UNIVERSITY OF TRENTO

DOCTORAL THESIS

Effective field theory description of α cluster nuclei:

The ^{9}Be ground state and ^{9}Be photodisintegration

Author:
Elena FILANDRI

Supervisor:
Winfried LEIDEMANN

Department of Physics

XXXIV CICLO

April 6, 2022

Contents

List of Figures

List of Tables

Chapter 1

Introduction

In this Thesis we present a description of α cluster nuclei, focusing on the case of ^{9}Be, within Cluster Effective Field Theory.

In some particular nuclei some of the nucleons, contained within them, aggregate in certain substructures. These are called halo or cluster nuclei. The clustering structures emerge from a delicate equilibrium among repulsive short-range forces and Pauli blocking effects, attractive medium-range nuclear interactions, and long-range Coulomb potential [1]. Seeking for this balance, four nucleons will tend then to aggregate by forming a spin zero entity known as α particle. The α particle has the highest binding energy per nucleon among the light nuclei ($\sim$ 7 MeV) and this suggests that this is a natural state for nucleons to fall in.

The study of nuclear clustering has a long history back to Rutherford's discovery of alpha radiation and the development of quantum mechanics (see [1] and references therein). In 1928 Gamow and, separately, Gurney and Condon described the α-particle as undergoing quantum-mechanical tunneling from inside the decaying nucleus [2]. About a decade later, came the work of Hafstad and Teller [3], which depicted even-even $N = Z$ nuclei in terms of an α-particle model with bonds connecting clusters. Along the same lines, Dennison proposed a model of the low-lying ^{16}O states in terms of four α-clusters at the vertices of a regular tetrahedron [4, 5] and, few years later, Morinaga suggested that linear chains of α-clusters could describe some specific nuclear states [6]. One of the candidates for such a description was the second 0^+ state of ^{12}C postulated by Hoyle [7] as responsible for enhancing the triple-α reaction in stars and experimentally observed soon after [8]. Concurrent with these theoretical developments, new experiments provided high-quality data on elastic α-α scattering [9, 10, 11]. This in turn led to the development of an effective α-α interaction [12]. At the same time, Ikeda, Takigawa, and Horiuchi noticed that α-clustering appeared close to the so-called α-decay thresholds [13], which represents the energy required for the decay of the system into constituent α-particles. These α-clustering were then schematized in the so-called Ikeda diagram, Figure 1.1. Despite the early start of cluster studies, it is only recently that radioactive ion beam experiments allowed new generation of studies, in which the data are compared to theoretical predictions with or without assumptions of a cluster core.

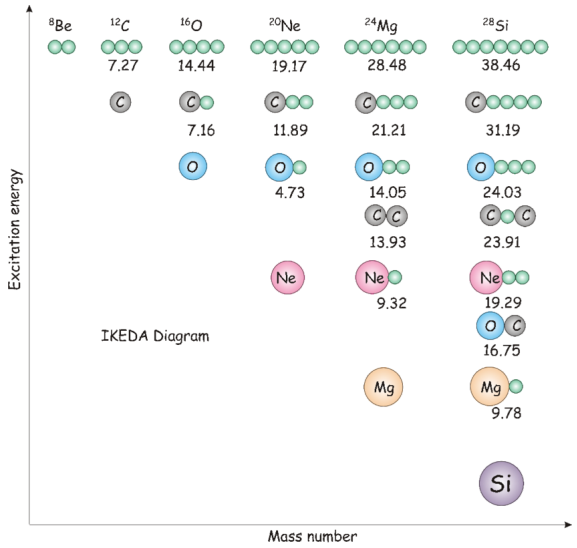

FIGURE 1.1: The Ikeda diagram. The threshold energies for each configuration are given in MeV. The smallest, unlabelled clusters are alpha particles. Decreasing excitation energy more and more complex cluster structures are formed. Figure from Ref. [14]

Nowadays, many experimental evidences for the cluster structure of nuclei have been found and they are well documented [1]. In particular we mention the observation of some cluster systems predicted by the Ikeda diagram (^{20}Ne,^{24}Mg,^{28}Si) and other more recent experimental studies that seems to support the alpha cluster structure in ^{56}Ni [15] and in the ground state of ^{40}Ca [16]. In spite of numerous experimental successes several nuclei are still under investigation as cluster nuclei candidates, among which are Beryllium-9 and the ground state of Carbon-12. In all these nuclei one in fact can recognize the presence of a natural separation of scales, indeed, the energy required in order to separate the system into clusters is much less than the separation energy of a nucleon from the cluster. For instance, in the case of ^{9}Be the energy needed to separate the system into the three effective degrees of freedom is ~ 1.572 MeV, while the proton separation energy of ^{4}He is $S_p(^4\text{He})$ ~ 19.813 MeV. By comparing of these two energies one can conclude that a separation of scales exists. Thus the necessary requirement for the creation of an Effective Field Theory potential is fulfilled.

An Effective Field Theory (EFT) captures the most general dynamics among low-energy degrees of freedom that is consistent with some assumed symmetries. In nuclear physics where the fundamental theory of Quantum chromodynamics (QCD), formulated in terms of quarks and gluons, is non perturbative at ~ 1 GeV, one can construct an EFT using the QCD symmetries. All the details of the QCD dynamics at short distances are encoded in the EFT interaction strengths, called Wilson coefficients or low-energy constants, which can be determined from experimental data or lattice calculations. Scattering amplitudes are calculated as expansions in Q/M_{hi} and M_{lo}/M_{hi}, with Q being the typical momentum of the effective particles inside the nucleus. Here M_{hi} is the momentum scale where the EFT breaks down and M_{lo}

stands for low-energy scales of physics we want to capture. An EFT is renormalizable in the sense that at each order in the expansion the sensitivity to unaccounted short-distance physics is small, that is, of relative $O(Q/M_{hi}, M_{lo}/M_{hi})$. It is crucial to formulate a power counting that justifies a controlled truncation of the Lagrangian and of the transition amplitude according to the desired accuracy. Nuclei offer a non-trivial challenge because one wants such a perturbative expansion in addition to the non-perturbative treatment of certain leading operators, which is required due to the existence of shallow bound states [17]. Most of the ab initio studies of nuclear structure, based on the explicit solution of the Schrödinger equation or its equivalents, are now carried out with potentials inspired by EFT. Up to now, two, three, four and even more nucleon systems have been studied with EFT. While much remains to be understood, many successes have been achieved [18, 19]. The extension of EFTs with nucleons as degrees of freedom to larger nuclei faces computational challenges. As a first step in this extension, we can specialize at very low energies in which clusters of nucleons behave coherently in such a way that they can be chosen as new degrees of freedom. Even though many interesting issues of nuclear structure cannot be resolved, one can still investigate ground states of cluster or halo nuclei and some low-energy reactions of astrophysical interest involving them.

In this Thesis the main emphasis is on the system provided by the nucleus of ^{9}Be, but also the ground states of ^{12}C,^{16}O and ^{20}Ne are considered. For $E \lesssim 20$ MeV the dynamics describing the cluster configuration is insensitive to the internal dynamics of the α particles. Therefore, in order to describe these systems at low energy, we can use a three-body approach with interactions between the neutron and an alpha particle and between alpha particles.

The cluster approach is not new for the study of ^{9}Be. The cluster description was employed by Efros et al. in [20], where this nucleus has been depicted as an $\alpha\alpha n$ system and a calculation of the ground state has been made using phenomenological local potentials. Within the same three-body approach, another calculation by Casal et al. [21] has been performed, where in addition a phenomenological three-body force has been introduced. A similar model has been also used in Ref. [22] where the ground state of ^{9}Be has been investigated by using the coupled-rearrangement-channel Gaussian expansion method.

In this work, instead, contact interactions derived from Cluster EFT, with a more solid theoretical background, are used. The potentials are regularized by a Gaussian cutoff which treats the short-distance dependence of the interaction. We choose the cutoff regularization, because of its ability to reproduce known features, such as the correct sign of the parameters in the effective range expansion [23, 24]. Then, the potential coefficients are found to reproduce these scattering parameters in the calculated scattering T-matrix. Furthermore, we extend our EFT approach by including many-body forces.

In the same framework of Cluster EFT we describe also the photodisintegration

of ^{9}Be. This reaction is particularly interesting in the astrophysical context of nucleosynthesis since the inverse reaction might represent an alternative to the triple alpha process in the formation of ^{12}C, one of the key elements for life. In particular astrophysical settings, as during neutron stars mergers or supernova explosions, nucleosynthesis is driven by r-processes. In this environment, due to the high density of neutrons, an alternative channel to reach ^{12}C could become relevant and interesting to be investigated. Specifically, this process begins with the formation of ^{8}Be from two α particles and it proceeds with the reaction

$$^8\mathrm{Be} + n \rightarrow {}^9\mathrm{Be} + \gamma \tag{1.1}$$

followed then by

$$^9\mathrm{Be} + \alpha \rightarrow {}^{12}\mathrm{C} + n. \tag{1.2}$$

The reaction (1.2) could represent the main contribution to the abundance of ^{12}C, determining the initial condition for the synthesis of heavier elements. Since ^{8}Be is a resonance above the continuum threshold of two α-particles, we will concentrate on the following reaction

$$\alpha + \alpha + n \rightarrow {}^9\mathrm{Be} + \gamma, \tag{1.3}$$

which, due to time reversal invariance, gives the same transition amplitude as the corresponding ^{9}Be photodisintegration.

Since the 1940s measurements of the ^{9}Be photodisintegration cross-section have been performed using several different photon sources, as, for instance, radioactive isotopes [25], bremsstrahlung [26] and, more recently, laser-induced Compton backscattered γ rays [27, 28, 29]. The experimental data of the cross-section identify a region of interest at low energy, between gamma energies of 1.5 MeV and 5.2 MeV. Here the first pronounced peak, at around 1.7 MeV, has been connected to the $1/2^+$ channel of the reaction, while the other, at around 3 MeV, is linked to the $5/2^+$ channel. Regarding higher energy regions, in Ref. [27] a large resonance at around 10 MeV, already observed by A. M. Goryachev et al. in [26], was measured. Since it seems to be related to the $\alpha\alpha n$ cluster nature of ^{9}Be this resonance is known as Cluster Dipole Resonance (CDR). Above the latter the so-called giant dipole resonance (GDR) appears. A comparison among different sets of experimental data is given in Figure 1.2.

Although numerous experimental data have focused on the same regions of interest, there are significant discrepancies between the resonance features emerging from different data sets. For instance, the $1/2^+$ peak in Ref. [28] (red squares) is 20% smaller than the one found in Ref. [29] (filled diamonds). With regard to the CDR, the experimental data in Ref. [27] (blue squares) show a more enhanced cross-section than the bremsstrahlung ones in [26] (crosses). Clearly, such discrepancies can affect significantly supernovae nucleosynthesis models, which can be highly sensitive to

the $\alpha\alpha n$ reaction rate [30]. For this reason a solid theoretical study of ^{9}Be photodisintegration, based on ab initio calculations, could help.

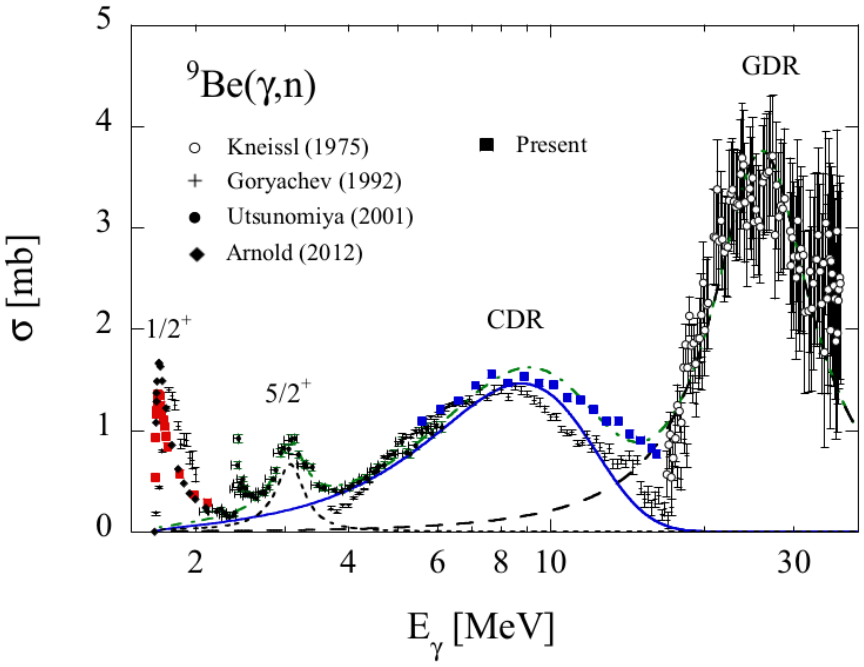

FIGURE 1.2: Comparison of different sets of data for the ^{9}Be photodisintegration in the energy range between 1.5 MeV and 30 MeV. The figure is taken from Ref. [27], to which the label "present" is referred. Data are shown for positron annihilation in flight measurements by U. Kneissl et al. [31] (empty circles), bremsstrahlung ones by A. M. Goryachev et al. [26] (crosses), laser-induced Compton backscattered γ rays ones by C. W. Arnold et al. [29] (filled diamonds) and by H. Utsunomiya et al. (filled circles [28], filled squares [27]).

Here, we present a fully ab initio calculations of the ground state wave functions and energies performed by solving the Schrödinger equation. Eigenvalues and eigenvectors are obtained, through the variational principle, from the diagonalization of the Hamiltonian expanded on a complete basis. Since the used potentials are interactions born in momentum space we have chosen to work with a Non-Symmetrized Hyperspherical Harmonic basis [32, 33] in this space. The continuum states, required to calculate the photodisintegration cross-section in a conventional way, are avoided via the use of the Lorentz Integral Transform (LIT) method [34].
The Thesis is structured as follows.

In Chapter 2 we present the general framework of the Cluster Effective field theory used in order to derive the interaction between the chosen nuclear constituents. After a brief overview on the general concepts of effective field theories, the Cluster EFT is described. In particular we show how to calculate the interactions between alpha particles and a nucleon. Some details of the EFT, such as the power counting and the limits on the cutoff value provided by the Wigner bound are also presented.

In Chapter 3 the method used to calculate the ground states of the studied nuclei is shown. The nuclear ground states have been calculated via the variational principle expanding their wave functions on a hyperspherical harmonics (HH) basis in momentum space. Moreover we discuss how to avoid the symmetrization of the HH basis elements thanks to the use of the Casimir operator. Finally, the application of this general method to our particular Hamiltonian is illustrated.

In Chapter 4, in the general context of nuclear reactions, the ^{9}Be photodisintegration process is presented showing in detail how to derive the currents within our theory. The final form of the cross-section is also given.

In Chapter 5 we explain the Lorentz Integral Transform (LIT) approach for the determination of the response function associated to inclusive processes. We analyse how the LIT method allows us to calculate the response function via a reduction of the continuum problem to a bound-state one and present the practical approaches for the computation of the LIT. The formalism of the LIT applied to the ^{9}Be photodisintegration reaction is then introduced.

In Chapter 6 the final results are presented. Starting from the discussion of the results obtained for the ground states of ^{12}C, ^{16}O, ^{20}Ne and of ^{9}Be, then the cross-section for the photodisintegration reaction of ^{9}Be will be shown.

Conclusions and future perspectives are drawn in Chapter 7.

Chapter 2

Cluster Effective Field Theory

In this Chapter we present the general structure of the Cluster Effective field theory (EFT) used in order to derive two and three-body interactions among a neutron and alpha particles. After a brief overview on the general concepts of EFTs in nuclear physics, Section 2.1, the Cluster or Halo EFT is described in Section 2.2. In this context two different kinds of approaches for the calculation of the interactions are presented: the perturbative one, Section 2.3, and the resummation, Section 2.4. The potentials for the α-α and α-n dominant partial waves are derived and, then, cured from ultraviolet divergences using the cutoff regularization scheme. In particular, we consider for the $\alpha\alpha$ system the S_0 wave interaction while for αn pair the $P_{\frac{3}{2}}$ and $S_{\frac{1}{2}}$ partial waves. The potential coefficients are found comparing the calculated scattering T-matrix with the effective range expansion. In Section 2.5 we introduce the power counting, a fundamental requirement for the solidity of any EFT. Furthermore, the limits on the cutoff values provided by the Wigner bound are shown in Section 2.6. Finally, in Section 2.7 we deal with the three-body force introduced in the theory.

2.1 Effective Field Theories

The separation of energy scales is a fundamental point in most physics problems since it permits to select the relevant degrees of freedom and the dominant interactions [35]. Then, eventually, a systematic treatment of the less relevant interactions is required, which can be accomplished in a variety of ways.

In nuclear physics this problem was already faced when it was realized that the deuteron scattering length results large compared to the range of the nuclear force. Also by analysing the slow-neutron scattering from bound protons, the need to separate the effects of the nuclear force from those of the longer-range electromagnetic interactions arose. This led to the treatment of short range interactions with various techniques among those, for instance, the effective range expansion [36] and parametrizations of the nuclear force in terms of meson exchange, which were perceived as more fundamental. Meanwhile, at the end of the 20th century, the method of effective field theories (EFTs) has been developed in particle physics. The general idea is starting from the most general Lagrangian involving the relevant low-energy

degrees of freedom and invariant under some chosen symmetries. Depending on whether or not an underlying theory is known there are two ways to construct an EFT.

When the high-energy fundamental theory is known, an effective theory can be obtained in a top-down approach by a process in which the effects of high energy are systematically eliminated. Starting from a known theory, one then systematically eliminates the degrees of freedom associated with energies above a given high-energy scale M_{hi}. One method to do that was proposed by Wilson and others in the 1970 [37]. There the high-energy degrees of freedom, also defined as high momenta or heavy fields, are identified and integrated out in the action. The result of this integration is an effective action that describes the interactions among the low-energy degrees of freedom in a certain energy range.

When the fundamental high-energy theory is not known another way to construct an EFT is needed. In this case, it may still be possible to obtain a theory by a bottom-up approach where relevant symmetries and naturalness constraints are imposed on the candidate Lagrangians. One simply begins introducing all operators, allowed by the low-energy symmetries of the fundamental theory. Each term is then multiplied by a coupling constant which depends inversely on the high energy scale Λ^n with n the correct power for the dimension of the operator. These couplings encode all the dynamics of the underlying theory at short distances, they are the so-called Wilson coefficients or low-energy constants (LECs). In general they are determined from experimental data or by a possible comparison with the fundamental theory.

The bottom-up EFT is particularly useful for nuclear physics. The Quantum Chromodynamics (QCD) in fact, formulated in terms of quarks and gluons, is highly non perturbative for processes characterized by external momenta $Q \leq M_{\mathrm{QCD}} \sim 1\,\mathrm{GeV}$. Historically the first nuclear EFT was the Chiral EFT [38, 39], which is designed for momenta $\ll 1$ GeV. In addition to nucleons, it includes explicit pions and the interactions are constrained by an approximate global symmetry of QCD, the chiral symmetry. This is the symmetry for independent flavour rotations in the isospin space of the left-handed and the right-handed components of the quark field. Chiral EFT has proven to be extremely challenging to renormalize due to the singularity of the dominant interactions, which has to be treated non-perturbatively in order to produce bound states and resonances, namely nuclei.

A simpler EFT, Pionless (or Contact) EFT, focuses on momenta below the pion mass [40]. This theory, whose renormalization is better under control, is constrained only by QCD spacetime symmetries. It presents a high degree of universality, and except for the degrees of freedom which change depending on the application, it is formally identical to other EFTs where all interactions are of short range. The same framework has been successful also for atomic systems with large scattering lengths (for example, near a Feshbach resonance)[41]. A variant of pionless EFT is the Halo or Cluster EFT applicable to describe bound states and reactions involving halo or

cluster nuclei in an energy range such that clusters of nucleons can be treated as elementary degrees of freedom [42]. This represent a first step in this extension of EFTs to larger nuclei and even though many interesting issues of nuclear structure cannot be resolved, one can still describe anomalously shallow nuclei and some reactions of astrophysical interest.

2.2 Cluster EFT

In nuclear physics, in general, nucleons are used as effective degree of freedom, however this is not the only possible choice.

In particular, some nuclei have some parts of the system which can be seen as separated subsystems, these are called halo or cluster nuclei. We can, for example, focus on one of these systems provided by the nucleus of ^{9}Be. As already mentioned in Chapter 1, the energy needed in order to separate the system into the three effective degrees of freedom α, α, and n is $\sim$ 1.572 MeV, while the proton separation energy of ^{4}He is $S_p(^4\text{He}) \sim 19.813$ MeV. Comparing these two energy values, one can already see a separation of scales, needed for an Effective Field Theory approach. In order to describe this kind of systems, in the low-energy range, we can use an EFT taking nucleons and alpha particles as degrees of freedom. The α-α interaction is dominated by the S_0 resonant state, while the αn system has a resonance in the $P_{\frac{3}{2}}$ partial wave [43].

As stated in the previous Section, when we use a bottom up approach the first step is to look for a theory that respects, in a chosen energy range, the same symmetries as the fundamental one. Therefore the effective Lagrangian for non-relativistic nucleons and alpha particles must obey the symmetries of the strong interactions at low energies, i.e. parity, charge-conjugation, time-reversal and Galilean invariance. After having identified the symmetries, it is necessary to write all the independent terms compatible with the restrictions imposed by these one.

The most general interaction Lagrangian density for systems including α particles and a neutron with only contact interaction and ignoring spin and isospin indices, up to Q^2 order is given by

$$\begin{aligned}\mathcal{L}_{int} = {} & \lambda_{0\alpha\alpha,l}(\Psi(\overleftrightarrow{\nabla}^l)\Psi)^\dagger(\Psi(\overleftrightarrow{\nabla}^l)\Psi) + \lambda_{1\alpha\alpha,l}\Big((\Psi\overleftrightarrow{\nabla}^2(\overleftrightarrow{\nabla}^l)\Psi)(\Psi(\overleftrightarrow{\nabla}^l)\Psi) + hc\Big) \\ & + \lambda_{0\alpha n,l}(\Psi(\overleftrightarrow{\nabla}^l)n)^\dagger(\Psi(\overleftrightarrow{\nabla}^l)n) + \lambda_{1\alpha n,l}\Big((\Psi\overleftrightarrow{\nabla}^2(\overleftrightarrow{\nabla}^l)n)(\Psi(\overleftrightarrow{\nabla}^l)n) + hc\Big) + \dots ,\end{aligned} \tag{2.1}$$

with $\overleftrightarrow{\nabla}$ the left and right derivative acting as

$$\Psi_a \overleftrightarrow{\nabla} \Psi_b = \frac{m_b\partial_a - m_a\partial_b}{m_a + m_b}, \tag{2.2}$$

Ψ and n representing the non-relativistic approximation of the alpha particle and nucleon fields, respectively,

$$\Psi(\boldsymbol{x}) = V \int \frac{d\boldsymbol{k}}{(2\pi)^3}\, a_{\boldsymbol{k}}\, \frac{e^{i\boldsymbol{k}\cdot\boldsymbol{x}}}{\sqrt{V}}\,, \tag{2.3}$$

$$\Psi^{\dagger}(\boldsymbol{x}) = V \int \frac{d\boldsymbol{k}}{(2\pi)^3}\, a^{\dagger}_{\boldsymbol{k}}\, \frac{e^{-i\boldsymbol{k}\cdot\boldsymbol{x}}}{\sqrt{V}}\,, \tag{2.4}$$

$$n(\boldsymbol{x}) = V \int \frac{d\boldsymbol{k}}{(2\pi)^3}\, b_{\boldsymbol{k}}\, u(\boldsymbol{k})\, \frac{e^{i\boldsymbol{k}\cdot\boldsymbol{x}}}{\sqrt{V}}\,, \tag{2.5}$$

$$n^{\dagger}(\boldsymbol{x}) = V \int \frac{d\boldsymbol{k}}{(2\pi)^3}\, b^{\dagger}_{\boldsymbol{k}}\, \bar{u}(\boldsymbol{k})\, \frac{e^{-i\boldsymbol{k}\cdot\boldsymbol{x}}}{\sqrt{V}} \tag{2.6}$$

being $a_{\boldsymbol{k}}$ the annihilation operators, $u(\boldsymbol{k})$ the Dirac spinor. The $\lambda_{i,l}$ in Eq. (2.1) are the low-energy constants and the subscript l stands for the type of interaction considered, that is $l = 0$ for S-wave interaction, $l = 1$ P-wave and so on. Justifying the truncation of the Lagrangian is crucial to formulate a power counting for each kind of interaction examined.

From the Lagrangian (2.1) the α-α and α-n potentials in momentum space can be obtained, regularizing the ultraviolet divergences with a Gaussian cutoff $g(p) = e^{-(p/\Lambda)^{2m}}$,

$$V(\mathbf{p},\mathbf{p}') = \langle \mathbf{p}|V|\mathbf{p}'\rangle = \sum_{l=0}^{\infty}(2l+1)V_l(p,p')P_l(\hat{\mathbf{p}}\cdot\hat{\mathbf{p}}')\,, \tag{2.7}$$

where $P_l(\hat{\mathbf{p}}\cdot\hat{\mathbf{p}}')$ is the l-th Legendre polynomial, $\boldsymbol{p}, \boldsymbol{p}'$ relative momenta and $V_l(p,p')$ is given by

$$V_l(p,p') = p^l p'^l g(p) g(p') \sum_{ij=0}^{1} p^{2i} \lambda_{ij} p'^{2j} \qquad \lambda = \begin{pmatrix} \lambda_0 & \lambda_1 \\ \lambda_1 & 0 \end{pmatrix}. \tag{2.8}$$

The choice of the cutoff regularization is due to its ability to reproduce known features, such as the correct sign of the effective range parameter in the T-matrix expansion or the right scaling of the renormalized scattering amplitude [23, 24].

The LECs of our effective theory will then be determined by comparing the calculated T-matrix with the effective range expansion (ERE). In this way we will obtain equations that relate the coupling constants to the effective range parameters α_l, r_l for each interaction examined. To calculate the T-matrix there are two different approaches depending on the case in question [35]. The first case occurs when the effective-range parameters are of "natural" size, namely given by the appropriate power of the high momentum scale M_{hi}. In particular, a resonance or a bound state, if present, generally occurs at the momentum scale M_{hi}. In this natural case, a perturbative approach can be used to calculate the T-matrix considering only the diagrams which give the largest contribution to it. However, in most cases the interactions are finely tuned in such a way as to produce a resonance close to threshold, at a scale M_{lo} much smaller than M_{hi}, violating the naive dimensional-analysis estimate. This situation can occur when one or more of the effective-range parameters have unnatural sizes related to the low-momentum scale M_{lo}. In the latter case, to describe the correct behaviour near the resonance, the T-matrix has to be resummed

to all orders in the loop expansion.

At this point it is important to emphasise that in an EFT two different expansions in power of Q (typical momentum of the particles) are present. The first one, which we already mentioned, is the expansion of the Lagrangian in the number of derivatives at the vertex. It depends on the relative size of the coupling constant, $\lambda_1 Q^2/\lambda_0$. The second one is the loop expansion governed by $mQ\lambda_0$ where m is in general the reduced mass of the system.

In the next sections we explain how to build potentials both in natural and in the fine-tuning case, although in this work we only implement the non-perturbative approach. This is due to the ab initio method used: the bound energies and wave functions are calculated by solving the Schrödinger equation with the EFT potentials, thus in a non-perturbative approach. For reasons of consistency, hence, the potentials used for the computation of the observables should be derived in the same approach.

2.3 Natural case

Let us consider first the simplest scenario, the so-called natural case.

When the scattering length and the effective range have natural values of order $a \sim r \sim 1/M_{hi}$, the theory has only a single mass scale M_{hi} thus no fine-tuning is present. We present here for the sake of simplicity the S-wave case, the generalization for the other waves will be then straightforward. The aim is to calculate the LECs λ_0 and λ_1 for the following potential,

$$V_0(p,p') = g(p)g(p') \sum_{i,j=0}^{1} p^{2i} \lambda_{ij} p'^{2j}, \tag{2.9}$$

where again $g(p) = e^{-(p/\Lambda)^{2m}}$.

As already mentioned in Section 2.2, in order to do this, we calculate the on shell T-matrix and we compare this expression with the effective range expansion (ERE)

$$\frac{1}{T_0^{on}(E)} = -\frac{\mu}{2\pi}\left(-\frac{1}{a_0} + \frac{1}{2} r_0 k^2 ..\right) + O(k^4) \tag{2.10}$$

or after some manipulations,

$$T_0^{on}(E) = -\frac{2\pi}{\mu}\left(-a_0 - {a_0}^2 \frac{1}{2} r_0 k^2 ..\right) + O(k^4)\,, \tag{2.11}$$

with a_0 the scattering length, r_0 the effective range and μ the reduced mass.

We refer to Appendix A for more details on the T-matrix formalism and ERE.

The first step is to calculate the T-matrix. In this case, due to the natural values of scattering parameters, one can perform the calculation with the perturbative approach and calculate the diagrams that contribute the most to the T-matrix.

We consider the following diagrams:

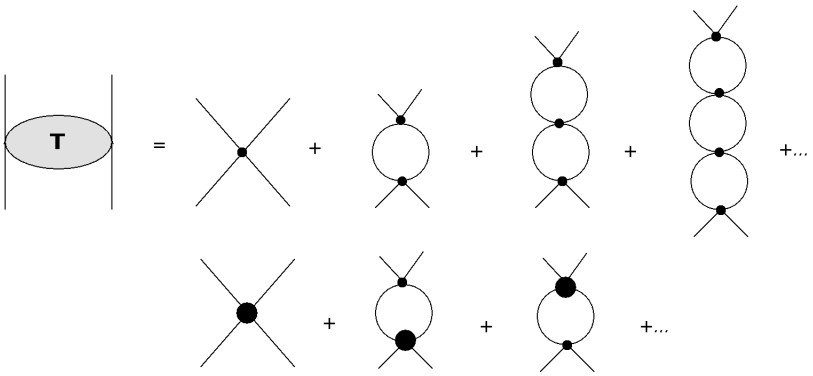

FIGURE 2.1: Diagrammatic expansion of the T-matrix.

In Figure 2.1 the small dot stands for a Q^0 contact interaction, and the bigger one for a Q^2 (or ∇^2) contact interaction. Considering the loop expansion up to next-to-next-to-next leading order (N3LO) and setting $p = p' = k$ we get

$$T^{on}_{l=0} = \lambda_0[g(k)^2 + \lambda_0 I_0 + (\lambda_0 I_0)^2 + (\lambda_0 I_0)^3] + 2\lambda_1 k^2 (g(k)^2 + 2\lambda_0 I_0)\,, \tag{2.12}$$

with

$$I_0 = -2\mu \int_0^\infty \frac{d^3q}{(2\pi)^3} \frac{g(q)^2}{q^2 - k^2 - i\epsilon} = -\frac{\mu}{\pi^2} \int_0^\infty dq q^2 \frac{g(q)^2}{q^2 - k^2 - i\epsilon}. \tag{2.13}$$

The I_0 term can be calculated solving the following integral as

$$\begin{aligned} &-\tfrac{\mu}{\pi^2} \textstyle\int_0^\infty dq q^2 \tfrac{g(q)^2}{q^2-k^2-i\epsilon} = \\ &-\tfrac{\mu}{\pi^2} \textstyle\int_0^\infty dq g(q)^2 - \tfrac{\mu k^2}{\pi^2} \textstyle\int_0^\infty dq \tfrac{g(q)^2}{q^2-k^2-i\epsilon} = \\ &-\tfrac{\mu}{\pi^2} 2^{\frac{-1}{2m}} \Gamma((2m+1)/2m)\Lambda - \tfrac{i\mu k}{2\pi} g^2(k)\,. \end{aligned} \tag{2.14}$$

In Eq. (2.14) the expression of the regulator $g(p)^2$ can be simplified as

$$g(p)^2 = e^{-(2p/\Lambda)^{2m}} \sim 1 - (2p/\Lambda)^{2m} \sim 1 \qquad m \geq 2\,, \tag{2.15}$$

and substituting the expression of I_0 and $g(k)^2$ in Eq. (2.12), one obtains

$$\begin{aligned} T^{on}_{l=0} = \lambda_0[1 + \lambda_0(-f(\Lambda) - \tfrac{i\mu k}{2\pi}) + \lambda_0^2(-f(\Lambda) - \tfrac{i\mu k}{2\pi})^2 + \lambda_0^3(-f(\Lambda) - \tfrac{i\mu k}{2\pi})^3] \\ +2\lambda_1 k^2(1 + 2\lambda_0(-f(\Lambda) - \tfrac{i\mu k}{2\pi})]\,, \end{aligned} \tag{2.16}$$

where $f(\Lambda) = \frac{\mu}{\pi^2}\Gamma((2m+1)/2m)2^{\frac{-1}{2m}}\Lambda$.

Finally comparing the expression of the calculated T-matrix with the ERE (2.10) one gets

$$\frac{\alpha_0 2\pi}{\mu} = \lambda_0[1 - \lambda_0 f(\Lambda) + \lambda_0^2 (f(\Lambda))^2 - \lambda_0^3 (f(\Lambda))^3]\,, \tag{2.17}$$

$$\frac{r_0 \alpha_0^2 \pi}{\mu} = \lambda_1[2 - 4\lambda_0 f(\Lambda) + 3\frac{\lambda_0^4}{\lambda_1} f(\Lambda) \frac{\mu^2}{4\pi^2} - \frac{\lambda_0^3}{\lambda_1} \frac{\mu^2}{4\pi^2}]. \tag{2.18}$$

It is worth noting that in the case of a perturbative approach in principle it would be possible a 'standard' renormalization approach by sending the cutoff to infinity, since the number of counter-terms to the considered order is finite [35]. In this way the renormalized parameters λ_{0R} and λ_{1R}, containing only the Λ-dependent infinite terms, can be defined as

$$\lambda_{0R} = \lambda_0[1 - \lambda_0 f(\Lambda) + \lambda_0^2 (f(\Lambda))^2 - \lambda_0^3 (f(\Lambda))^3] \tag{2.19}$$

$$\lambda_{1R} = \lambda_1[1 - 2\lambda_0 f(\Lambda) + 3\tfrac{\lambda_0^4}{\lambda_1} f(\Lambda) \tfrac{\mu^2}{8\pi^2}]. \tag{2.20}$$

According to the Wigner bound, explained later in Section 2.6, removing the cutoff by sending it to infinity inevitably leads to a negative value of the effective range. For for this reason we will adopt in this work the so-called 'implicit' renormalization scheme by keeping the cutoff finite [44]. This latter is a more flexible procedure which is also optimal in case of non-perturbative calculation of the T-matrix. For each value of the cutoff λ_0 and λ_1 are obtained using the experimental values for a_0 and r_0 in Eqs. (2.17), (2.18).

As example of natural case we can take the $S_{\frac{1}{2}}$-wave of the α-n interaction. The natural values of the scattering length and of the effective range [45],

$$a_0 = 2.4641\,\text{fm} \qquad r_0 = 1.385\,\text{fm}\,, \tag{2.21}$$

indicate that $a_0 \sim r_0 \sim 1/M_{hi}$. Substituting these experimental values in Eqs. (2.17), (2.18) we obtain four solutions for λ_0 and λ_1, however just two of them are real. In Figure 2.2 a comparison with the experimental data for the αn S-wave phase shift can be seen.

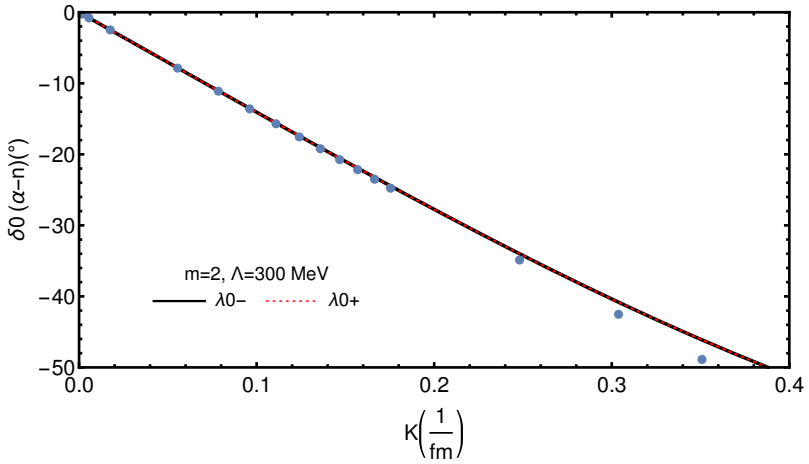

FIGURE 2.2: α-n calculated phase shift in comparison with the R-matrix analysis [46]. K is the relative momentum in the center of mass frame. The black curve represents one real solution of the two coupling constants, the red one the other. In this calculation we set $\Lambda = 300$ MeV and $g(p)^2 = e^{-(2p/\Lambda)^4}$, i.e. we set the m parameter in the regulator as $m = 2$.

We conclude this paragraph by remarking that the assumption of naturalness implies a perturbative amplitude. Since terms in the Q/M expansion of the amplitude are in correspondence to terms in the derivative expansion of the effective Lagrangian, the accuracy of description of low-energy data can be improved systematically by considering higher-order terms in the interaction Lagrangian. Not surprisingly, the EFT here can only describe scattering. Bound states or narrow resonances, if they exist, have typical momenta $\sim M_{lo}$, and are outside the region of validity of the expansion.

2.4 Fine-tuning

In this Section we discuss the non-perturbative treatment of the T-matrix. The following calculation for the P-wave case only can be also found in Ref. [47], where the αn $P_{3/2}$ resonance was considered.

The fine-tuning occurs when we want to describe narrow low-energy resonances with very large scattering parameters. In this case the large scattering length is a signal of non-perturbative physics which indicates that another energy scale M_{lo} is present, i.e.

$$\frac{1}{\alpha_0} \sim M_{lo}^3/M_{hi}^2\,, \quad r_0 \sim 1/M_{hi}\,; \quad \frac{1}{\alpha_1} \sim M_{lo}^2 M_{hi}\,, \quad r_1 \sim M_{hi}. \tag{2.22}$$

When between two particles only a short range interaction is present we can simply write the Lippmann-Schwinger equation as

$$T(\mathbf{p},\mathbf{p}') = V(\mathbf{p},\mathbf{p}') + \int \frac{d\mathbf{q}}{(2\pi)^3} V(\mathbf{p},\mathbf{q}) \frac{1}{E' - \frac{q^2}{2\mu_{\alpha n}} + i\epsilon} T(\mathbf{q},\mathbf{p}')\,, \tag{2.23}$$

where $E' = k^2/2\mu_{\alpha n}$.

In this case, in order to describe the right behaviour near the resonance $\sim M_{lo}$, the calculation of the T-matrix cannot be performed perturbatively since such energy range is outside the region of validity of the expansion; the series of diagrams must be resummed. Hence, the next step consists in the resolution of the Lippmann-Schwinger equation. In order to do this, the T-matrix can be expanded in partial waves. The result is

$$T(\mathbf{p},\mathbf{p}') = \sum_{l=0}^{\infty} (2l+1) T_l(p,p') P_l(\hat{\mathbf{p}},\cdot\,\hat{\mathbf{p}}')\,, \tag{2.24}$$

where one assumes

$$T_l(p,p') = p^l p'^l g(p) g(p') \sum_{i,j=0}^{1} p^{2i} \tau_{ij}(E) p'^{2j}. \tag{2.25}$$

At this point, we can substitute Eqs. (2.23), (2.24) in Eq. (2.25) getting

$$\tau_{ij}(E) = \lambda_{i,j} + \sum_{m,n=0}^{1} \lambda_{im} \int \frac{d^3q}{(2\pi)^3} \frac{q^{2l+2m+2n}}{E - \frac{q^2}{2\mu_{\alpha n}} + i\epsilon} g^2(q) \tau_{nj}(E) \tag{2.26}$$

or, in matrix form,

$$\tau(E) = \lambda + \lambda \phi^{(l)} \tau(E)\,, \tag{2.27}$$

where

$$\phi^{(l)} = \begin{pmatrix} \phi_0^{(l)} & \phi_2^{(l)} \\ \phi_2^{(l)} & \phi_4^{(l)} \end{pmatrix}, \tag{2.28}$$

being

$$\phi_{2n}^{(l)} = \int \frac{d^3q}{(2\pi)^3} \frac{q^{2l+2n}}{E - \frac{q^2}{2\mu_{\alpha n}} + i\epsilon} g^2(q)\,. \tag{2.29}$$

Solving for τ one finds

$$\tau(E) = \frac{1}{\det \tau^{-1}} \begin{pmatrix} -\frac{\lambda_0}{\lambda_1^2} - \phi_4^{(l)} & -\frac{1}{\lambda_1} + \phi_2^{(l)} \\ -\frac{1}{\lambda_1} + \phi_2^{(1)} & -\phi_0^{(l)} \end{pmatrix}, \tag{2.30}$$

where $\det \tau^{-1} = \phi_0^{(l)} \phi_4^{(l)} + \frac{\lambda_0}{\lambda_1^2} \phi_0^{(l)} - \left(\phi_2^{(l)} - \frac{1}{\lambda_1}\right)^2$.

For our derivation we need the on-shell T-matrix, which can be calculated inserting Eq. (2.30) into Eq. (2.26) and putting $p = p' = k$ as

$$T_l^{on}(E) = \frac{k^{2l}}{\det \tau^{-1}} g^2(k) \left[-\frac{\lambda_0}{\lambda_1^2} - \phi_4^{(l)} + \left(-\frac{1}{\lambda_1} + \phi_2^{(l)} \right) 2k^2 - \phi_0^{(l)} k^4 \right]. \tag{2.31}$$

The quantity $\phi_{2n}^{(l)}$ of Eq. (2.29) can be expressed through a useful recursion relation

$$\phi_{2n}^{(l)} = I_{2n+2l+1} + k^2 \phi_{2n-2}^{(l)}\,, \tag{2.32}$$

where $I_n \sim \Lambda^n$ is defined by

$$I_n = -\frac{\mu_{\alpha n}}{\pi^2} \int_0^\infty dq q^{n-1} g^2(q). \tag{2.33}$$

Using this result, we find

$$\frac{k^{2l}}{T_l^{\text{on}}(E)} = \frac{1}{g^2(k)} \left[\frac{\left(I_{2l+3} - \frac{1}{\lambda_1}\right)^2}{I_{2l+5} + \frac{\lambda_0}{\lambda_1^2} - k^2 \left(I_{2l+3} - \frac{2}{\lambda_1}\right)} - \phi_0^{(l)} \right]. \tag{2.34}$$

The above equation is a general result in absence of long range interactions. In the case of fine tuning and therefore a non-perturbative approach, it is clear that renormalizing with an infinite cutoff is no longer possible, due to the infinite number of counter terms.

The following step is to expand Eq. (2.34) in power of k^2/Λ^2,

$$\frac{k^{2l}}{T_l^{on}(E)} = \frac{1}{g^2(k)}\left[\frac{\left(I_{2l+3}-\frac{1}{\lambda_1}\right)^2}{I_{2l+5}+\frac{\lambda_0}{\lambda_1^2}}+k^2\left(\frac{I_{2l+3}-\frac{1}{\lambda_1}}{I_{2l+5}+\frac{\lambda_0}{\lambda_1^2}}\right)^2\left(I_{2l+3}-\frac{2}{\lambda_1}\right)-\phi_0^{(l)}\right]. \tag{2.35}$$

In this expansions it can been assumed again that the contribution due to $g(k)$ is negligible[1]

$$g(k) \overset{k\to 0}{\longrightarrow} 1-\left(\frac{k}{\Lambda}\right)^{2m} \qquad \text{with} \qquad m \geq 2\,. \tag{2.36}$$

To simplify notation, one can define

$$f_{n,m} = \frac{n}{\Lambda^n}\int_0^\infty dq q^{n-1} e^{-2\left(\frac{q^2}{\Lambda}\right)^{2m}} = \left(\frac{1}{2}\right)^{\frac{n}{2m}}\Gamma\left(\frac{n}{2m}+1\right), \tag{2.37}$$

in this way the quantity in Eq. (2.33) can be rewritten as

$$I_n = -\frac{\mu_{\alpha n}}{\pi^2}\frac{\Lambda^n}{n}f_{n,m}\,. \tag{2.38}$$

Moreover it is useful to introduce the adimensional coefficients c_0 and c_1 defined through the following relations,

$$\lambda_0 = -\frac{\pi^2}{\mu_{\alpha n}}\frac{c_0}{\Lambda^{2l+1}}\,, \quad \lambda_1 = -\frac{\pi^2}{\mu_{\alpha n}}\frac{c_1}{\Lambda^{2l+3}}. \tag{2.39}$$

The expression for the T-matrix can be now compared to the ERE

$$\frac{2k^l}{T_l^{on}(E)} = -\frac{\mu}{2\pi}\left(-\frac{1}{\alpha_l}+\frac{1}{2}r_l k^2 - ik^{2l+1}\right)+O(k^4)\,, \tag{2.40}$$

what we get from the comparison are two coupled equations.

For example in the S-wave case,

$$\begin{gathered}\frac{\left(\frac{f_{3,m}}{3}-\frac{1}{c_1}\right)^2}{\frac{f_{5,m}}{5}+\frac{c_0}{c_1^2}} = f_{1,m}-\frac{\pi}{2\alpha_0\Lambda} \\ \frac{4}{\pi\Lambda}\left(1-\frac{1}{\left(\frac{1}{3}c_1 f_{3,m}-1\right)^2}\right)\left(f_{1,m}-\frac{\pi}{2\alpha_0\Lambda}\right)^2\frac{3}{f_{3,m}} = r_0.\end{gathered} \tag{2.41}$$

While for the P-wave case,

$$\begin{gathered}\frac{\left(\frac{f_{5,m}}{5}-\frac{1}{c_1}\right)^2}{\frac{f_{7,m}}{7}+\frac{c_0}{c_1^2}} = \frac{f_{3,m}}{3}-\frac{\pi}{2\alpha_1\Lambda^3} \\ -\frac{4\Lambda}{\pi}\left\{f_{1,m}-\left(\frac{f_{3,m}}{3}-\frac{\pi}{2\alpha_1\Lambda^3}\right)^2\frac{5}{f_{5,m}}\left[1-\left(c_1\frac{f_{5,m}}{5}-1\right)^{-2}\right]\right\} = r_1.\end{gathered} \tag{2.42}$$

[1] We performed the calculation even with $m = 1$, this does not add other complications to the calculation but only the addition of a term in Eqs. (2.41),(2.42). However parameters $m \geq 2$ give better results in the phase shift and for this reason we will use the calculation presented in the text.

From Eqs. (2.41) and (2.42) we can notice that a bound on Λ is provided.
In the limit $\Lambda \to \infty$ $r_0 \to 0$ while $r_1 \to \infty$. Since we want a finite r_l, Λ needs to be finite. This is the implicit renormalization procedure, also related to the concept of the Wigner bound. More details about this topic will be provided later in the text in Section 2.6.

Now, we focus on the P-wave case for the α-n interaction. Using Eq. (2.42) one obtains c_0 and c_1 as functions of Λ,

$$c_0 = \left[\frac{\left(\frac{f_{5,m}}{5} - \frac{1}{c_1}\right)^2}{\frac{f_{3,m}}{3} - \frac{\pi}{2a_1\Lambda^3}} - \frac{f_{7,m}}{7} \right] c_1^2 , \tag{2.43}$$

$$c_1 = \frac{5}{f_{5,m}} \left\{ 1 \pm \left[1 - \frac{\left(f_{1,m} + \frac{r_1\pi}{4\Lambda}\right)\frac{f_{5,m}}{5}}{\left(\frac{f_{3,m}}{3} - \frac{\pi}{2a_1\Lambda^3}\right)^2} \right]^{-\frac{1}{2}} \right\} ,$$

then the $P_{3/2}$ experimental scattering parameters $a_1 = -62.951$ fm^3 and $r_1 = -0.8819$ fm^{-1} [45] can be used in order to get an explicit solution for c_0 and c_1. Clearly from the second degree Eqs. (2.43) we obtain two solutions for c_0 and c_1.

In principle, both solutions reproduce the correct T-matrix, but we choose the smaller ones of most natural size, which also provide a weakly attractive potential at large distance. In Figure 2.3 we show the two pairs of solutions in function of the αn cutoff Λ.

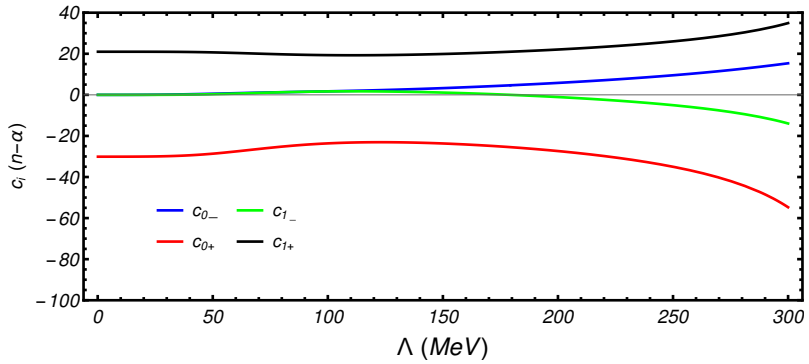

FIGURE 2.3: Coupling constant c_i for the $P_{3/2}$ wave of the αn potential. As one can see, the set c_{i-} is composed of coupling constants with natural size and thus preferable to the set c_{i+}.

The α-n $P_{3/2}$ phase shift is shown in Figure 2.4. For cutoffs between 200 and 300 MeV one finds a good agreement with experimental data. In the inset of the Figure one sees that the total cross-section correctly reproduces the $^2P_{3/2}$ resonance at $E_R = Q_{\alpha-\text{decay}}(^5\text{He}) = 0.798$ MeV with a width of 0.648 MeV [48].

In Section 2.3 we described the case of the $S_{\frac{1}{2}}$ wave of α-n interaction. As already mentioned, in this case the natural values of the scattering length and the effective range suggest a perturbative approach. However in our work we will carry out also in this case the resummation of the T-matrix. Our purpose is, in fact, to obtain the ground state of these cluster nuclei by solving the Schrödinger equation, that

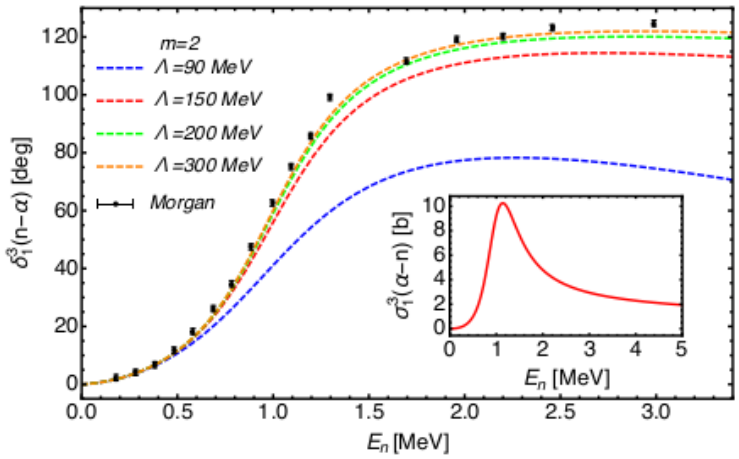

FIGURE 2.4: Phase shifts $\delta_{13}(E_n)(l = 1, J = 3/2)$ with experimental data from Morgan and Walter [49] and in the inset the cross-section $\sigma_{13}(E_n)$ obtained with $\Lambda = 300$ MeV. Figure from Ref. [47].

is a non-perturbative calculation. Therefore we apply the same non-perturbative approach to the calculation of the potential, in order to make the whole approach more consistent. Using, then, Eqs. (2.41) and the experimental values given in (2.21), we get again two sets of coupling constants. As in the previous case between these we choose those of natural values, therefore the c_{i-} set, Figure 2.5.

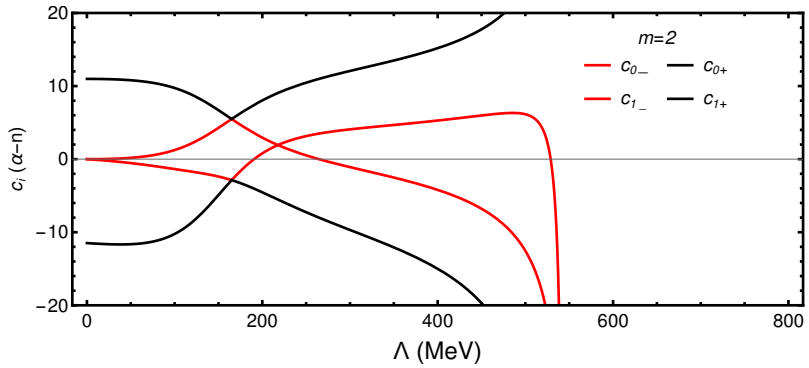

FIGURE 2.5: Coupling constant c_i for the αn interaction $S_{1/2}$ wave. Also in this case the set c_{i-} provides more natural values.

In Figure 2.6 the α-n $S_{\frac{1}{2}}$ phase shift is shown. As one can see the agreement with the experimental data is quite good within a range of energy that increasing the cutoff becomes wider and wider.

Unfortunately, the operation of resummation of the T-matrix creates bound states forbidden by the Pauli principle. For the Pauli principle, in fact, the nucleon can not occupy the state S since it is already occupied by other four nucleons. The potential obtained following this approach provides an αn bound state at about −13 MeV for most of the cutoff values greater than 150 MeV. This state, not being physical, must be projected out. In order to remove this pole we follow the method of Ref. [50],

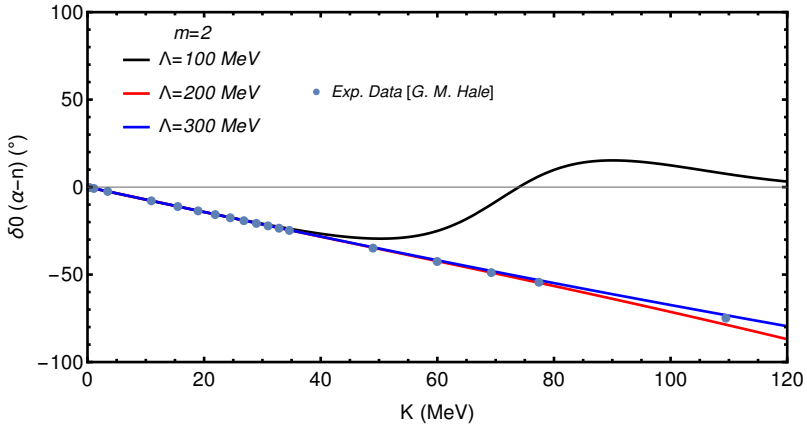

FIGURE 2.6: δ_0 α-n phase shift calculated for different cutoff values and experimental data. Here K is the relative momentum in the center of mass frame.

adding in the S-wave α-n potential the term

$$V(p,p') = \Gamma|\Phi(p)\rangle\langle\Phi(p')|\,, \tag{2.44}$$

where $\Phi(p)$ is the wave function of the forbidden state and Γ the projection parameter. Formally $\Gamma \to \infty$ but in practice Γ must be large enough such that the results for the three-body bound state and scattering, in the considered energy regime, become independent of it.

2.4.1 The presence of the Coulomb interaction

Now we proceed to the analysis of the case where a narrow resonance occurs between charged particles, for example the S-wave α-α interaction. In this case, the T-matrix form is more complicated due to the fact that the effect of the long-range Coulomb repulsion has to be considered. As a consequence, the T-matrix can be separated in two different contributions:

$$T = T_C + T_{SC} \tag{2.45}$$

where T_C is the one connected to the pure Coulomb interaction V_C, while T_{SC} is the one associated to the Coulomb-distorted short-range interaction; this latter term is the one we are interested in.

According to Ref. [17], the Coulomb-distorted S on-shell T-matrix can be written in effective range expansion at second order as

$$T_{SC}^{on} = -\frac{2\pi}{\mu_{\alpha\alpha}} \frac{C_\eta^2(k) e^{2i\sigma_0(k)}}{-\frac{1}{a_0} + \frac{1}{2} r_0 k^2 - 2k_C H(\eta)}\,, \tag{2.46}$$

being $\eta = k_C/k$, $k_C = 4\alpha\mu_{\alpha\alpha}$ and

$$C_\eta(k) = \sqrt{2\pi\eta/(e^{2\pi\eta}-1)}\,. \tag{2.47}$$

The parameter σ_l is the pure Coulomb scattering phase shift, defined by

$$e^{2i\sigma_l} = \frac{\Gamma(1+l+i\eta)}{\Gamma(1+l-i\eta)}\,, \tag{2.48}$$

where we have indicated with $\Gamma(z)$ the Gamma function, while

$$H(\eta) = Re[\Psi(1+i\eta)] + \frac{i}{2\eta}C_\eta^2 - ln(\eta) \tag{2.49}$$

is expressed in terms of the digamma function $\Psi(z) = (d/dz)ln\Gamma(z)$.
The Lippmann-Schwinger equation in this case turns out to be

$$T_{SC}(\boldsymbol{p},\boldsymbol{p}') = \langle\psi_{\boldsymbol{p}}^{(-)}|V_S|\psi_{\boldsymbol{p}'}^{(+)}\rangle - 2\mu_{\alpha\alpha}\int\frac{d\boldsymbol{p}''}{(2\pi)^3}\langle\psi_{\boldsymbol{p}}^{(-)}|V_S G_C^+|\psi_{\boldsymbol{p}''}^{(-)}\rangle\frac{T_{SC}(\boldsymbol{p}'',\boldsymbol{p}')}{p''^2-k^2+i\epsilon}\,, \tag{2.50}$$

being V_S our short-range interaction, $G_C^{(\pm)} = \frac{1}{E-H_0-V_C\pm i\epsilon}$ the Coulomb Green's function with H_0 the free Hamiltonian and $|\psi_{\mathbf{p}'}^{(\pm)}\rangle = |[1+G_C^{(\pm)}V_C]\mathbf{p}'\rangle$.

We recall that in the S-wave case the potential takes the form

$$V_0(p,p') = g(p)g(p')\sum_{i,j=0}^{1} p^{2i}\lambda_{ij}p'^{2j} \tag{2.51}$$

and knowing that $\psi_{\mathbf{p}}^{(-)} = e^{-2i\sigma_0(p)}\psi_{\mathbf{p}}^{(+)}$ one has

$$\langle\psi_{\mathbf{p}}^{(-)}|V_S|\psi_{\mathbf{p}'}^{(+)}\rangle = e^{2i\sigma_0(p)}\langle\psi_{\mathbf{p}}^{(+)}|V_S|\psi_{\mathbf{p}'}^{(+)}\rangle = \sum_{i,j=0}^{1}\lambda_{ij}X_{2i}(p)^*X_{2j}(p'), \tag{2.52}$$

with

$$X_{2j}(p) = \frac{1}{2\pi^2}\int_0^\infty dq q^{2j+2}\psi^+{}_p(q)g(q). \tag{2.53}$$

We use the following expression of Coulomb wave function in momentum space [51],

$$\psi_p^+(q) = \frac{4\pi C_\eta e^{i\sigma_0(q)}}{q(p^2-q^2)}\lim_{\gamma\to0^+}Im\left(\frac{q+p+i\gamma}{q-p+i\gamma}\right)^{i\eta}. \tag{2.54}$$

For the sake of simplicity it is useful to define the following quantities,

$$\gamma_0(p) = \tfrac{2}{\pi}\textstyle\int_0^\infty dq\frac{q}{p^2-q^2}\lim_{\gamma\to0^+}Im\left(\frac{q+p+i\gamma}{q+p+i\gamma}\right)^{i\eta}g(q), \tag{2.55}$$

$$\gamma_1(p) = \tfrac{2}{\pi}\textstyle\int_0^\infty dqq\lim_{\gamma\to0^+}Im\left(\frac{q+p+i\gamma}{q+p+i\gamma}\right)^{i\eta}g(q), \tag{2.56}$$

$$\gamma_2(p) = p^2\gamma_0(p), \tag{2.57}$$

thus we have,

$$X_0(p) = C_\eta e^{i\sigma_0(p)}\gamma_0(p), \tag{2.58}$$
$$X_2(p) = C_\eta e^{i\sigma_0(p)}(-\gamma_0(p) + \gamma_2(p)). \tag{2.59}$$

Inserting the definitions (2.55)-(2.59) in the expression of the potential (2.52) we get the T-matrix in the following matrix form,

$$T_{sc}(p,p') = e^{i\sigma_0(p)}C_\eta(p)\left[\sum_{ij=0}^{2}\tau_{ij}\gamma_i(p)\,\gamma_j(p')\right]C_\eta(p')e^{i\sigma_0(p')}, \tag{2.60}$$

and defining

$$\left\{v_{ij}\right\}_{ij=0,1,2} = \begin{pmatrix} \lambda_0 & -\lambda_1 & \lambda_1 \\ -\lambda_1 & 0 & 0 \\ \lambda_1 & 0 & 0 \end{pmatrix} = -\frac{\pi^2}{\mu}\begin{pmatrix} \tilde{\lambda}_0 & -\tilde{\lambda}_1 & \tilde{\lambda}_1 \\ -\tilde{\lambda}_1 & 0 & 0 \\ \tilde{\lambda}_1 & 0 & 0 \end{pmatrix}, \tag{2.61}$$

one obtains

$$\tau = \frac{v}{1 - v\Phi}, \tag{2.62}$$

with

$$\Phi_{a,b} = -\frac{\mu}{\pi^2}\int_0^\infty dq \frac{q^2}{q^2 - k^2 - i\epsilon}C_\eta^2(q)\gamma_a(q)\gamma_b(q). \tag{2.63}$$

At this point an expansion in powers of k^2/Λ^2 of T_{sc}^{on} can be performed.

In order to do this the only assumption we make is

$$\gamma_0(k) \sim \gamma_0(0)e^{\theta_0\frac{k^2}{\Lambda^2}} \sim \gamma_0(0)[1 + \theta_0\frac{k^2}{\Lambda^2}], \tag{2.64}$$
$$\gamma_1(k) \sim \gamma_1(0)e^{\theta_1\frac{k^2}{\Lambda^2}} \sim \gamma_1(0)[1 + \theta_1\frac{k^2}{\Lambda^2}], \tag{2.65}$$

where θ_0 and θ_1 are appropriate interpolating functions.

From the comparison term to term of this expansion with Eq. (2.46), one gets the equations for $\tilde{\lambda_0}$ and $\tilde{\lambda_1}$

$$\tilde{\lambda}_0 = \tilde{\lambda}_1^2\left(\frac{A^2}{I_1 - \frac{\pi}{2a_0}g_0(0)^2} - 2\frac{g_0(0)}{g_1(0)}A - I_5 + 2J_3 - s_1\right), \tag{2.66}$$
$$\tilde{\lambda}_1 = \frac{1}{I_3 - u_1 - A},$$

with

$$\begin{aligned} I_{2n+1} &= \int_0^\infty dq q^{2n}C_\eta^2(q)\gamma_0^2(q), \\ u_n &= \int_0^\infty dq q^{n-1}\left[\frac{\gamma_1(q)}{\gamma_0(q)} - \frac{\gamma_1(0)}{\gamma_0(0)}\right]\gamma_0^2(q)C_\eta(q)^2, \\ J_3 &= \int_0^\infty dq q^{2n}C_\eta^2\gamma_0(q)\gamma_1(q), \\ s_n &= \int_0^\infty dq q^{n-1}\left[\frac{\gamma_1(q)^2}{\gamma_0(q)^2} - \frac{\gamma_1(0)^2}{\gamma_0(0)^2}\right]\gamma_0^2(q)C_\eta(q)^2, \\ g_n(q) &= \int_0^\infty dq q^{n-1}\left[\gamma_1(q)^2 - \gamma_1(0)^2\right]C_\eta(q)^2, \end{aligned} \tag{2.67}$$

and the quantity A is calculated from the following equation,

$$\begin{aligned}&\{\tfrac{2\theta_0}{\Lambda^2}[I_1-\tfrac{\pi}{2a_0}\gamma_0^2]+g_{-1}+\tfrac{\pi}{4}r_0\gamma_0(0)^2-2\theta_0\tfrac{I_1}{\Lambda^2}\}A^2\\ +&\{2(u_{-1}-\tfrac{\theta_1-\theta_0}{\Lambda^2}I_1\tfrac{\gamma_1(0)}{\gamma_0(0)})[I_1-\tfrac{\pi}{2a_0}\gamma_0^2]-2(1-\tfrac{\theta_1-\theta_0}{\Lambda^2}\tfrac{\gamma_1(0)}{\gamma_0(0)})[I_1-\tfrac{\pi}{2a_0}\gamma_0^2]^2\}A\\ &-(2u_1-I_3+\tfrac{2\gamma_1}{\gamma_0(0)}u_{-1}-s_{-1})=0\,.\end{aligned}\tag{2.68}$$

Being Eq. (2.66) a second degree equation, there are again two distinct solutions for λ_0 and λ_1. One gives a negative λ_0 value, the other one positive.

Let us now take the explicit case of the S_0 wave for the α-α interaction with [9],

$$a_{0\alpha\alpha}=-1920\,\text{fm}\qquad r_{0\alpha\alpha}=1.099\,\text{fm}\,.$$

In Figure 2.7 the two sets of coupling constant λ_i in function of Λ is shown while in Figure 2.8 one can see the phase shifts, calculated with both solutions, compared with the experimental data. It is interesting to note that the agreement with the

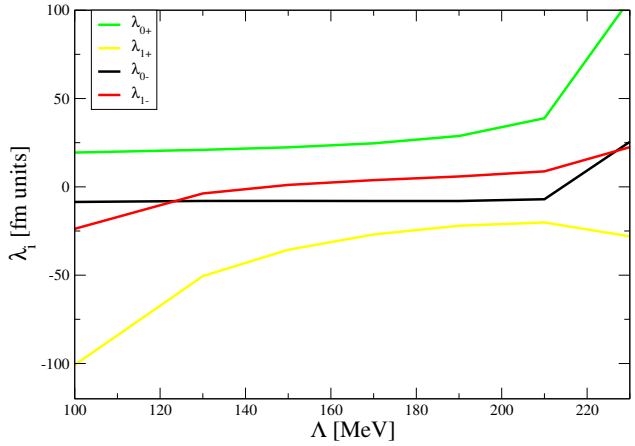

FIGURE 2.7: Values of the two pairs of coupling constant in function of the cutoff Λ. We indicate with + (−) symbol the solution which provides a positive (negative) λ_0 value.

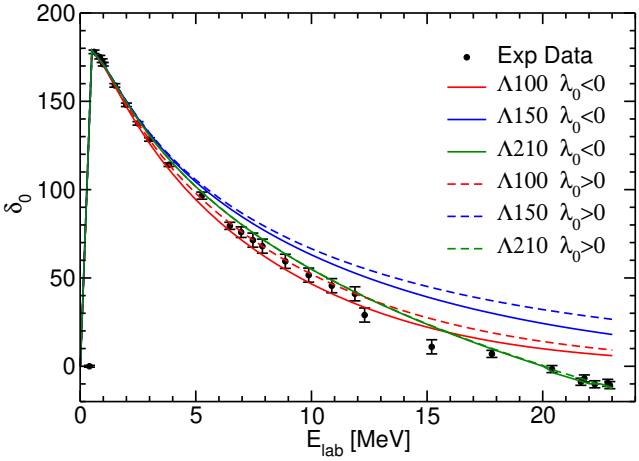

FIGURE 2.8: Comparison between the calculated α-α $l=0$ phase shift and experimental data [9] for different cutoff values Λ.

experimental data is quite good even at rather high energies.

In Figure 2.9 we show our results for the α-α phase shift with a cutoff of 100 MeV in comparison with experimental data and with another theoretical approach, where a different halo EFT expansion has been employed [17].

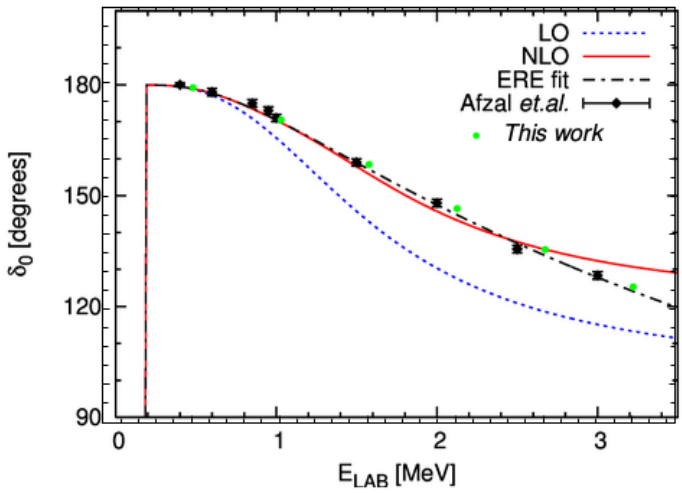

FIGURE 2.9: α-α scattering phase shift δ_0 ($l = 0, j = 0$) with cutoff $\Lambda = 100$ MeV [43] in comparison with experimental data from Azfal et al. [9] and with another Halo EFT calculation [17] in lowest order (LO) and Next-to-leading order (NLO). We also show the fit to the experimental data (ERE fit).

There, a T-matrix expansion in power of k_R/k_c is performed, with $k_R = \sqrt{\mu\alpha E_R} \sim 20\,\text{MeV}$. In our expansion in power of k/Λ the momentum k can be either close to k_R or of the same size of k_C. For this reason the phase shift obtained can describe the experimental data in the whole considered energy range, whereas the results of [17] have a less realistic energy behaviour beyond 2.5 MeV.

2.5 Power Counting

An essential feature required for an EFT approach is the power counting.

For the α-n case, from a physical interpretation one would expect that the two scales are given by $M_{lo} = \sqrt{2\mu_{\alpha n} Q_{\alpha decay}(^5\mathrm{He})} \approx 30\,\mathrm{MeV}$, $M_{hi} = \sqrt{2\mu_{\alpha n} S_p(^4\mathrm{He})} \approx 170\,\mathrm{MeV}$ [43]. The chosen power counting should also reproduce the known P-wave resonance of the system at low energy $\sim M_{lo}$, therefore we need to keep the scattering length term $\frac{1}{a_1}$ and the effective range r_1 to be of the same order of M_{lo} to guarantee a resonance pole in the T-matrix. We adopt the following power counting [52]

$$\frac{1}{a_0} \sim M_{hi}\,, \quad r_0 \sim 1/M_{hi}\,, \tag{2.69}$$

$$\frac{1}{a_1} \sim M_{lo}^2 M_{hi}\,, \quad r_1 \sim M_{hi}, \tag{2.70}$$

Hence, using experimental values for a_1 and r_1, we get $M_{lo} \approx 50$ MeV and $M_{hi} \approx 170$ MeV while for a_0 and r_0, we get $M_{hi} \approx 180$ MeV.[2]

In the $\alpha\alpha$ case we have three different scales of interest $M_{lo} = \sqrt{2\mu_{\alpha\alpha} Q_{\alpha decay}(^8\mathrm{Be})} \approx 20$ MeV, $M_{hi} = \sqrt{2\mu_{\alpha\alpha} S_p(^4\mathrm{He})} \approx 260\,\mathrm{MeV}$ and the Coulomb one $k_C = 4\alpha\mu_{\alpha\alpha}$. In a similar way to the previous case, but with the following power counting

$$a_0 \sim \frac{M_{hi}^2}{M_{lo}^3}\,, \quad r_0 \sim \frac{1}{3k_C} \sim \frac{1}{M_{hi}}, \tag{2.71}$$

using again the experimental values we obtain $M_{lo} \approx 20$ MeV and $M_{hi} \approx 170$ MeV.

With the adopted power counting in the α-n interaction the scattering length a_1 and the effective range r_1 contribute to the leading order (LO), there are a_0, r_0 contributions at the next-to-leading order (NLO) and the shape parameter P_1 is next-to-next-to leading order (N2LO). In the α-α interaction a_0 and r_0 give contribution to the LO, there are no contributions at the NLO and the shape parameter P_0 is of a higher order. Therefore, we perform an EFT expansion up to NLO with a precision given in the αn case by $O\left(M_{lo,\alpha n}^2/M_{hi,\alpha n}^2\right) \sim 0.09$ where $M_{hi} = min\{M_{hi,l=0}, M_{hi,l=1}\}$. In the $\alpha\alpha$ one has $O\left(M_{lo,\alpha\alpha}^2/M_{hi,\alpha\alpha}^2\right) \sim 0.01$. Moreover in order to evaluate the range of validity of our EFT, we should also consider the breakdown scale of the $\alpha\alpha n$ system. Since we consider a three-body problem we have to take the strictest constraint $M_{hi} = min\{M_{hi,\alpha n}, M_{hi,\alpha\alpha}\} = 170$ MeV.

[2] We find for M_{hi} the scales 80 MeV from a_0, 280 MeV from r_0. The average of the two values gives $M_{hi} \approx 180$ MeV.

2.6 The Wigner bound

An interesting aspect of short range interactions is the existence of a Wigner bound [53]. Long ago, assuming only causality and unitarity, Wigner proved that if a potential vanishes beyond range R then the rate at which phase shifts can vary with energy is bounded by

$$\frac{d\delta(k)}{dk} \geq -R + \frac{1}{2k}\sin(2\delta(k) + 2kR) \tag{2.72}$$

this translates into an upper limit on the effective range, which, for instance, in the S-wave case reads

$$r_0 \leq 2\left[R - \frac{R^2}{a} + \frac{R^3}{3a^2}\right], \tag{2.73}$$

while in the P-wave case

$$r_1 \lesssim -\frac{1}{2R}. \tag{2.74}$$

From these general results it is clear that the effective range was found to be negative in the EFT calculation when the cutoff Λ was removed [54]. When a cutoff is employed in order to regulate an Hamiltonian, the latter satisfies all physical principles and therefore it is a physical theory with the cutoff identified with the range; i.e. $\Lambda \sim 1/R$. In the limit $\Lambda \to \infty$ attempting to produce a positive effective range using zero-range potentials is impossible. As a result of Wigner bound, there is no EFT scattering analysis with only contact interactions in which the cutoff can be removed from the problem. One might think that including explicit pions in the EFT will improve the situation. Indeed, the Wigner bound has been proven to be a general property of contact interactions that is still true in the presence of pions [55].

In our case, the Wigner bound, Eqs. (2.73) and (2.74), translates in an explicit constraint on the parameter determining the range of our EFT potential, namely the cutoff Λ. Using in fact for each interaction the equations that relate r_l to Λ and imposing the correct sign of the experimental value of r_l, a Λ limit is obtained. One must have $\Lambda_{l=0,an} < 843$ MeV, $\Lambda_{l=1,an} < 340$ MeV and $\Lambda_{l=0,aa} < 230$ MeV.

2.7 A three-body interaction

The two-body potentials described in the previous Sections generate a rather significant cutoff dependence in the observables of three-body systems. This dependence can be interpreted as a lack of a three-body force in our EFT. Many-body forces are generally suppressed by power counting, but in some cases it is necessary to promote them to a lower order to have a cutoff-independent description of observables. Three-body force promotion at the LO is a feature present in the pionless EFT and its variants. A theory with only interactions of near-zero range exhibits a discrete scale invariance (DSI) [56] and the peculiarities of Efimovian physics occur [57]. Potentials that predict the same observables on the two-body system generate a sequence of shallow 3-body bound states called "Efimov states".

In our EFT we used implicit renormalization by maintaining finite values for the cutoff [44] and thus effectively introducing an energy scale, breaking the discrete scale invariance. Although with this procedure many features of Efimov physics are avoided, the system still exhibits a remanence of the DSI and the three-body observables turn out to be strictly dependent on the choice of two-body cutoff. To cure this dependence, the three-body force is typically promoted to the leading order. This is not the only way to proceed. An alternative approach would be to set the two-body cutoffs to a particular values that reproduces the experimental observables of the three-body system. This assumption seems to give physical meaning to the cutoff in the theory. On the other hand when an implicit renormalization is done keeping finite values for this parameter, it is not wrong to think that this introduced scale is somehow related to a physical energy scale. However, without a 3-body force at LO, the scale of the 3-body system would then be given only by the cutoff effect and is affected by considerable uncertainty.

For these reasons we insert in the theory a three-body force that at leading order is given by

$$\mathcal{L}^3_{int} = \lambda_{3\alpha\alpha n}\Psi^\dagger\Psi\Psi^\dagger\Psi n^\dagger n + \lambda_{3\alpha\alpha\alpha}\Psi^\dagger\Psi\Psi^\dagger\Psi\Psi^\dagger\Psi\,, \tag{2.75}$$

where $\lambda_3 = \frac{c_3}{\Lambda^5}$, from the above equation one obtains a momentum space potential as

$$V_3 = \lambda_3\, e^{-(p_{12}^2+p_{23}^2+p_{31}^2)/\Lambda^2} e^{-(p'^2_{12}+p'^2_{23}+p'^2_{31})/\Lambda^2}\,, \tag{2.76}$$

where p_{ij} are the relative momenta.

In this case the LECs will be determined for each cutoff value by the physical quantities of the three-body systems. It is interesting to note that in the three-body force case the cutoff is not limited by any constraint.

Chapter 3

Calculation of the ground state: The HH Method

After describing the EFT interactions between particles, hence our Hamiltonian, in this Chapter we show the method used to calculate the ground states of the studied nuclei. Our aim is to solve the Schrödinger equation in order to find the binding energy and the wave function of the considered nuclei. To do this we expand the wave function on a proper basis and we use the Rayleigh-Ritz variational principle, to find the coefficients of the expansion, $\delta \langle \Psi | H - E | \Psi \rangle = 0$. This reduces the search for the coefficients to an eigenvalue problem. We use the Lanczos algorithm [58], see Appendix B for the details, in order to calculate the lowest eigenvalues and eigenvectors of the Hamiltonian matrix. Here, the formalism which is required in order to define this approach in a proper way is shown. As first step, we introduce the set of coordinates. In Section 3.1, we present the Jacobi coordinates and in Section 3.2 how they can be transformed into hyperspherical coordinates. In Section 3.3, we illustrate the characteristics of the complete HH basis. Since the potentials are born in momentum space, we discuss how the HH expansion is performed in this space, Section 3.4. In Section 3.5 the NSHH method, which avoids the symmetrization of the HH basis elements using the Casimir operator, is presented. Finally, in Section 3.6 we calculate the expansion of our EFT Hamiltonian on the NSHH basis. This Chapter is mainly inspired by Refs. [59, 60, 61].

3.1 Jacobi coordinates

The first step in order to construct the hyperspherical basis and, subsequently, the HH functions, is given by the Jacobi coordinates.

The use of this type of coordinate system allows us to obtain a translation invariant picture of an $\mathcal{N}$-particle system, separating the relative motion of the particles from the center-of-mass one. In a system of $\mathcal{N}$ particles, where $\boldsymbol{r}_i$ and m_i are the Cartesian position and the mass of the i-th particle respectively, we introduce the

mass-weighted Jacobi coordinates by adopting the so-called reversed order convention [62],

$$\boldsymbol{\eta}_{\mathcal{N}-i} = \sqrt{\frac{m_{i+1}M_i}{mM_{i+1}}}\left(\boldsymbol{r}_{i+1} - \frac{1}{M_i}\sum_{j=1}^{i} m_j \boldsymbol{r}_j\right), \tag{3.1}$$

where $i = 1, .., N$, $N = \mathcal{N} - 1$, the constant m is a reference unit mass (in our case it is the nucleon mass) and

$$M_i = \sum_{j=1}^{i} m_j. \tag{3.2}$$

As one can see the choice of Jacobi coordinates is not unique. These are order dependent, which means that changing the order, mass parameters and coupling sequence between each of the $\mathcal{N}$ particles results in a completely different set of coordinates. However, as shown later in Section 3.5, it is always possible to pass from one set of Jacobi coordinates to another with different ordering and parameters, by means of suitable transformations.

From the above expressions it is evident that each $\boldsymbol{\eta}_{\mathcal{N}-i}$ vector (for $i > 1$) represents the $(i+1)$-th particle position with respect to the center of mass of the first i particles. In particular, the last Jacobi coordinate, $\boldsymbol{\eta}_N$, is directly proportional to the relative distance between the first two particles

$$\boldsymbol{\eta}_N = \sqrt{\frac{m_1 m_2}{mM_2}}(\boldsymbol{r}_2 - \boldsymbol{r}_1). \tag{3.3}$$

In the reversed order convention then $\boldsymbol{\eta}_0$ represents the rescaled CM coordinate

$$\boldsymbol{\eta}_0 = \sqrt{\frac{M_{\mathcal{N}}}{m}}\boldsymbol{R}_{cm} = \frac{1}{\sqrt{mM_{\mathcal{N}}}}\sum_i m_i \boldsymbol{r}_i. \tag{3.4}$$

We can define the transformation between the Cartesian and Jacobian bases using the following matrix $\mathcal{T}$

$$\mathcal{T} = \begin{pmatrix} -\sqrt{\frac{m_2}{m_1 M_2}} & \sqrt{\frac{m_1}{m_2 M_2}} & 0 & \cdots & 0 \\ -\sqrt{\frac{m_3}{M_2 M_3}} & -\sqrt{\frac{m_3}{M_2 M_3}} & \sqrt{\frac{M_2}{m_3 M_3}} & \cdots & 0 \\ -\sqrt{\frac{m_4}{M_3 M_4}} & -\sqrt{\frac{m_4}{M_3 M_4}} & -\sqrt{\frac{m_4}{M_3 M_4}} & \cdots & 0 \\ \vdots & \vdots & \vdots & \ddots & \vdots \\ \sqrt{\frac{1}{M_{\mathcal{N}}}} & \sqrt{\frac{1}{M_{\mathcal{N}}}} & \sqrt{\frac{1}{M_{\mathcal{N}}}} & \cdots & \sqrt{\frac{1}{M_{\mathcal{N}}}} \end{pmatrix} \cdot \mathcal{M}, \tag{3.5}$$

where $\mathcal{M}_{ij} = \sqrt{m_i}\delta_{ij}$. Then one can verify the following properties

$$\mathcal{T}^T \cdot \mathcal{T} = \mathbf{I} \qquad \det(\mathcal{T}) = 1, \tag{3.6}$$

thus $\mathcal{T}$ belongs to the $SO(N)$ group.

Given a vector $\boldsymbol{v}_r$ defined in the Cartesian basis and the same vector $\boldsymbol{v}_\eta$ defined in the Jacobian one, we have the following relation

$$\boldsymbol{v}_r = \frac{1}{\sqrt{m}} \mathcal{M} \cdot \mathcal{T}^T \cdot \boldsymbol{v}_\eta. \tag{3.7}$$

The relation between volume elements is

$$dV_\eta = \prod_{i=1}^{N} d\boldsymbol{\eta}_i = \prod_{i=1}^{N} \sqrt{\frac{m_i}{m}} d\boldsymbol{r}_i = \Big(\prod_{i=1}^{N} \sqrt{\frac{m_i}{m}} \Big) dV_r. \tag{3.8}$$

From Eq. (3.7) one can then easily express the Cartesian kinetic operator in the Jacobi version

$$\begin{aligned} T = -\sum_{i=1}^{\mathcal{N}} \frac{\hbar^2}{2m_i} \Delta_{r_i} &= -\frac{\hbar^2}{2} \nabla_r^T \cdot (\mathcal{M}^{-1})^2 \cdot \nabla_r \\ &= -\frac{\hbar^2}{2m} \nabla_\eta^T S \cdot \mathcal{M} \cdot (\mathcal{M}^{-1})^2 \cdot \mathcal{M} \cdot S^T \cdot \nabla_\eta \\ &= -\frac{\hbar^2}{2m} \sum_{i=0}^{N} \Delta_{\eta_i}, \end{aligned} \tag{3.9}$$

where $\nabla_r^T = (\nabla_{r_1}^T, \nabla_{r_2}^T, \cdots)$ and ∇_η^T has an analogous definition.

3.2 Hyperspherical coordinates

Once a set of Jacobi coordinates is chosen, every single vector $\boldsymbol{\eta_k}$ needs to be expressed in spherical coordinates. For each $\boldsymbol{\eta_k}$ one has one radial coordinate η_k and two angular coordinates $\hat{\eta}_k = (\theta_k, \varphi_k)$. Let us first consider the case of two Jacobi radial coordinates, η_1 and η_2. We can parametrize them, using the hyperradial coordinate ρ_2 and the hyperradial angle Φ_2, in polar coordinates

$$\begin{cases} \eta_1 = \rho_2 \cos \Phi_2, \\ \eta_2 = \rho_2 \sin \Phi_2. \end{cases} \tag{3.10}$$

Adding another angle and with a different hyperradius ρ_3 we can describe three Jacobi radial coordinates using the following spherical parametrization

$$\begin{cases} \eta_1 = \rho_3 \cos \Phi_3 \cos \Phi_2, \\ \eta_2 = \rho_3 \cos \Phi_3 \sin \Phi_2, \\ \eta_3 = \rho_3 \sin \Phi_3. \end{cases} \tag{3.11}$$

We can end up with $N-1$ angles, in order to describe N η_i radial coordinates

$$\begin{cases} \eta_1 = \rho_N \cos\Phi_N ... \cos\Phi_3 \cos\Phi_2, \\ \eta_2 = \rho_N \cos\Phi_N ... \cos\Phi_3 \sin\Phi_2, \\ \vdots \\ \eta_i = \rho_N \cos\Phi_N ... \cos\Phi_{i+1} \sin\Phi_i, \\ \vdots \\ \eta_{N-1} = \rho_N \cos\Phi_N \sin\Phi_{N-1}, \\ \eta_N = \rho_N \sin\Phi_N. \end{cases} \tag{3.12}$$

Therefore we can determined N different radial coordinates using a S_+^{N-1} hypersphere in $\mathbf{R}^N$. We can invert the previous definitions and define the hyperradius ρ and every hyperangle Φ_i with the radial Jacobi coordinates

$$\begin{cases} \sin\Phi_N = \eta_N/\rho_N \\ \cos\Phi_N = \rho_{N-1}/\rho_N \end{cases} \Rightarrow \begin{cases} \rho_N^2 = \rho_{N-1}^2 + \eta_N^2 = \sum_{j=1}^N \eta_j^2 \\ \sin\Phi_i = \frac{\eta_i}{\sqrt{\eta_1^2+...+\eta_i^2}} \end{cases} . \tag{3.13}$$

Note that the hyperradial coordinate $\rho = \rho_N$ is symmetric with respect to permutations of the particles. With these formulae then the $3N = 3(\mathcal{N}-1)$ internal coordinates for an $\mathcal{N}$-particle system can be expressed by an hyperradial coordinate ρ and $3N-1 = 3A-4$ hyperangular coordinates $\Omega_{(N)}=\{\hat{\eta}_1, \hat{\eta}_2,.., \hat{\eta}_N, \Phi_2,.., \Phi_N\}=\{\Omega_1, \Omega_2, .., \Omega_N, \Phi_2,..,\Phi_N\}$, with the hyperangles Φ_N varying in the range $0 \le \Phi_N \le \frac{\pi}{2}$.

Summarizing, we have developed the following parametrization:

$$\boldsymbol{\eta}(\rho, \Omega_{(N)}) : \mathbf{R}^{3N} \to \mathbf{R}_+ \times S_+^{N-1} \times (S^2)^N. \tag{3.14}$$

We can then define the hyperradial volume element as

$$\begin{aligned} dV_{3N} &= \rho^{3N-1} d\rho dS_{3N-1} = \\ &= \rho^{3N-1} d\rho \sin^2(\Phi_N) \cos^{3N-4}\Phi_N d\Phi_N d\Omega_N dS_{3N-4} \\ &= \rho^{3N-1} d\rho \sin\theta_1 d\theta_1 d\varphi_1 \prod_{i=2}^{N} \sin\theta_i d\theta_i d\varphi_i (\sin\Phi_i)^2 (\cos\Phi_i)^{3i-4} d\Phi_i , \end{aligned} \tag{3.15}$$

where dS_{3N-1} is the volume element associated with the $3N-1$ dimensional hypersphere and $d\Omega_N$ is the volume associated with the angular part of the Nth Jacobi coordinate $\boldsymbol{\eta}_N$. As for the Jacobi coordinates also in the hyperspherical case we can choose among several different sets of coordinates. A powerful tool in representing the variety of such sets is given by the tree diagram, first introduced by N. Ya. Vilenkin et al. in [63]. In Figure 3.1 the set of Eq. (3.12) is schematized.

Each hyperangle Φ_i is related to the i-th node: if the segment joining this node with the upper one extends to the right, a factor equal to $\sin\Phi_i$ is associated, otherwise $\cos\Phi_i$. Each η_i is obtained by the product of ρ with each sine or cosine factor

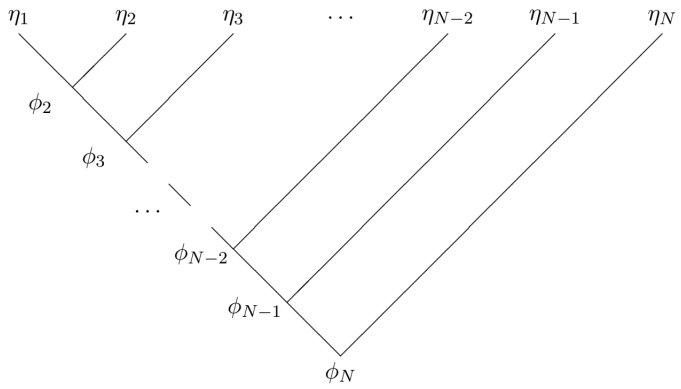

FIGURE 3.1: Tree diagram representing the standard scheme of hyperangular coordinates. The explicit relations are shown in Eq. (3.12). Figure from Ref. [61].

associated to each node starting from the lowest vertex and following the path to the η_i termination.

3.3 Hyperspherical harmonic functions

As well as the hyperspherical coordinates are a generalization of the spherical coordinates for a $\mathcal{N}$-body system, the hyperspherical harmonic functions are a generalization of the spherical harmonic functions. For $\mathcal{N} = 2$ these are eigenfunctions of the angular momentum operator contained in the relative kinetic energy operator. Therefore, in order to generate the HH for $\mathcal{N} > 2$, we need a generalization of the Laplace operator in terms of the hyperradius $\rho = \rho_N$ and the hyperangle Φ_N. This results in [64]

$$\Delta_{(N)} = \Delta_{\rho_N} - \frac{1}{\rho_N^2}\hat{K}_N^2\,, \tag{3.16}$$

where the hyperradial part is

$$\Delta_{\rho_N} = \frac{\partial^2}{\partial\rho_N^2} + \frac{3N-1}{\rho_N^2}\frac{\partial}{\partial\rho_N} = \frac{1}{\rho_N^{3N-1}}\frac{\partial}{\partial\rho_N}\rho_N^{3N-1}\frac{\partial}{\partial\rho_N}. \tag{3.17}$$

The hyperspherical or grand angular momentum operator $\hat{K}_n^2$, $n = 2, ..., N$, can then be expressed in terms of the squared angular momentum associated to the n-th Jacobi coordinate, $\hat{l}_n^2$, and $\hat{K}_{n-1}^2$ as

$$\hat{K}_n^2 = -\frac{\partial^2}{\partial\phi_n^2} - \frac{3n-6-(3n-2)\cos(2\phi_n)}{\sin(2\phi_n)}\frac{\partial}{\partial\phi_n} + \frac{1}{\cos^2\phi_n}\hat{K}_{n-1}^2 + \frac{1}{\sin^2\phi_n}\hat{l}_n^2, \tag{3.18}$$

where we define $\hat{K}_1^2 = \hat{l}_1^2$ and the internal n particle angular momentum operator as $\hat{L}_n = \hat{L}_{n-1} + \hat{l}_n$. The operators $\hat{K}_N^2, \hat{K}_{N-1}^2, \ldots, \hat{K}_2^2$, $\hat{L}_N, \hat{L}_{N-1}, \ldots, \hat{L}_2, \hat{M}_{N_z}$ and

$\hat{l}_N, \hat{l}_{N-1}, \ldots, \hat{l}_2, \hat{l}_1$ commute each other giving us the possibility of labelling each hyperspherical state with a complete set of quantum numbers indicated as $[K]$. We define the hyperspherical harmonics $\mathcal{Y}_{[K]}$ as the eigenstates of the grandangular momentum operator

$$\hat{K}_N^2 \mathcal{Y}_{[K]} = K(K+3N-2)\mathcal{Y}_{[K]}. \tag{3.19}$$

The explicit form of the hyperspherical harmonics in terms of the spherical harmonics $Y_{lm}(\theta,\phi)$ and of the Jacobi polynomials $P_\mu^{(a,b)}(z)$ is

$$\begin{aligned}
\mathcal{Y}_{[K]}(\Omega_N) &= \prod_{j=1}^{N} Y_{l_j m_j}(\theta_j,\phi_j) \\
&\times \sum_{m_1,\ldots,m_N} \langle l_1 m_1 l_2 m_2 | L_2 M_2\rangle \ldots \langle L_{N-1} M_{N-1} l_N m_N | L_N M_N\rangle \\
&\times \prod_{j=1}^{N} \mathcal{N}(K_j; l_j, K_{j-1}) (sin\alpha_j)^{l_j} (cos\alpha_j)^{K_{j-1}} P_{\mu_j}^{[l_j+1/2],[K_{j-1}+(3j-5)/2]}(cos(2\alpha_j)),
\end{aligned} \tag{3.20}$$

where l_i and m_i correspond to the angular momentum and its projection associated to the i-th Jacobi coordinate while L_i and M_i are the total angular momentum and its projection, respectively. The latter results from the composition of all the angular momenta from the first one to the i-th coordinate one. In addition, the normalization constant is given by

$$\mathcal{N}_j(K_j; l_j, K_{j-1}) = \sqrt{\frac{(2K_j+3j-2)\mu_j!\Gamma(\mu_j+K_{j-1}+l_j+(3j-2)/2)}{\Gamma(\mu_j+l_j+3/2)\Gamma(\mu_j+K_{j-1}+(3j-3)/2)}}, \tag{3.21}$$

where μ_j is a positive integer and $K_j = K_{j-1} + 2\mu_j + l_j$. We observe that the hyperspherical harmonics are characterised by $3N-1$ quantum numbers:

$$[K] = (l_1, ..., l_N, L_2, ..., L_N, M_N, K_2, ...K_N). \tag{3.22}$$

3.3.1 The complete basis

It is relevant to point out that the hyperspherical harmonics alone do not represent a complete basis set on which we can perform the expansion of the wave function under consideration. In fact, not only the hyperradial part is still missing but also the spin and isospin one. A basis function in this space is of the form

$$|\Phi_i\rangle = |\mathcal{R}_{r_i}\mathcal{Y}_{[K_N]_i}\rangle \otimes |\chi_{[S_\mathcal{N}]_i}\chi_{[T_\mathcal{N}]_i}\rangle\ , \tag{3.23}$$

where $\mathcal{R}_{r_i}$ are the hyperradial basis functions, $\chi_{[S_\mathcal{N}]_i}$ and $\chi_{[T_\mathcal{N}]_i}$ are the spin and isospin states. The hyperradial basis is chosen to be the generalized Laguerre polynomials $L_n^{(\nu)}(\rho/\beta)$ coupled with the appropriate weights

$$\mathcal{L}_n(\rho) = \left(\frac{1}{\beta}\right)^{\frac{3\mathcal{N}+5}{2}} \sqrt{\frac{n!}{(n+\nu)!}} L_n^{(\nu)}(\rho/\beta) e^{-\frac{\rho}{2\beta}} \left(\frac{\rho}{\beta}\right)^{\frac{\nu-3\mathcal{N}+4}{2}}\ , \tag{3.24}$$

where we take ν integer, β is a variational parameter with dimension of a length and n is an integer number $n \geq 0$. Choosing $\nu = 3N-1$ the hyperradial contribution to the volume element Eq. (3.15) in the basis functions is naturally included. By using the properties of the Laguerre polynomials we can analytically evaluate the kinetic radial matrix elements

$$\langle \mathcal{L}_n(r)| \nabla_\rho |\mathcal{L}_{n'}(r)\rangle = \frac{1}{4}\delta_{nn'} - \frac{3N-1+2n'}{2} R^{\nu;-1}_{n,n'} + (3N-\nu+2)\times \\ \times \left[n' R^{\nu;-2}_{n,n'} - \sqrt{n'(n'+\nu)} R^{\nu;-1}_{n,n'-1}\right], \tag{3.25}$$

with

$$\begin{aligned} R^{\nu;a}_{n,n'} &= \langle \mathcal{L}_n(r)| r^a |\mathcal{L}_{n'}(r)\rangle = \\ &= \sqrt{\frac{n!n'!}{(n+\nu)!(n'+\nu)!}} \int_0^\infty dr e^{-r} r^\nu L_n(r) L_{n'}(r) r^a = \\ &= \sqrt{\frac{n!(n+\nu)!}{n'!(n'+\nu)!}} \sum_{m=0}^{n} (-1)^m \frac{(\nu+a+m)!(-a-m)_{n'}}{(n-m)!(\nu+m)!m!}. \end{aligned} \tag{3.26}$$

The spin and the isospin basis were both defined on a reversed sequential coupling. By denoting as s_i and t_i, respectively, the spin and the isospin quantum numbers of the i-th particle, each spin and isospin state can be identified as

$$[S_\mathcal{N}] = s_\mathcal{N}, s_{\mathcal{N}-1}, ..., s_1; S_2, ..., S_{\mathcal{N}-1}, S_\mathcal{N} \tag{3.27}$$

$$[T_\mathcal{N}] = t_\mathcal{N}, t_{\mathcal{N}-1}, ..., t_1; T_2, ..., T_{\mathcal{N}-1}, T_\mathcal{N}; T_{\mathcal{N}_z}; \tag{3.28}$$

where S_i (T_i) is the total spin (isospin) quantum number of the system composed by particles from $\mathcal{N}$ to $\mathcal{N}-i+1$. $T_{\mathcal{N}_z}$ is the projection on the z axis of the total isospin $T_\mathcal{N}$. The isospin coupling scheme can be represented in the tree diagram as shown in Figure 3.2. In the case of a central force L_N and S_N are conserved, meaning

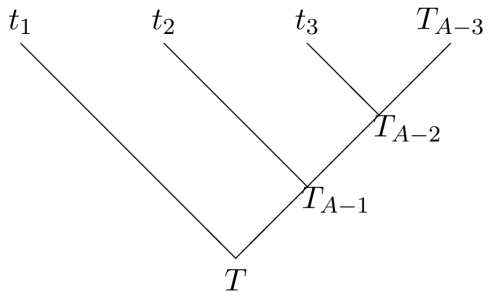

FIGURE 3.2: Tree diagram representing the sequential reversed-order $\mathcal{N}$-body isospin coupling [61].

that they are good quantum numbers for defining the eigenstates of $\hat{H}$. In the non-central case however S_N and L_N are not good quantum numbers anymore, and only the total angular momentum J, together with the isospin numbers $T_\mathcal{N}$ and $T_{\mathcal{N}_z}$, can

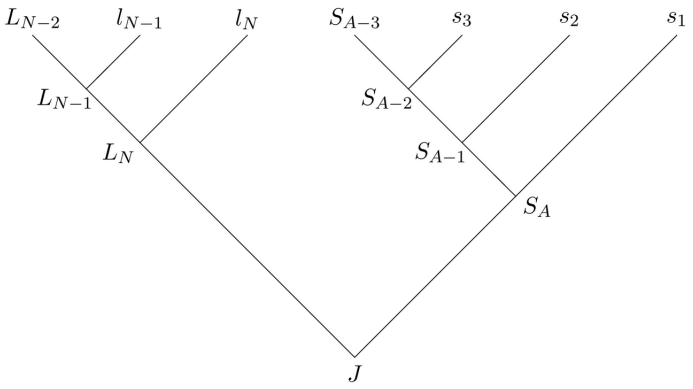

FIGURE 3.3: Tree diagram representing the coupling scheme between the orbital angular momentum L_N and the total spin $S_{\mathcal{N}}$ in a $\mathcal{N}$-body non-central basis [61].

be used to define the angular plus spin/isospin wave function, leading to a much bigger basis, Figure 3.3.

3.4 Momentum space

The α-α and α-n potentials analyzed in this Thesis are born in momentum space as they are calculated from a Lagrangian within an EFT. For this reason, this space represents the natural frame for our calculations. At this point, it becomes crucial to understand how to transfer the HH formalism in the aforementioned space. As there is a wide choice to mix the coordinates of real space in order to build a complete set of Jacobian coordinates, in principle the same freedom is also present in the momentum space. However, fixed a proper set of Jacobi coordinates $\boldsymbol{\eta}_i$ in coordinate space then the coordinates in momentum space $\boldsymbol{\pi}_i$ are defined as the conjugate variables through,

$$[\eta_i^\alpha, \pi_j^\beta] = i\hbar\delta_{\alpha\beta}\delta_{ij}, \tag{3.29}$$

where $i, j = 1, ..., N$ and $\alpha, \beta = x, y, z$.

For $\mathcal{N}$ body system we introduce the following coordinates

$$\begin{aligned}
\boldsymbol{\pi}_{\mathcal{N}-i} &= \sqrt{\frac{mM_i}{m_{i+1}M_{i+1}}}\left(\boldsymbol{p}_{i+1} - \frac{m_{i+1}}{M_i}\sum_{i=1}^{N}\boldsymbol{p}_i\right), \\
\boldsymbol{\pi}_0 &= \sqrt{\frac{m}{M_{\mathcal{N}}}}\sum_{i=0}^{N}\boldsymbol{p}_i\,,
\end{aligned} \tag{3.30}$$

where $N = \mathcal{N} - 1$, m is a reference unit mass and $M_i = \sum_{j=1}^{i} m_j$. The $\boldsymbol{\pi}_0$ coordinate is the rescaled center of mass momentum. As we can see, with this particular ordering the last Jacobi coordinate, $\boldsymbol{\pi}_N$, is directly proportional to the relative momentum

between the first two particles

$$\boldsymbol{\pi}_N = \sqrt{\frac{mM_2}{m_1 m_2}}\boldsymbol{p}_{12}, \tag{3.31}$$

with

$$\boldsymbol{p}_{12} = \frac{m_1\boldsymbol{p}_2 - m_2\boldsymbol{p}_1}{M_2} = \frac{m_1\boldsymbol{p}_2 - m_2\boldsymbol{p}_1}{m_1 + m_2}. \tag{3.32}$$

The Jacobian determinant for the transformation $(\boldsymbol{p}_1, \ldots, \boldsymbol{p}_\mathcal{N}) \to (\boldsymbol{\pi}_0, \boldsymbol{\pi}_1, \ldots, \boldsymbol{\pi}_N)$ is the opposite as the coordinate space one

$$\mathcal{J} = \prod_{i=1}^{\mathcal{N}} \sqrt{\frac{m}{m_i}}. \tag{3.33}$$

Explicitly the definitions (3.30) for $N = 2$, a three-body system, lead to the following result:

$$\begin{aligned}
\boldsymbol{\pi}_2 &= \sqrt{\frac{mM_2}{m_1 m_2}}\left(\frac{m_1\boldsymbol{p}_2 - m_2\boldsymbol{p}_1}{M_2}\right), \\
\boldsymbol{\pi}_1 &= \sqrt{\frac{mM_2}{m_3 M_3}}\left(\boldsymbol{p}_3 - \frac{m_3}{M_2}(\boldsymbol{p}_1 + \boldsymbol{p}_2)\right), \\
\boldsymbol{\pi}_0 &= \sqrt{\frac{m}{M_3}}(\boldsymbol{p}_1 + \boldsymbol{p}_2 + \boldsymbol{p}_3),
\end{aligned} \tag{3.34}$$

and the inverse relations read,

$$\begin{aligned}
\boldsymbol{p}_1 &= \sqrt{\frac{m_1}{m}}\left(\sqrt{\frac{m_1}{M_3}}\boldsymbol{\pi}_0 - \sqrt{\frac{m_1 m_3}{M_3 M_2}}\boldsymbol{\pi}_1 - \sqrt{\frac{m_2}{M_2}}\boldsymbol{\pi}_2\right) \\
\boldsymbol{p}_2 &= \sqrt{\frac{m_2}{m}}\left(\sqrt{\frac{m_2}{M_3}}\boldsymbol{\pi}_0 - \sqrt{\frac{m_2 m_3}{M_3 M_2}}\boldsymbol{\pi}_1 + \sqrt{\frac{m_1}{M_2}}\boldsymbol{\pi}_2\right) \\
\boldsymbol{p}_3 &= \sqrt{\frac{m_3}{m}}\left(\sqrt{\frac{m_3}{M_3}}\boldsymbol{\pi}_0 + \sqrt{\frac{M_2}{M_3}}\boldsymbol{\pi}_1\right).
\end{aligned} \tag{3.35}$$

Once the Jacobi coordinates are determined, the transformation to the hyperspherical coordinate system can be carried out following the same procedure for the coordinate space case.

The N hyperspherical coordinates in the momentum space are

$$\begin{cases} \pi_1 = Q_N \cos\Phi_N ... \cos\Phi_3 \cos\Phi_2, \\ \pi_2 = Q_N \cos\Phi_N ... \cos\Phi_3 \sin\Phi_2, \\ \vdots \\ \pi_i = Q_N \cos\Phi_N ... \cos\Phi_{i+1} \sin\Phi_i, \\ \vdots \\ \pi_{N-1} = Q_N \cos\Phi_N \sin\Phi_{N-1}, \\ \pi_N = Q_N \sin\Phi_N \end{cases} \tag{3.36}$$

defining the hyperradius Q and every single hyperangle Φ_i as

$$\begin{cases} \sin\Phi_N = \pi_N/Q_N \\ \cos\Phi_N = \pi_{N-1}/Q_N \end{cases} \Rightarrow \begin{cases} Q_N^2 = Q_{N-1}^2 + \pi_N^2 = \sum_{j=1}^{N} \pi_j^2 \\ \sin\Phi_i = \frac{\pi_i}{\sqrt{\pi_1^2+...+\pi_i^2}} \end{cases} . \tag{3.37}$$

The volume element can be written as

$$\begin{aligned} dV_{3N} &= Q^{3N-1} dQ dS_{3N-1} = \\ &= Q^{3N-1} dQ \sin^2(\Phi_N) \cos^{3N-4}\Phi_N d\Phi_N d\Omega_N dS_{3N-4} \\ &= Q^{3N-1} dQ \sin\theta_1 d\theta_1 d\varphi_1 \prod_{i=2}^{N} \sin\theta_i d\theta_i d\varphi_i (\sin\Phi_i)^2 (\cos\Phi_i)^{3i-4} d\Phi_i , \end{aligned} \tag{3.38}$$

where dS_{3N-1} is the volume element associated with the $3N-1$ dimensional hypersphere and $d\Omega_N$ is the volume associated with the angular part of the Nth Jacobi coordinate $\boldsymbol{\pi}_N$. The only significant difference between the coordinate and momentum spaces is in the kinetic energy operator construction. While the internal kinetic energy of the system in real space is calculated using the hyperlaplacian, the derivation of the internal kinetic energy in momentum space is much simpler. The total kinetic energy is

$$T_{total} = \sum_{i=1}^{\mathcal{N}} \frac{p_i^2}{2m_i}, \tag{3.39}$$

that can be written in Jacobian coordinates in the following compact form

$$T_{total} = \frac{\sum_{i=0}^{N} \pi_i^2}{2m}. \tag{3.40}$$

The internal kinetic energy is defined as

$$T_{int} = T_{total} - T_{CM} = T_{total} - \frac{P_{CM}^2}{2M_{\mathcal{N}}} = T_{total} - \frac{(\sum_{i=1}^{\mathcal{N}} p_i)^2}{2M_{\mathcal{N}}}, \tag{3.41}$$

inserting Eq. (3.30) and (3.40) in this definition, one gets

$$T_{int} = \frac{\sum_{i=1}^{N} \pi_i^2}{2m}. \tag{3.42}$$

Remembering then the definition of hypermomentum Q

$$Q = \sqrt{\sum_{i=1}^{N} \boldsymbol{\pi}_i^2}, \tag{3.43}$$

one simply obtains

$$T_{int} = \frac{Q^2}{2m}. \tag{3.44}$$

At this point one can introduce the complete basis in the momentum space.

A significant advantage of the HH formalism consists in the fact that the hyperangular part of the basis remains unaltered moving from coordinate to momentum space. In fact, it is possible to show that $\mathcal{Y}_{[K]}(\Omega_r) \xrightarrow[FT]{} \mathcal{Y}_{[K]}(\Omega_p)$ [65]. With regard to the hyperradial part of the basis, we can choose to work again with the Laguerre polynomials basis functions rewritten in terms of the hypermomentum Q. Therefore we can define our basis wave function Ψ as a product of a purely hypermomentum function, a purely hyperangular one and the spin and isospin states,

$$\Psi_{[n]}(\boldsymbol{\pi}_1, ..., \boldsymbol{\pi}_N) = \Psi_{[n]}(Q, \Omega_{(N)}) = g_n(Q)\mathcal{Y}_{[K_n]}(\Omega_{(N)}) \otimes |\chi_{[S_\mathcal{N}]_i}\chi_{[T_\mathcal{N}]_i}\rangle\,, \tag{3.45}$$

with $\chi_{[S_\mathcal{N}]_i}$($\chi_{[T_\mathcal{N}]_i}$) the spin (isospin) states, $g_n(Q)$ defined as

$$g_n(Q) = \left(\frac{1}{\beta}\right)^{\frac{3N}{2}} \sqrt{\frac{n!}{(n+\nu)!}} \left(\frac{Q}{\beta}\right)^{\frac{\nu}{2}-\frac{3N-1}{2}} e^{-\frac{Q}{2\beta}} L_n^\nu\left(\frac{Q}{\beta}\right) \tag{3.46}$$

and $\mathcal{Y}_{[K_n]}(\Omega_{(N)})$ the hyperspherical harmonic of the full system, with set of hyperangular quantum numbers $[K_N]$, given in Eq. (3.20).

3.5 The Symmetrized and the Non-Symmetrized HH Basis

A well-known feature of the wave function of a quantum particle system is the defined symmetry under particle permutations. The HH functions, however, do not possess any intrinsic symmetry and must be manually symmetrized.

One method consists in constructing HH functions recursively by realizing irreducible representations not only of the orthogonal group $O(3N)$ but also of the group $O(N)$, accordingly to the chain $O(3N) \subset O(3) \otimes O(N)$:

$$\begin{array}{ccccccccc} O(3N-3) \supset O(3) \otimes & O(N-1) & \supset & O(N-2) & \cdots & \supset & O(2) & & \\ & \cup & & \cup & & & \cup & & \\ & S_N & \supset & S_{N-1} & \cdots & \supset & S_3 & \supset & S_2 \end{array} \tag{3.47}$$

Such an approach was developed more than two decades ago by N. Barnea [66] through an efficient technique, and it resulted in the first 6-body computation using the HH method [63]. Up to 7-body calculations have also been performed [67]. This method is particularly efficient for a few-body system of N identical fermions, since given an antisymmetric wave function Ψ_A, all the matrix elements for a potential can be determined by computing only the matrix element of one pair of particles as

$$\langle \Psi_A | \sum_{i<j} V_{ij} | \Psi_A \rangle = \frac{N(N-1)}{2} \langle \Psi_A | V_{N,N-1} | \Psi_A \rangle . \tag{3.48}$$

Then because of the recursivity proprieties of the HH and remembering that the last Jacobi coordinate is expressed as only function of the relative coordinate between the N and $N-1$ particle, one can realise that the matrix element $\langle \Psi_A | \sum_{i<j} V_{ij} | \Psi_A \rangle$ will only involve two integrations in the N and $N-1$ coordinates. Unfortunately the method becomes computationally heavy for increasing N and dealing with particles with different masses and symmetries it is no longer feasible.

An alternative HH approach has been developed a few years ago by M. Gattobigio et al. in Ref. [32] which is based on the use of the Hyperspherical Harmonic basis without previous symmetrization (NSHH). Let us see, in this case, how to deal with the problem caused by the lack of an intrinsic symmetry of the wave function, having to calculate the matrix elements for all the couples of particle ij. In order to do this the permutation matrices can be used

$$\langle \Psi_{NSHH} | V_{ij} | \Psi_{NSHH} \rangle = \langle \Psi_{NSHH} | P_{1i}^{-1} P_{2j}^{-1} V_{12} P_{1i} P_{2j} | \Psi_{NSHH} \rangle , \tag{3.49}$$

with

$$P_{ab} = \prod_{s=a}^{b-1} \mathcal{P}^{(s)} \prod_{s=b-2}^{a} \mathcal{P}^{(s)}, \quad a < b. \tag{3.50}$$

The unitary matrix $\mathcal{P}^{(j)}$ is defined as

$$\mathcal{P}^{(j)}_{[K_N][K'_N]} = \int \mathcal{Y}^*_{[K_N]}(\Omega_N)\mathcal{Y}_{[K'_N]}(\Omega^{(j)}_N)d\Omega_N \tag{3.51}$$

and represents the kinematic rotation between the two mass-position pairs (m_j, r_j) and (m_{j+1}, r_{j+1}) in the HH basis. It can be shown (see [61]) to be equal to

$$\begin{aligned}\mathcal{P}^{(j)}_{[K_N][K'_N]} =& \left[\prod_{\alpha=1}^{i-2}\delta_{l_\alpha,l'_\alpha}\prod_{k=2}^{i-2}\delta_{L_k,L'_k}\delta_{K_k,K'_k}\right]^{(i)}\mathcal{B}^{L_{i-2}K_{i-2}L_iK_i}_{l_{i-1}l'_{i-1}L_{i-1}L'_{i-1}K'_{i-1}} \\ &\cdot\left[\prod_{\alpha=i+1}^{N}\delta_{l_\alpha,l'_\alpha}\prod_{k=i+1}^{N}\delta_{L_k,L'_k}\delta_{K_k,K'_k}\right].\end{aligned} \tag{3.52}$$

The $\mathcal{B}$ matrices represent the blocks of the $\mathcal{P}$ matrix and are combination recouplings by means of the T and the Raynal-Revai coefficients as

$$\begin{aligned}{}^{(i)}\mathcal{B}^{L_{i-2}K_{i-2}L_iK_i}_{l_{i-1}l'_{i-1}L_{i-1}L'_{i-1}K'_{i-1}} =& \sum_{L_{i,i-1}} T^{L_{i-2}l_{i-1}l_i}_{L_{i-1},L_{i,i-1},L_i}T^{L_{i-2}l'_{i-1}l'_i}_{L_{i-1},L_{i,i-1},L_i}\times \\ &\times\sum_{K_{i-1,i}} T^{\alpha_{K_{i-1}}\alpha_{l_{i-1}}\alpha_{l_i}}_{K_{i-1}Ki,i-1K_i}T^{\alpha_{K_{i-1}}\alpha'_{l_{i-1}}\alpha'_{l_i}}_{K_{i-1}Ki,i-1K_i}\cdot\mathcal{R}^{K_{i,i-1},L_{i,i-1}}_{l_{i-1}l_i,l'_{i-1}l'_i},\end{aligned} \tag{3.53}$$

with

$$\begin{aligned}T^{L_{i-2}l_{i-1}l_i}_{L_{i-1},L_{i,i-1},L_i} =& (-1)^{L_{i-2}+l_{i-1}+l_i+L_i}\sqrt{2L_{i-1}+1}\times \\ &\times\sqrt{2L_{i,i-1}+1}\begin{Bmatrix} L_{i-2} & l_{i-1} & l_i \\ l_i & L_i & L_{i,i-1}\end{Bmatrix},\end{aligned} \tag{3.54}$$

and $\mathcal{R}^{K_{i,i-1},L_{i,i-1}}_{l_{i-1}l_i,l'_{i-1}l'_i}(\beta_j)$ the Raynal-Revai coefficients as described in [68].

Now we need to figure out how to restore the correct symmetry of the wave function. The well defined symmetries of the $\mathcal{N}$-body Hamiltonian eigenvectors can be identified by means of the application of the Casimir operator of the group of permutations of $\mathcal{N}$ objects, $C(\mathcal{N})$. [1]

N. Barnea et al. in Ref. [33] proposed a variation on this non-symmetrized HH (NSHH) method which is based on the definition of a pseudo-Hamiltonian as an appropriate combination of the $\mathcal{N}$-body Hamiltonian and the $C(\mathcal{N})$ operator. The lowest eigenvectors of such an operator have the requisite permutational symmetry and can be calculated using fast diagonalization procedures, in our instance the Lanczos algorithm (illustrated in Appendix B) was chosen.

This last approach is the one adopted in the present work. If we examine a system of identical particles, the Casimir operator is defined by

$$\hat{C}(\mathcal{N}) = \sum_{i<j}^{\mathcal{N}} P_{ij}\,, \tag{3.55}$$

[1] Clearly in case of particles with spin and isospin degrees of freedom one has to extend the basis and in this case the permutation operators will contain also spin and isospin recouplings [61].

where P_{ij} is the operator that permutes the i-th particle with the j-th one. Since the Hamiltonian commutes with $\hat{C}(\mathcal{N})$, these two operators share the same set of eigenstates. In particular, the eigenvalue of the Casimir operator for a symmetric state is $\lambda_S = \frac{\mathcal{N}(\mathcal{N}-1)}{2}$, for an antisymmetric state it is equal to $\lambda_A = \frac{-\mathcal{N}(\mathcal{N}-1)}{2}$ and for a mixed state it corresponds to λ_M, where $\lambda_A < \lambda_M < \lambda_S$. In Ref. [61], a generalised form of the Casimir operator for different particle species is defined by

$$\hat{C}(\mathcal{N}) = \sum_{s=1}^{n} b_{\Lambda_s} \hat{C}_s(\mathcal{N}_s)\,, \tag{3.56}$$

where $\hat{C}_s(\mathcal{N}_s)$ is the Casimir operator given by Eq. (3.55) for $\mathcal{N}_s$ particles of the same species, n is the number of different species in the system and the parameter b_{Λ_s} comes out to be equal to 1 for antisymmetric and mixed states, and to -1 for symmetric states. The original Hamiltonian can now be modified, by adding a new term which depends on $\hat{C}(\mathcal{N})$, as

$$\hat{H}' = \hat{H} + \gamma \hat{C}(\mathcal{N}). \tag{3.57}$$

The eigenvalues of H' for a specific symmetry configuration Λ assume the form

$$E'_{k,\Lambda} = E_{k,\Lambda} + \gamma \sum_{s=1}^{n} b_{\Lambda_s} \lambda_{\Lambda_s}\,, \tag{3.58}$$

where k varies from 0 to the maximum number of states N_{max} with the same symmetry configuration. As a result, after the parameter γ is fixed, we are able to distinguish the states with the desired symmetry configuration Γ from the others since the associated eigenvalues will be the lowest. Indicating the shifted value for the ground state energy with $E'_{0,\Gamma}$, the following relation holds:

$$E'_{0,\Gamma} = E_{0,\Gamma} + \gamma \sum_{s=1}^{n} b_{\Gamma_s} \lambda_{\Gamma_s} < E_{0,\Lambda} + \gamma \sum_{s=1}^{n} b_{\Lambda_s} \lambda_{\Lambda_s}\,, \tag{3.59}$$

where $\Lambda \neq \Gamma$. This inequality implies the presence of a lower bound on the parameter γ given by

$$\gamma > \frac{E_{0,\Gamma} - E_{0,\Lambda}}{\sum_{s=1}^{n} (b_{\Lambda_s} \lambda_{\Lambda_s} - b_{\Gamma_s} \lambda_{\Gamma_s})}. \tag{3.60}$$

At this point, the true ground-state energy $E_{0,\Gamma}$ can be obtained by subtracting the term $\gamma \sum_{s=1}^{n} b_{\Gamma_s} \lambda_{\Gamma_s}$ to $E'_{0,\Gamma}$. We would like to emphasize that the avoidance of the symmetrization technique is partially compensated by the larger dimension of the basis, which is no longer constrained a priori by permutational symmetry.

3.6 Application to Cluster EFT Hamiltonian

In the previous Sections we presented the complete HH basis in momentum space. Furthermore we showed how, even without explicit symmetrization, we could compute the potential solely between the N-th and N-1-th particle by using permutations and then selecting the correct symmetry by the additional pseudo-potential with the Casimir operator. Let us now illustrate the explicit calculation of the expansion of the Hamiltonian on the basis of the NSHH. To calculate the matrix elements $H_{mn} = \langle \psi_m | H | \psi_n \rangle$ the kinetic and potential parts of the Hamiltonian $H_{mn} = T_{mn} + (V_{N,N-1})_{mn}$ are considered separately.

For the kinetic term T_{mn} one simply gets

$$T_{mn} = \frac{n!}{(n+\nu)!} \int dQ Q^{3N-1} g_m(Q) \frac{Q^2}{2m} g_n(Q)\, \delta_{[K],[K']}. \tag{3.61}$$

Concerning the two-body potential, as we have seen in Chapter 2, they depend on the two relative momenta p, p' in the following way

$$V(\mathbf{p},\mathbf{p}') = \sum_{l=0}^{\infty}(2l+1)(p^l p'^l g(p) g(p') \sum_{ij=0}^{1} p^{2i} \lambda_{ij} p'^{2j}) P_l(\hat{\mathbf{p}}\cdot\hat{\mathbf{p}}') \qquad \lambda = \begin{pmatrix} \lambda_0 & \lambda_1 \\ \lambda_1 & 0 \end{pmatrix}, \tag{3.62}$$

where $P_l(\hat{\mathbf{p}}\cdot\hat{\mathbf{p}}')$ indicates the l-th Legendre polynomial.
Equivalently in terms of the Jacobi coordinates the potential is a function of $\boldsymbol{\pi}_N, \boldsymbol{\pi}'_N$ as

$$V(\mathbf{p},\mathbf{p}') \to V(\sqrt{\frac{mM_2}{m_1 m_2}}\boldsymbol{\pi}_N, \sqrt{\frac{mM_2}{m_1 m_2}}\boldsymbol{\pi}'_N). \tag{3.63}$$

The dependence on the variables $\boldsymbol{\pi}$ and $\boldsymbol{\pi}'$, beyond the particular case under consideration, represents a general feature of the potentials in momentum space even if the corresponding potential in the coordinate space is local.

Therefore in order to expand $V(\boldsymbol{\pi}_N, \boldsymbol{\pi}'_N)$ we need to introduce

$$\begin{cases} \pi_N = Q \sin(\Phi_N) \\ \Omega_N = (\varphi_N, \theta_N) \end{cases}, \tag{3.64}$$

where

$$Q = \sum_{i=1}^{N} \pi_i^2, \tag{3.65}$$

and the new variable

$$\begin{cases} \pi'_N = Q' \sin(\Phi'_N) \\ \Omega'_N = (\varphi'_N, \theta'_N) \end{cases} \tag{3.66}$$

with

$$Q' = \sum_{i=1}^{N-1} \pi_i^2 + \pi_N'^2. \tag{3.67}$$

Using Eq. (3.66) together with Eq. (3.67) one obtains

$$Q'^2 = \sum_{i=1}^{N-1} \pi_i^2 + \pi_N'^2 = \sum_{i=1}^{N-1} \pi_i^2 + Q'^2 \sin^2(\Phi_N') \Rightarrow \sum_{i=1}^{N-1} \pi_i^2 = Q'^2(1 - \sin^2(\Phi_N')), \tag{3.68}$$

then one can make the same argument with Eq. (3.64) and Eq. (3.65) getting

$$\sum_{i=1}^{N-1} \pi_i^2 = Q^2(1 - \sin^2(\Phi_N)) = Q^2 \cos^2(\Phi_N). \tag{3.69}$$

Putting the two results together

$$Q^2 \cos^2(\Phi_N) = Q'^2 \cos^2(\Phi_N') \Rightarrow \cos^2(\Phi_N') = \cos^2(\Phi_N) \frac{Q^2}{Q'^2} \tag{3.70}$$

we have a relation with which we can remove Φ_N' as a free variable in the integration, meaning that the final element of volume is

$$d\Omega = \pi_N'^2 d\pi_N' = Q'^2 \sin^2(\Phi_N') \frac{dQ'}{\sin(\Phi_N')} = Q'^2 \sin(\Phi_N') dQ'. \tag{3.71}$$

Now the integral $(V_{N,N-1})_{mn}$ can be rewritten in HH coordinates as

$$\begin{aligned}
(V_{N,N-1})_{mn} = \mathcal{N} \int & dQ dQ' d\Phi_N d\Omega_{(N-1)} d\Omega_N d\Omega_N' Q^{3N-1} Q'^2 g_m(Q) g_n(Q') \times \\
& \times (\sin(\Phi_N))^{l_N+2} (\cos(\Phi_N))^{K_{N-1}+3N-4} P_{n_N}^{(l_n+\frac{1}{2}, K_{N-1}+\frac{3N-5}{2})} (\cos(2\Phi_N)) \times \\
& \times \sum_{M_{N-1}, m_N} (\langle L_{N-1} M_{N-1} l_N m_N | L_N M_N \rangle \mathcal{Y}_{[K_{N-1}]}(\Omega_{(N-1)})) Y_{l_N}^{m_N}(\Omega_N)) \times \\
& \times V(\boldsymbol{\pi}_N, \boldsymbol{\pi}_N') (\sin(\Phi_N'))^{l_N'+1} (\cos(\Phi_N'))^{K_{N-1}'} P_{n_N'}^{(l_n'+\frac{1}{2}, K_{N-1}'+\frac{3N-5}{2})} (\cos(2\Phi_N')) \times \\
& \times \sum_{M_{N-1}', m_N'} (\langle L_{N-1}' M_{N-1}' l_N' m_N' | L_N' M_N' \rangle \mathcal{Y}_{[K_{N-1}']}(\Omega_{(N-1)})) Y_{l_N'}^{m_N'*}(\Omega_N')),
\end{aligned} \tag{3.72}$$

with $\mathcal{N} = \mathcal{N}(K_N, l_N, K_{N-1}) \mathcal{N}(K_N', l_N', K_{N-1}')$ the product of all normalization factors of the various functions in the integral.
As detailed in Ref. [60] the Eq. (3.72), after some mathematical manipulations, can

be cast in the following compact expression

$$\begin{aligned}(V_{N,N-1})_{mn} = {} & \delta_{[K_{N-1}][K'_{N-1}]}\delta_{l_N l'_N}\delta_{m_N m'_N}\delta_{L_N L'_N}\delta_{M_N M'_N}\delta_{m''0}\times \\ & \times 2\pi\mathcal{N}\int dQdQ'Q^{3N-1}Q'^2 g_m(Q)g_n(Q')\times \\ & \times \int d\Phi_N(\sin\Phi_N)^{l_N+2}(\cos\Phi_N)^{K_{N-1}+3N-4}P_{n_N}^{(l_N+\frac{1}{2},K_{N-1}+\frac{3N-5}{2})}(\cos(2\Phi_N))\times \\ & \times (\sin\Phi'_N)^{l_N+1}(\cos\Phi'_N)^{K'_{N-1}}P_{n_N}^{(l_N+\frac{1}{2},K_{N-1}+\frac{3N-5}{2})}(\cos(2\Phi'_N))V_{l_N}(\pi_N,\pi'_N)\,,\end{aligned} \tag{3.73}$$

where

$$V_{l_N}(\pi_N,\pi'_N) = \int_{-1}^{1} dtV(\pi_N,\pi'_N,t)P_{l_N}^0(t) \tag{3.74}$$

being $t = \hat{\pi}_N\cdot\hat{\pi}'_N$.

3.6.1 The three-body potential

As we mentioned in the Chapter 2, in the Hamiltonian a three-body potential of the form

$$V_3 = \lambda_3\, e^{-(p_{12}^2+p_{23}^2+p_{31}^2)/\Lambda^2}e^{-(p'^2_{12}+p'^2_{23}+p'^2_{31})/\Lambda^2} \tag{3.75}$$

is included, where p_{ij} are the relative momenta. In this case the Jacobi variables present are four: $\boldsymbol{\pi}_1$, $\boldsymbol{\pi}_2$, $\boldsymbol{\pi}'_1$ and $\boldsymbol{\pi}'_2$. However, the calculation of the matrix $(V_3)_{mn}$ can be considerably simplified since it is possible to rewrite the potential in terms of the hypermomenta Q and Q' as,

$$V_3 = \lambda_3\, e^{-(Q^2/\Lambda_3^2)}e^{-(Q'^2/\Lambda_3^2)}\,. \tag{3.76}$$

Therefore this potential takes the form of a hypercentral potential and $(V_3)_{mn}$ is simply given by

$$(V_3)_{mn} = \mathcal{N}\int dQdQ'Q^{3N-1}Q'^{3N-1}g_m(Q)g_n(Q')V_3(Q,Q')\,\delta_{[K],[K']}\,. \tag{3.77}$$

Chapter 4

Nuclear photodisintegration reactions

In this Chapter we propose the derivation of the electromagnetic currents used in the calculation of the ^{9}Be photodisintegration cross-section. In Section 4.1 we introduce the general aspects of nuclear reactions, with particular attention to their inclusion in the EFT framework. In Section 4.2 we then analyze the photodisintegration process for the ^{9}Be, showing how to derive the current within our theory. There we also discuss the continuity equation for the current and the charge density. Finally, in Section 4.3, we derive the expression for the cross-section of the process using the Fermi golden rule.

The notations used in this Chapter for the particle fields, the interaction Hamiltonian, the T-matrix and the S-matrix can be found in Appendix C.

4.1 Nuclear reactions

Nuclear reactions are a fundamental tool for the investigation of nuclear structure and dynamics. Calculating the cross-section of a given process and comparing it with experimental data is essential to understand the reliability of the model. The nuclear response function is directly related to the interaction Hamiltonian or more precisely to the relative T-matrix, hence the nuclear currents can be derived within the EFT framework.

Most of the recent current calculations in the literature are based on EFTs [69, 70]. Differently from the calculations of bound states or resonances, the derivation of the currents follows the perturbative approach. In this way the calculation can be inserted in a systematic context where the error at each order is due to the truncation of the Lagrangian and of the T-matrix used.

The general approach starts considering an interaction Lagrangian density. If we are describing the reaction within an EFT then the Lagrangian is constructed in a similar way as explained in Chapter 2. From the Lagrangian it is possible to derive the associated Hamiltonian by means of the Legendre transform. Then in order to obtain the cross-section it is necessary to calculate the matrix T_{fi} of the process and here the perturbative approach and power counting of the theory are required to

justify the contributions of the matrix that will contribute most to the process. As we have already seen in Section 2.3, the various terms of the T-matrix are visualized through diagrams that facilitate the power counting of their perturbative order. In general given an interaction Hamiltonian H_{int} and the initial and final states $|I;\mathbf{q},\boldsymbol{k}\rangle$ and $|F;\boldsymbol{k}'\rangle$, combination of a scattering particle with momentum $\boldsymbol{k}$, a photon with momentum $\boldsymbol{q}$ and nucleus states, the T-matrix reads

$$\begin{aligned} T_{fi} &= \langle F;\boldsymbol{k}'|H_{int}|I;\mathbf{q},\boldsymbol{k}\rangle \\ &+ \frac{\sum_{INT}\langle F;\boldsymbol{k}'|H_{int}|INT\rangle\langle INT|H_{int}|I;\mathbf{q},\boldsymbol{k}\rangle}{E_I+E_k+E_q-E_{\mathrm{INT}}+i\epsilon} \\ &+ \cdots . \end{aligned} \tag{4.1}$$

Above $|INT\rangle$ indicates the possible intermediate states of particles produced during the reaction and the dots mean higher orders in the calculation. Finally the scattering matrix element S_{fi}, between the initial (i) and final (f) states, is given by

$$S_{fi} = \delta_{fi} - 2\pi i\delta(E_f - E_i)T_{fi} \tag{4.2}$$

and the cross-section is calculated by the Fermi golden rule [71]. In this work we focus on the photodisintegration process which is when a nucleus absorbs a photon and then breaks up into fragments. The typical spectrum for this reaction is shown in Figure 4.1.

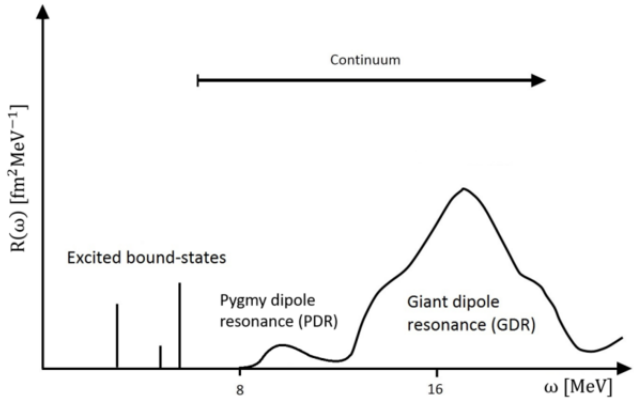

FIGURE 4.1: Figure from Ref.[72]

At low energy one can see the discrete spectrum representing the excited bound-states, above the break-up threshold the continuum region appears. This region is dominated by resonant peaks originated, in most cases, by dipole excitations. The first area in this region is populated by the so-called pygmy dipole resonances (PDRs), typical of neutron-rich nuclei and often explained as due to the oscillation of the excess neutrons against all other nucleons. In the higher energy region the giant dipole resonances (GDRs) are found. These are interpreted as the collective modes of all protons oscillating against all neutrons [73].

4.2 Electromagnetic currents

The starting point to derive the electromagnetic currents is given by a Lagrangian density. We can firstly consider the one body free Lagrangian for the alpha particle

$$\mathcal{L}_\alpha = \frac{1}{2}\left(\frac{1}{2m_\alpha}\partial_\mu\Psi^\dagger\partial^\mu\Psi - m_\alpha^2\Psi^+\Psi + h.c.\right), \tag{4.3}$$

where we use the definitions of the quantum fields shown in Eqs. (2.3)-(2.6).
The photon field can be included in the above Lagrangian via minimal coupling,

$$\partial_\mu \to \partial_\mu + ie\hat{Q}A_\mu. \tag{4.4}$$

being $\hat{Q}$ the charge operator, which takes different values depending on the field is acting on, and

$$A^\mu(\boldsymbol{x}) = \sum_{\lambda=4,\pm1,0} V\int \frac{d\boldsymbol{q}}{(2\pi)^3}\frac{1}{\sqrt{2\omega_q}}(a_{\boldsymbol{q},\lambda}\epsilon^\mu_{\boldsymbol{q},\lambda}\frac{e^{iqx}}{\sqrt{V}} + a^\dagger_{\boldsymbol{q},\lambda}\epsilon^{\mu\,*}_{\boldsymbol{q},\lambda}\frac{e^{-iqx}}{\sqrt{V}}) \tag{4.5}$$

is the field of a photon with energy $\omega_{\mathbf{q}} = |\mathbf{q}| = q$. The polarization four vectors $\epsilon^\mu_{\boldsymbol{q},\lambda}$ are defined as,

$$\epsilon^\mu_{\mathbf{q},\lambda} = (1,\hat{\mathbf{0}}) \quad \lambda = 4, \tag{4.6}$$
$$\epsilon^\mu_{\mathbf{q},\lambda} = (0,\hat{\epsilon}_{\mathbf{q},\lambda}) \quad \lambda \neq 4, \tag{4.7}$$

where $\hat{\mathbf{0}}$ is a three-dimensional vector with null components, $\hat{\epsilon}_{\mathbf{q},0} = \hat{\mathrm{q}}$ and the vectors $\hat{\epsilon}_{\mathbf{q},\pm1}$ are defined in circular polarization. The $\hat{\epsilon}_{\mathbf{q},\lambda}$ satisfy the relations

$$\hat{\epsilon}^\dagger_{\mathbf{q},\lambda} = (-)^\lambda\hat{\epsilon}^\dagger_{\mathbf{q},-\lambda}, \tag{4.8}$$
$$\hat{\epsilon}^\dagger_{\mathbf{q},\lambda}\cdot\hat{\epsilon}_{\mathbf{q},\lambda'} = \delta_{\lambda,\lambda'}. \tag{4.9}$$

With the substitution (4.4) the Lagrangian (4.3) becomes,

$$\mathcal{L}^{em}_\alpha \simeq \frac{1}{4m_\alpha}\left(\partial_\mu\Psi\right)^\dagger(2ieA^\mu\Psi) + h.c., \tag{4.10}$$

where we considered only the linear terms in the electromagnetic field and the covariant derivative acts on the field of the alpha particle as,

$$\partial_\mu\Psi = V\int\frac{d\boldsymbol{k}}{(2\pi)^3}a_{\boldsymbol{p}}\,(-ik_\mu)\frac{e^{i\boldsymbol{k}\cdot\boldsymbol{x}}}{\sqrt{V}}. \tag{4.11}$$

Considering only the minimal coupling with the electromagnetic field (4.4), proportional to the charge operator, the free Lagrangian of the neutron will not make any further contribution. The use of only the minimal coupling and no other couplings with the electromagnetic field in case of focus on electric dipole transition is justified by the fact that it represents, at low energy, the main contribution to the

current [74].

Now we can move to consider the EFT interaction Lagrangian density, described in detail in Eq. (2.1). Here for the sake of simplicity we write only the dominant interactions for the particles pairs, which are the S_0 partial wave interaction for $\alpha\alpha$ and the $P_{\frac{3}{2}}$ for αn,

$$\begin{aligned}\mathcal{L}_{\alpha\alpha n} &= \lambda_{0\alpha\alpha,0}\Psi^\dagger\Psi\Psi^\dagger\Psi + \lambda_{1\alpha\alpha,0}\left(\Psi\overleftrightarrow{\nabla}^2\Psi\Psi\Psi + h.c.\right) \\ &+ \lambda_{0\alpha n,1}(\Psi\overleftrightarrow{\nabla}n)^\dagger(\Psi\overleftrightarrow{\nabla}n) + \lambda_{1\alpha n,1}\left((\Psi\overleftrightarrow{\nabla}^2\overleftrightarrow{\nabla}n)(\Psi\overleftrightarrow{\nabla}n) + h.c.\right). \end{aligned} \tag{4.12}$$

Writing the covariant expression of the gradient as

$$\Psi_a\overleftrightarrow{\nabla}\Psi_b = \frac{m_b\partial_a - m_a\partial_b}{m_a+m_b} \to \frac{m_b\partial_{a\mu} - m_a\partial_{b\mu}}{m_a+m_b} \equiv \partial_{a\mu} - \partial_{b\mu} \tag{4.13}$$

and introducing again the electromagnetic field via minimal coupling

$$\partial_{a\mu} - \partial_{b\mu} \to \partial_{a\mu} + (ie\hat{Q}A_\mu)_a - \partial_{b\mu} - (ie\hat{Q}A_\mu)_b \equiv \overleftrightarrow{\partial}_\mu + (ie\hat{Q}A_\mu)_a - (ie\hat{Q}A_\mu)_b\,, \tag{4.14}$$

from the first term of αn Lagrangian we get

$$\begin{aligned}&\lambda_{0\alpha n,1}(\Psi\overleftrightarrow{\nabla}n)^\dagger(\Psi\overleftrightarrow{\nabla}n) \to \\ &= \lambda_{0\alpha n,1}[(\Psi\overleftrightarrow{\partial}_\mu n + ie\hat{Q}A_\mu\Psi n)(\Psi\overleftrightarrow{\partial}^\mu n + ie\hat{Q}A^\mu\Psi n)^\dagger)] \\ &\simeq \lambda_{0\alpha n,1}[\Psi\overleftrightarrow{\partial}_\mu n(ie\hat{Q}A^\mu\Psi n)^\dagger + (\Psi\overleftrightarrow{\partial}^\mu n)^\dagger(ie\hat{Q}A_\mu\Psi n)]\,, \end{aligned} \tag{4.15}$$

where again in the last line we considered only the linear terms in A_μ.
From the λ_1 term of the αn Lagrangian one has

$$\begin{aligned}&\lambda_{1\alpha n,1}\left((\Psi\overleftrightarrow{\nabla}^2\overleftrightarrow{\nabla}n)(\Psi\overleftrightarrow{\nabla}n) + h.c.\right) \to \\ &\lambda_{1\alpha n,1}[\Psi(\overleftrightarrow{\partial}_\mu + ie\hat{Q}A_\mu)^2(\overleftrightarrow{\partial}_\mu + ie\hat{Q}A_\mu)n)^\dagger)](\Psi(\overleftrightarrow{\partial}^\mu + ie\hat{Q}A^\mu)n)^\dagger)) + h.c. \\ &\simeq 4\lambda_{1\alpha n}\left(\left(\Psi\overleftrightarrow{\partial}^3_\mu n\right)((2ieA^\mu\Psi n) + h.c.)\right). \end{aligned} \tag{4.16}$$

Regarding the $\alpha\alpha$ interaction Lagrangian the $\lambda_{0\alpha\alpha,0}$ term in Eq. (4.12) does not have a derivative to be coupled to the electromagnetic field. While from the $\lambda_{1\alpha\alpha,0}$ terms one obtains

$$\Psi_a(\partial_{a\mu} + (ie\hat{Q}A_\mu)_a - \partial_{b\mu} - (ie\hat{Q}A_\mu)_b)^2\Psi_b\,, \tag{4.17}$$

which has not A_μ-dependent linear terms since the two α fields have the same charge $Q_a = Q_b$. It is interesting to note that the Lagrangian terms written in Eqs. (4.15), (4.16) are the only interaction Lagrangian terms with a linear coupling with the electromagnetic field, since considering also the NLO of the αn interaction or the three-body interaction we do not have additional terms. Such interactions, in fact, do not contain any further derivative.

Putting all the terms together we get the expression of the $\alpha\alpha n$ electromagnetic Lagrangian density, that is

$$\mathcal{L}^{em}_{\alpha\alpha n} = \lambda_{0\alpha n}\left(\left(\Psi \overleftrightarrow{\partial}_{\mu} n\right)(2ieA^{\mu}\Psi n)^{\dagger} + h.c.\right) + 4\lambda_{1\alpha n}\left(\left(\Psi \overleftrightarrow{\partial}^{3}_{\mu} n\right)((2ieA^{\mu}\Psi n) + h.c.)\right). \tag{4.18}$$

At this point the Hamiltonian can be calculated by the Legendre transformation of the Lagrangian. Neglecting higher-order terms one simply has [75],

$$\mathcal{L}_{int} \simeq -\mathcal{H}_{int} \tag{4.19}$$

$$H_{int}(x) = \int d^3x \mathcal{H}_{int}(x)\,. \tag{4.20}$$

Then, the T-matrix element from an initial state $|i\rangle = |\alpha_1\alpha_2 nq\rangle$, with two alpha particles of quantum numbers $\alpha_1\alpha_2$, a neutron n and a photon q, to a final state $|f\rangle = |\alpha'_1\alpha'_2 n'\rangle$ is given by

$$\begin{aligned} T_{fi} &= \left\langle \alpha'_1\alpha'_2 n' \middle| -\int d^3x \mathcal{L}^{em}_{\alpha} \middle| \alpha_1\alpha_2 nq \right\rangle \\ &+ \sum_{\mathrm{INT}} \frac{\left\langle \alpha'_1\alpha'_2 n' \middle| -\int d^3x \mathcal{L}^{em}_{\alpha} \middle| \mathrm{INT} \right\rangle \left\langle \mathrm{INT} \middle| -\int d^3x \mathcal{L}_{\alpha\alpha n} \middle| \alpha_1\alpha_2 nq \right\rangle}{E_{\alpha_1} + E_{\alpha_2} + \mathcal{E}_n + \omega_{\boldsymbol{q}} - E_{\mathrm{INT}} + i\epsilon} \\ &+ \cdots, \end{aligned} \tag{4.21}$$

where $|\mathrm{INT}\rangle = \left|\alpha''_1\alpha''_2 n''\right\rangle$ represents an intermediate state of the process consisting of α, α, n particles. Each term of the above expression can be visualized through an time-ordered diagram.

There is an one-to-one correspondence between the diagrams and the expressions of the contributions to the T-matrix. If we consider the time running upward, the various factors are ordered starting from the top of the diagrams and going backward. Every time we meet a vertex, we associate the corresponding vertex function; between two vertices we have a propagator or better an energy denominator which takes into account of the flying particles in the intermediate state. For each vertex there is a δ-function conserving the momenta. After the elimination of the sum over the intermediate state momenta with the δ-functions, it remains an integrations over a momentum for each remaining loop. It is important to notice that these diagrams are not Feynman diagrams. Unlike the latter, we must consider here all time orderings. This is due to the analytical integration over time we have performed when we have written the S-matrix in terms of the T-matrix. To establish how many terms of the above equation it is necessary to calculate, let us start considering the diagrams in Figure 4.2.

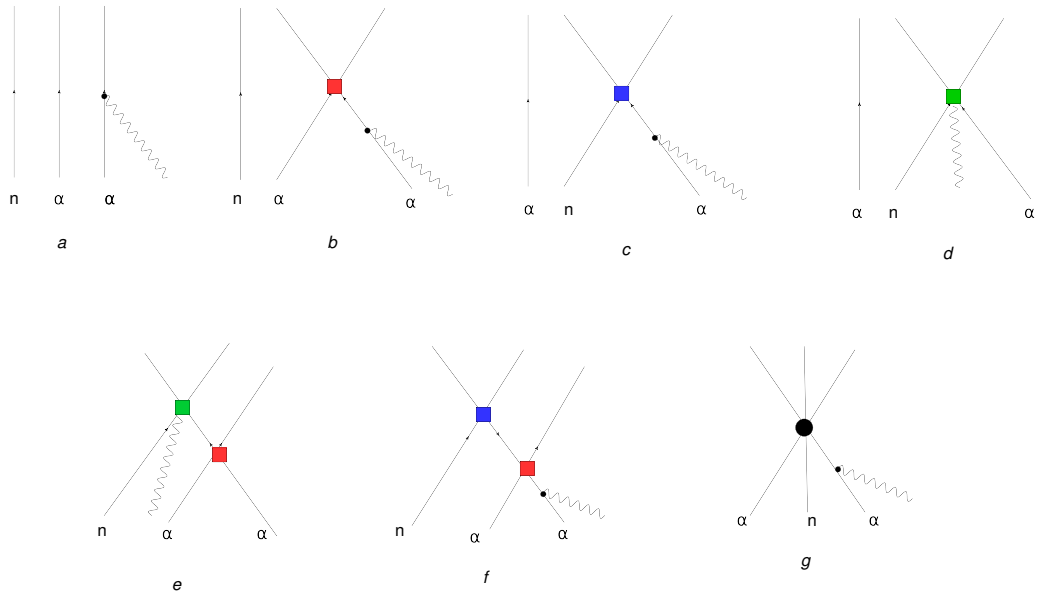

FIGURE 4.2: T-matrix contributions described in the text.

Here we adopt the naive power counting [76] which simply corresponds to the dimensional analysis and gives an idea about the magnitude of each term in the expansion. We considered each delta function, in addition to that of energy conservation, as Q^{-3}. This is because each of these deltas eliminates an integral over the momenta $d\boldsymbol{p}$. The energy denominator in Eq. (4.21) is considered of order Q, since it corresponds to the energy of the photon. The contribution of the vertex derives from the interaction Lagrangians. In the diagrams above the electromagnetic vertex of the α particle with a photon, of Eq. (4.10), is represented with a dot and at the leading order gives $\sim \frac{\boldsymbol{p}}{m\sqrt{\omega_q}} \sim Q^{-\frac{1}{2}}$. The red square represents the $\alpha\alpha$ interaction of Eq. (4.12), while the blue square represents the αn interaction of Eq. (4.12). The bigger dot stands for a three-body force contact interaction and the green square for the interaction (4.18). Regarding the constants of the EFT potential we considered $\lambda_{0\alpha\alpha} \sim \Lambda^{-2}$ and $\lambda_{0\alpha n} \sim \Lambda^{-4}$, see Eq. (2.39). In this way it is easy to see that diagram (a) represents the dominant contribution $\sim Q^{-13/2}$ and diagram (b) is suppressed by a factor Q^2/Λ^2 with respect to the first one, due to the lack of one delta function and to the energy denominator. Therefore it is $O(Q^{-11/2}/\Lambda^2)$, the (c) diagram is suppressed by Q^4/Λ^4, thus $\sim O(Q^{-5/2}/\Lambda^4)$ and the other diagrams are of higher order.

Let us now return to consider Eq. (4.21), the first term of the sum represents the diagram (a) of Figure 4.2, that is the LO contribution, while the second term stands for the diagram (b) when we consider an intermediate state of two α particles and a neutron and taking only the $\alpha\alpha$ terms of Eq. (4.12). In this work we only consider the contribution of diagram (a). Regarding the higher order diagrams, as also shown in Ref. [74], for our purposes their contributions can be neglected.

Therefore substituting Eq. (4.10) into Eq. (4.21), the LO contribution of the T-matrix reads

$$\begin{aligned} T_{fi} &= \left\langle \alpha_1' \alpha_2' n' \left| - \int d^3x \frac{1}{2m_\alpha} \left(\partial_\mu \Psi\right)^\dagger (ieA^\mu \Psi) + h.c. \right| \alpha_1 \alpha_2 n q \right\rangle \\ &= \frac{ie}{2m_\alpha} \langle 0 | a_{\boldsymbol{p}_{\alpha_1'}} a_{\boldsymbol{p}_{\alpha_2'}} b_{\boldsymbol{p}_{n'}} \Big(- \int d^3x V \int \frac{d\boldsymbol{k}'}{(2\pi)^3} a^\dagger_{\boldsymbol{k}'} (ik'_\mu) \frac{e^{-i\boldsymbol{k}'\cdot\boldsymbol{x}}}{\sqrt{V}} \\ &\times V \sum_{\lambda'} \int \frac{d\boldsymbol{q}'}{(2\pi)^3} \frac{1}{\sqrt{2\omega_{\boldsymbol{q}'}}} a_{\boldsymbol{q}',\lambda'} \epsilon^\mu_{\boldsymbol{q}',\lambda'} \frac{e^{i\boldsymbol{q}'\cdot\boldsymbol{x}}}{\sqrt{V}} V \int \frac{d\boldsymbol{k}}{(2\pi)^3} a_{\boldsymbol{k}} \frac{e^{i\boldsymbol{k}\cdot\boldsymbol{x}}}{\sqrt{V}} \\ &+ h.c. \Big) a^\dagger_{\boldsymbol{p}_{\alpha_1}} a^\dagger_{\boldsymbol{p}_{\alpha_2}} b^\dagger_{\boldsymbol{p}_n} a^\dagger_{\boldsymbol{q}} |0\rangle \,, \end{aligned} \tag{4.22}$$

where p_{α_1}, p_{α_2} ($p_{\alpha_1'}$, $p_{\alpha_2'}$) indicate the initial (final) alpha particle four-momenta, p_n ($p_{n'}$) the initial (final) neutron four-momentum, q the photon one and $|0\rangle$ is the vacuum state. Using the commutation rules of creation and annihilation operators of the fields,

$$[a_{\boldsymbol{p}}, a^\dagger_{\boldsymbol{p}'}] = \frac{(2\pi)^3}{V} \delta^3(p - p') \,, \tag{4.23}$$

$$[a_{\boldsymbol{q},\lambda}, a^\dagger_{\boldsymbol{q}',\lambda'}] = \frac{(2\pi)^3}{V} \delta^3(q - q') \delta_{\lambda\lambda'} \,, \tag{4.24}$$

one has

$$\begin{aligned} T_{fi} =& \frac{-ie\,\epsilon^\mu_{\boldsymbol{q},\lambda}}{2m_\alpha V^3 \sqrt{V 2\omega_{\boldsymbol{q}}}} (2\pi)^9 \delta^3(p_{n'} - p_n) \Big[\delta^3(p_{\alpha_2'} - p_{\alpha_2}) (p_{\alpha_1 \mu} + p_{\alpha_1' \mu}) \int d^3x e^{i(p_{\alpha_1} + q - p_{\alpha_1'})x} \\ &+ \delta^3(p_{\alpha_1'} - p_{\alpha_1}) (p_{\alpha_2 \mu} + p_{\alpha_2' \mu}) \int d^3x e^{i(p_{\alpha_2} + q - p_{\alpha_2'})x} \Big] + (\alpha_1' \leftrightarrow \alpha_2') \\ =& \frac{-ie\,\epsilon^\mu_{\boldsymbol{q},\lambda}}{2m_\alpha V^3 \sqrt{V 2\omega_{\boldsymbol{q}}}} (2\pi)^9 \delta^3(p_{n'} - p_n) \Big[(p_{\alpha_1 \mu} + p_{\alpha_1' \mu}) \delta^3(p_{\alpha_1} + q - p_{\alpha_1'}) \delta^3(p_{\alpha_2'} - p_{\alpha_2}) \\ &+ (p_{\alpha_2 \mu} + p_{\alpha_2' \mu}) \delta^3(p_{\alpha_2} + q - p_{\alpha_2'}) \delta^3(p_{\alpha_1'} - p_{\alpha_1}) \Big] + (\alpha_1' \leftrightarrow \alpha_2') \,. \end{aligned} \tag{4.25}$$

In Eq. (4.25) the terms $(\alpha_1' \leftrightarrow \alpha_2')$ are obtained by exchanging p'_{α_1} with p'_{α_2}. They are they so-called exchange terms of the T-matrix. In the following text we consider only the direct T-matrix T^d_{fi}, since the exchange terms will be automatically considered from the symmetry of the nuclear wave function in Eq. (4.53).
Calling $\alpha'\alpha = \{\alpha_1'\alpha_1, \alpha_2'\alpha_2, n'n\}$, the nuclear current $J^{(1)}_{\mu\ \alpha'\alpha}$ can be defined through the following relation

$$T^d_{fi} \equiv J^{(1)}_{\mu\ \alpha'\alpha} \cdot \frac{\epsilon^\mu_{\boldsymbol{q},\lambda}}{V^{1/2}\sqrt{2\omega_{\boldsymbol{q}}}} \,, \tag{4.26}$$

as

$$\begin{aligned} J^{(1)}_{\mu\ \alpha'\alpha} = & -\tfrac{ie}{2m_\alpha V^3} (2\pi)^9 \delta^3(p_{n'} - p_n) \big(\delta^3(p_{\alpha_2'} - p_{\alpha_2}) \delta^3(p_{\alpha_1} + q - p_{\alpha_1'}) (p_{\alpha_1 \mu} + p_{\alpha_1' \mu}) \\ & + \delta^3(p_{\alpha_1'} - p_{\alpha_1}) \delta^3(p_{\alpha_2} + q - p_{\alpha_2'}) (p_{\alpha_2 \mu} + p_{\alpha_2' \mu}) \big) \,. \end{aligned} \tag{4.27}$$

Separating the charge density contribution from the space current and using the momentum conservation relation, we get

$$\rho^{(1)}_{\alpha'\alpha} = -\frac{ie}{2m_\alpha V^3}(2\pi)^9\delta^3(p_{n'}-p_n)\delta^3(p_{\alpha_1}-p_{\alpha'_1}+q)\delta^3(p_{\alpha'_2}-p_{\alpha_2})(E_{\alpha_1}+E_{\alpha'_1})\,(1\leftrightarrow 2)\,, \tag{4.28}$$

$$\boldsymbol{J}^{(1)}{}_{\alpha'\alpha}(\boldsymbol{p}_{\alpha_1},\boldsymbol{p}_{\alpha_2},\boldsymbol{q}) = -\frac{ie}{2m_\alpha V^3}(2\pi)^9\delta^3(p_{n'}-p_n)\delta^3(p_{\alpha_1}-p_{\alpha'_1}+q) \times \delta^3(p_{\alpha'_2}-p_{\alpha_2})\,(2\boldsymbol{p}_{\alpha_1}+\boldsymbol{q}) + (1\leftrightarrow 2)\,, \tag{4.29}$$

where $E_{\alpha_1} = \sqrt{m^2_{\alpha_1}+\boldsymbol{p}^2_{\alpha_1}}$ and the notation $(1\leftrightarrow 2)$ indicates the same term with p_{α_2}, p'_{α_2} instead of p_{α_1}, p'_{α_1}, respectively.

The NR expansion of the charge density contribution at leading order gives,

$$\rho^{(1)}_{\alpha'\alpha} \simeq -\frac{ie}{V^3}(2\pi)^9\delta^3(p_{n'}-p_n)\delta^3(p_{\alpha_1}-p_{\alpha'_1}+q)\delta^3(p_{\alpha'_2}-p_{\alpha_2}) + (1\leftrightarrow 2)\,. \tag{4.30}$$

In general the charge term gives, in addition to the Q^0 leading order contribution written above, a Q^2 relativistic correction term. If we wanted to take into account also these terms it would be necessary to use the relativistic formulation of the particle field.

Regarding $\boldsymbol{J}^{(1)}{}_{\alpha'\alpha}(\boldsymbol{p}_{\alpha_1},\boldsymbol{p}_{\alpha_2},\boldsymbol{q})$, in the case of real photons, only the transverse part of the current can be considered and supposing $q \parallel \hat{z}$ the spatial part of the current can be expanded over a set of 3 unit vectors. We choose the circular polarization vectors, already introduced in Eqs. (4.8), (4.9), defined as

$$\hat{\epsilon}_{\boldsymbol{q},0} \equiv \hat{\epsilon}_{\boldsymbol{q},z} \quad , \quad \hat{\epsilon}_{\boldsymbol{q},+1} \equiv -\frac{1}{\sqrt{2}}\left(\hat{\epsilon}_{\boldsymbol{q},x}+i\hat{\epsilon}_{\boldsymbol{q},y}\right) \quad , \quad \hat{\epsilon}_{\boldsymbol{q},-1} \equiv \frac{1}{\sqrt{2}}\left(\hat{\epsilon}_{\boldsymbol{q},x}-i\hat{\epsilon}_{\boldsymbol{q},y}\right)\,. \tag{4.31}$$

One obtains

$$\boldsymbol{J}^{(1)}_{\alpha'\alpha}\cdot\hat{\epsilon}_{q,\lambda} = J^{(1)}_{\lambda\ \alpha'\alpha}\hat{\epsilon}^*_{q,\lambda}\cdot\hat{\epsilon}_{q,\lambda} = J^{(1)}_{z\ \alpha'\alpha} - J^{(1)}_{1\ \alpha'\alpha} - J^{(1)}_{-1\ \alpha'\alpha} = -\sum_{\lambda=\pm1} J^{(1)}_{\lambda\ \alpha'\alpha}\,, \tag{4.32}$$

where

$$J^{(1)}_{\lambda\ \alpha'\alpha} = (\boldsymbol{J}^{(1)})_{\alpha'\alpha}\cdot\hat{\epsilon}_{q,\lambda}\,. \tag{4.33}$$

Using the following expressions of the spherical harmonics,

$$Y^1_1(\theta,\phi) = \tfrac{-1}{2}\sqrt{\tfrac{3}{2\pi}}e^{i\phi}sin\theta\,, \tag{4.34}$$

$$Y^{-1}_1(\theta,\phi) = \tfrac{1}{2}\sqrt{\tfrac{3}{2\pi}}e^{-i\phi}sin\theta\,, \tag{4.35}$$

the transverse current can be then rewritten as,

$$J^{(1)}_{\lambda\ \alpha'\alpha}(p_{\alpha_1}, p_{\alpha_2}) = \sqrt{\frac{4\pi}{3}}\frac{-ie}{m_\alpha}\frac{(2\pi)^9}{V^3}\delta^3(p_{n'} - p_n)\delta^3(p_{\alpha'_2} - p_{\alpha_2})$$
$$\delta^3(p_{\alpha_1} - p_{\alpha'_1} + q)\, p_{\alpha_1} Y^\lambda_1(\theta_1, \phi_1) + (1 \leftrightarrow 2)\ . \tag{4.36}$$

4.2.1 Continuity equation

Before proceeding with the discussion it is useful to make a clarification regarding the proof of the continuity equation. To deal with processes involving nuclear systems with photon absorption or emission, it is necessary to make use of the nuclear current and charge density operators. These operators contain both one-body contributions, where only one particle interacts with the considered photon and the others act as spectators, and many-body contributions. Here only one body operators are considered. Given $\boldsymbol{q}$ the momentum of the considered photon, we have the operators nuclear charge density and nuclear current written as

$$\rho(\mathbf{q}) = \sum_i \rho^{(1)}_i(\mathbf{q}) + \sum_{i<j} \rho^{(2)}_{ij}(\mathbf{q})\,, \tag{4.37}$$

$$\mathbf{j}(\mathbf{q}) = \sum_i \mathbf{j}^{(1)}_i(\mathbf{q}) + \sum_{i<j} \mathbf{j}^{(2)}_{ij}(\mathbf{q})\,, \tag{4.38}$$

where the summation is meant over all particles present and the superscripts "(1)" and "(2)" identify the one- and two-body contributions, respectively. The continuity equation, expressed in Schrödinger picture, in momentum space reads

$$\mathbf{q}\cdot\mathbf{j}(\mathbf{q}) = [H, \rho(\mathbf{q})]_- \tag{4.39}$$

and this relation has to be verified order by order in q. Considering non-interacting particles H is equal to H_0, the non-relativistic free Hamiltonian

$$H_0 = \sum_i \frac{p_i^2}{2m_i}\,. \tag{4.40}$$

Recalling the expression of the charge density and the current of Eqs. (4.29), (4.30) the one-body current and density operators in configuration representation can be constructed, obtaining [77, 78]

$$\rho(\mathbf{q}) = \sum_{i=1}^{N_\alpha} e_i e^{i\boldsymbol{q}\boldsymbol{x}_i}\,, \tag{4.41}$$

$$\mathbf{j}(\mathbf{q}) = \sum_{i=1}^{N_\alpha} e_i [\frac{\boldsymbol{p}_i}{2m_i}, e^{i\boldsymbol{q}\boldsymbol{x}_i}]_+\,, \tag{4.42}$$

with N_α number of α particles.

It is easy to prove that $\rho(\mathbf{q})$ and $\mathbf{j}(\mathbf{q})$ satisfy the Eq. (4.39) [77]

$$\begin{aligned}
\mathbf{q}\sum_{i=1}^{N_\alpha}\left(e_i\frac{\boldsymbol{p}_i}{2m_i}e^{i\mathbf{q}\boldsymbol{x}_i}+e_i e^{i\mathbf{q}\boldsymbol{x}_i}\frac{\boldsymbol{p}_i}{2m_i}\right) &= \sum_{i=1}^{N_\alpha}[\frac{\boldsymbol{p}_i^2}{2m_i},e_i e^{i\mathbf{q}\boldsymbol{x}_i}]_- \\
\mathbf{q}\sum_{i=1}^{N_\alpha}\left(e_i\frac{\boldsymbol{p}_i}{2m_i}e^{i\mathbf{q}\boldsymbol{x}_i}+e_i e^{i\mathbf{q}\boldsymbol{x}_i}\frac{\boldsymbol{p}_i}{2m_i}\right) &= \sum_{i=1}^{N_\alpha}\boldsymbol{p}_i[\frac{\boldsymbol{p}_i}{2m_i},e_i e^{i\mathbf{q}\boldsymbol{x}_i}]_-+[\frac{\boldsymbol{p}_i}{2m_i},e_i e^{i\mathbf{q}\boldsymbol{x}_i}]_-\boldsymbol{p}_i \\
\mathbf{q}\sum_{i=1}^{N_\alpha}\left(e_i\frac{\boldsymbol{p}_i}{2m_i}e^{i\mathbf{q}\boldsymbol{x}_i}+e_i e^{i\mathbf{q}\boldsymbol{x}_i}\frac{\boldsymbol{p}_i}{2m_i}\right) &= \mathbf{q}\sum_{i=1}^{N_\alpha}\left(e_i\frac{\boldsymbol{p}_i}{2m_i}e^{i\mathbf{q}\boldsymbol{x}_i}+e_i e^{i\mathbf{q}\boldsymbol{x}_i}\frac{\boldsymbol{p}_i}{2m_i}\right),
\end{aligned} \tag{4.43}$$

where in the last line we used

$$[\frac{\boldsymbol{p}_i}{2m_i},e_i e^{i\mathbf{q}\boldsymbol{x}_i}]_- = \frac{e_i}{2m_i}\boldsymbol{q}e^{i\mathbf{q}\boldsymbol{x}_i} \tag{4.44}$$

and the fact that the kinetic energy of the neutron commutes with the charge operator. Assuming to add a two-body interaction, V to the Hamiltonian

$$H = \sum_i\frac{\boldsymbol{p}_i^2}{2m_i}+\sum_{i<j}V_{ij} \tag{4.45}$$

in general, it is not said a priori that $\left[\sum_{i<j}V_{ij},\sum_i\rho_i^{(1)}(\mathbf{q})\right]_- = 0$ and Eq. (4.39) can be no longer satisfied. Developing in powers of q/m, the one-body charge density separates into a "non-relativistic" part of order q^0 and a part containing the relativistic corrections, of order q^2. As shown in Ref. [77], to the lowest order the continuity equation separates into

$$\mathbf{q}\cdot\mathbf{j}_i^{(1)}(\mathbf{q}) = \left[\frac{\boldsymbol{p}_i^2}{2m_i},\rho_i^{(1)}(\mathbf{q})\right]_- \tag{4.46}$$

$$\mathbf{q}\cdot\mathbf{j}_{ij}^{(2)}(\mathbf{q}) = \left[V_{ij},\rho_i^{(1)}(\mathbf{q})+\rho_j^{(1)}(\mathbf{q})\right]_-. \tag{4.47}$$

Our two body-potential depends only on the relative momenta and power of this,

$$V_{ij}\propto\boldsymbol{p}_{ij} = \frac{m_i\boldsymbol{p}_j-m_j\boldsymbol{p}_i}{m_i+m_j}, \tag{4.48}$$

hence in order to verify the relation (4.47) it is sufficient to prove

$$[\sum_{ij}\boldsymbol{p}_{ij},e_{\alpha_1}e^{i\mathbf{q}\boldsymbol{x}_{\alpha_1}}+e_{\alpha_2}e^{i\mathbf{q}\boldsymbol{x}_{\alpha_2}}]_- = 0 \tag{4.49}$$

and then use the commutator propriety

$$\begin{aligned}
[\sum_{ij}(\boldsymbol{p}_{ij})^n,e_{\alpha_1}e^{i\mathbf{q}\boldsymbol{x}_{\alpha_1}}+e_{\alpha_2}e^{i\mathbf{q}\boldsymbol{x}_{\alpha_2}}]_- = \sum_{ij}\quad & \boldsymbol{p}_{ij}^{n-1}[\boldsymbol{p}_{ij},e_{\alpha_1}e^{i\mathbf{q}\boldsymbol{x}_{\alpha_1}}+e_{\alpha_2}e^{i\mathbf{q}\boldsymbol{x}_{\alpha_2}}]_- \\
+\quad & [\boldsymbol{p}_{ij},e_{\alpha_1}e^{i\mathbf{q}\boldsymbol{x}_{\alpha_1}}+e_{\alpha_2}e^{i\mathbf{q}\boldsymbol{x}_{\alpha_2}}]_-\boldsymbol{p}_{ij}^{n-1}.
\end{aligned} \tag{4.50}$$

Therefore,

$$[\frac{m_i \boldsymbol{p}_j - m_j \boldsymbol{p}_i}{m_i + m_j}, e_{\alpha_1} e^{i\boldsymbol{q}\boldsymbol{x}_{\alpha_1}} + e_{\alpha_2} e^{i\boldsymbol{q}\boldsymbol{x}_{\alpha_2}}]_- =$$
$$e_{\alpha_1} \frac{m_i}{m_i + m_j} [\boldsymbol{p}_j, e^{i\boldsymbol{q}\boldsymbol{x}_{\alpha_1}}]_- + e_{\alpha_2} \frac{m_i}{m_i + m_j} [\boldsymbol{p}_j, e^{i\boldsymbol{q}\boldsymbol{x}_{\alpha_2}}] - (i \leftrightarrow j)\,, \tag{4.51}$$

where we indicated with $(i \leftrightarrow j)$ the term that is obtained by exchanging i for j. From the above expression it is clear that summing over ij means that the contribution from V_{ij} will be eliminated by the contribution of V_{ji}. Since we have a three-body system one of the two indices i and j is equal to α_1 or α_2 or both at the same time. Let us look explicitly at the case, for example, when index j represents the first alpha particle $j = \alpha_1$ and i indicates the neutron $i = n$. From Eq. (4.51) one has that the only non zero term is given by

$$e_{\alpha_1} \frac{m_n}{m_n + m_{\alpha_1}} [\boldsymbol{p}_{\alpha_1}, e^{i\boldsymbol{q}\boldsymbol{x}_{\alpha_1}}]_- = e_{\alpha_1} \frac{m_n}{m_n + m_{\alpha_1}} \boldsymbol{q} e^{i\boldsymbol{q}\boldsymbol{x}_{\alpha_1}} \tag{4.52}$$

and this contribution will be deleted by the term with $j = n$ and $i = \alpha_1$.

Therefore one has that Eq. (4.47) is verified.

Note that in addition to the longitudinal currents constrained by the continuity equation ("model independent" currents), one can also introduce currents that are purely transverse and therefore do not contribute to Eq. (4.39) ("model dependent" currents) [77].

4.3 Photodisintegration cross-section

In Eq. (4.22) we calculated the T-matrix between an initial state of two α particles, a neutron, a photon and a final state of two α particles plus a neutron.

Now we are interested in calculating the T-matrix between an initial state, consisting of a photon and the ^{9}Be ground state ψ_i, and a final state called ψ_f,

$$T_{fi} = \langle \psi_f | - \int d^3x \frac{1}{4m_\alpha} \left(\partial_\mu \Psi\right)^\dagger (2ieA^\mu \Psi) + h.c. | \psi_i \rangle$$
$$= \frac{1}{2} \sum_{p_{\alpha_1} p_{\alpha_2} p_n} \sum_{p_{\alpha_1'} p_{\alpha_2'} p_{n'}} \langle \psi_f | p_{\alpha_1'} p_{\alpha_2'} p_{n'} \rangle \langle p_{\alpha_1'} p_{\alpha_2'} p_{n'} | - \int d^3x \frac{1}{4m_\alpha} \left(\partial_\mu \Psi\right)^\dagger (2ieA^\mu \Psi) + h.c. | p_{\alpha_1} p_{\alpha_2} p_n q \rangle$$
$$\times \langle p_{\alpha_1} p_{\alpha_2} p_n | \psi_i \rangle$$
$$= \langle \psi_f(\boldsymbol{p}_{\alpha_1'}, \boldsymbol{p}_{\alpha_2'}, \boldsymbol{p}_{n'}) | J^{(1)}_{\mu\,\alpha'\alpha} \cdot \frac{\epsilon^\mu_{q,\lambda}}{V^{1/2}\sqrt{2\omega_q}} | \psi_i(\boldsymbol{p}_{\alpha_1}, \boldsymbol{p}_{\alpha_2}, \boldsymbol{p}_n) \rangle\,, \tag{4.53}$$

where $\psi_{i,f}(p_{\alpha_1}, p_{\alpha_2}, p_n)$ indicates the nuclear wave functions in momentum space and in the last line we use the definitions (4.26),(4.27).

In case of real photons, one can examine only the transverse part of the transition amplitude, which assuming $\hat{q} \parallel \hat{z}$ is given by

$$T_{fi} = \langle \psi_f(\boldsymbol{p}_{\alpha_1'}, \boldsymbol{p}_{\alpha_2'}, \boldsymbol{p}_{n'})| \sum_{\lambda=\pm 1} \frac{J^{(1)}_{\lambda\ \alpha'\alpha}}{V^{1/2}\sqrt{2\omega_q}} |\psi_i(\boldsymbol{p}_{\alpha_1}, \boldsymbol{p}_{\alpha_2}, \boldsymbol{p}_n)\rangle\,, \tag{4.54}$$

with $J^{(1)}_{\lambda\ \alpha'\alpha}$ defined in Eq. (4.36).

We can rewrite the Eq. (4.54) in function of the Jacobi coordinate through the relations (3.1) with $N = 2$ and (3.35). In order to do this, we assume the neutron in the last position and we set,

$$\boldsymbol{\pi}_0 = \frac{m_n}{(m_n + 2m_\alpha)} \boldsymbol{P}_{cm} = 0\,, \tag{4.55}$$

i.e. the target nucleus initially at rest. Regarding the wave function we can separate the center of the mass motion as

$$\psi(\boldsymbol{p}_{\alpha_1}, \boldsymbol{p}_{\alpha_2}, \boldsymbol{p}_n) \quad \rightarrow \quad \psi(\boldsymbol{\pi}_1, \boldsymbol{\pi}_2) \frac{e^{-i\boldsymbol{\pi}_0\cdot\boldsymbol{\eta}_0}}{\sqrt{V}}\,, \tag{4.56}$$

being $\boldsymbol{\eta}_0 = \frac{(m_n+2m_\alpha)}{m_n} \boldsymbol{R}_{cm}$.

Making such change of variable, the Eq. (4.54) reads

$$\begin{aligned}
T_{fi} \quad = \quad & -\sqrt{\frac{2\pi}{3}} \frac{ie}{m_\alpha} \frac{(2\pi)^9}{V^3 V^{1/2}\sqrt{\omega_q}} \sqrt{\frac{m_n^3}{m_\alpha m_\alpha m_n}} \delta^3(\boldsymbol{\pi}_0' - \sqrt{\frac{m_n}{M}}\boldsymbol{q}) \\
& \times \Bigg[\delta^3(\boldsymbol{\pi}_1 - \boldsymbol{\pi}_1' + \sqrt{\frac{m_n^2}{2m_\alpha M}}\boldsymbol{q}) \delta^3(\boldsymbol{\pi}_2 - \boldsymbol{\pi}_2' - \sqrt{\frac{m_n}{2m_\alpha}}\boldsymbol{q}) \\
& \times \langle \psi_f(\boldsymbol{\pi}_1 + \sqrt{\frac{m_n^2}{2m_\alpha M}}\boldsymbol{q}, \boldsymbol{\pi}_2 - \sqrt{\frac{m_n}{2m_\alpha}}\boldsymbol{q})| (-\sqrt{\frac{m_\alpha}{2M}}\boldsymbol{\pi}_{1_\perp} - \sqrt{\frac{m_\alpha}{2m_n}}\boldsymbol{\pi}_{2_\perp})|\psi_i(\boldsymbol{\pi}_1, \boldsymbol{\pi}_2)\rangle \\
+ \quad & \delta^3(\boldsymbol{\pi}_1 - \boldsymbol{\pi}_1' + \sqrt{\frac{m_n^2}{2m_\alpha M}}\boldsymbol{q}) \delta^3(\boldsymbol{\pi}_2 - \boldsymbol{\pi}_2' + \sqrt{\frac{m_n}{2m_\alpha}}\boldsymbol{q}) \\
& \times \langle \psi_f(\boldsymbol{\pi}_1 + \sqrt{\frac{m_n^2}{2m_\alpha M}}\boldsymbol{q}, \boldsymbol{\pi}_2 + \sqrt{\frac{m_n}{2m_\alpha}}\boldsymbol{q})| (-\sqrt{\frac{m_\alpha}{2M}}\boldsymbol{\pi}_{1_\perp} + \sqrt{\frac{m_\alpha}{2m_n}}\boldsymbol{\pi}_{2_\perp})|\psi_i(\boldsymbol{\pi}_1, \boldsymbol{\pi}_2)\rangle \Bigg],
\end{aligned} \tag{4.57}$$

where $M = (2m_\alpha + m_n)$ and we indicated with $\boldsymbol{\pi}_{1,2_\perp}$ the transverse part of the $\alpha_{1,2}$ momenta.

The delta function of the center of mass momentum conservation indicates that in the laboratory frame where $\boldsymbol{\pi}_0 = 0$ the final momentum of the center of mass will be equal to the photon momentum $\sqrt{\frac{M}{m_n}}\boldsymbol{\pi}_0' = \boldsymbol{q}$. Moreover in this reference system the transition operator does not depend on the center of mass motion.

Now we can consider the limit for low $\boldsymbol{q}$ of Eq. (4.57), thus $\boldsymbol{\pi}_1' = \boldsymbol{\pi}_1 + \sqrt{\frac{m_n^2}{2m_\alpha M}}\boldsymbol{q} \sim \boldsymbol{\pi_1}$, $\boldsymbol{\pi}_2' = \boldsymbol{\pi}_2 + \sqrt{\frac{m_n}{2m_\alpha}}\boldsymbol{q} \sim \boldsymbol{\pi_2}$ and $\boldsymbol{\pi}_0 \sim \boldsymbol{\pi}_0' - \sqrt{\frac{m_n}{M}}\boldsymbol{q}$. The latter is the same assumption

used in the low-energy calculation via the Siegert theorem [79], which consists of replacing the total current operator by its limit for $\boldsymbol{q} \to 0$ [80]. This represents a very good approximation for energies well below the pion production threshold [81]. In our case, since the Cluster EFT is a low-energy theory, this condition can be considered fulfilled without adding any further constraints to the description.

Therefore Eq. (4.57) can be approximated as

$$\begin{aligned} T_{fi} &= \frac{(2\pi)^9}{V^3 V^{1/2}\sqrt{\omega_q}}\sqrt{\frac{m_n^3}{m_\alpha m_\alpha m_n}}\delta^3(\boldsymbol{\pi}_1-\boldsymbol{\pi}_1')\delta^3(\boldsymbol{\pi}_2-\boldsymbol{\pi}_2') \\ &\quad\times\delta^3(\boldsymbol{\pi}_0'-\boldsymbol{\pi}_0)\langle\psi_f(\boldsymbol{\pi}_1,\boldsymbol{\pi}_2)|\hat{O}_\perp(\boldsymbol{\pi}_1)|\psi_i(\boldsymbol{\pi}_1,\boldsymbol{\pi}_2)\rangle\,, \end{aligned} \tag{4.58}$$

where

$$\hat{O}_\perp(\boldsymbol{\pi}_1) = -\sqrt{\tfrac{2\pi}{3}}\tfrac{ie}{m_\alpha}(-\sqrt{\tfrac{2m_\alpha}{M}}\boldsymbol{\pi}_{1\perp})\,, \tag{4.59}$$

is the transverse current operator which written in function of single particle momenta corresponds to[1]

$$\hat{O}_\perp \equiv -\sqrt{\frac{2\pi}{3}}\frac{ie}{m_\alpha}(\boldsymbol{p}_{\alpha_1\perp}+\boldsymbol{p}_{\alpha_2\perp})\,. \tag{4.60}$$

The next step to derive the cross-section is to calculate the matrix S_{fi} as

$$\begin{aligned} S_{fi} = &-2\pi i\delta(E_f-E_i-\omega_q)\frac{(2\pi)^9}{V^3V^{1/2}\sqrt{\omega_q}}\sqrt{\frac{m_n^3}{m_\alpha m_\alpha m_n}} \\ &\times\delta^3(\boldsymbol{\pi}_0-\boldsymbol{\pi}_0')\delta^3(\boldsymbol{\pi}_2-\boldsymbol{\pi}_2')\delta^3(\boldsymbol{\pi}_1-\boldsymbol{\pi}_1') \\ &\times\langle\psi_f(\boldsymbol{\pi}_1,\boldsymbol{\pi}_2)|\hat{O}_\perp(\boldsymbol{\pi}_1)|\psi_i(\boldsymbol{\pi}_1,\boldsymbol{\pi}_2)\rangle\,, \end{aligned} \tag{4.61}$$

with E_i the initial internal energy of the nucleus and E_f the final one, namely we neglected the nuclear recoil $\frac{q^2}{2M}$.

The differential cross-section is then given by the Fermi golden rules as a function of the target density ρ_t and the incoming flux $\mathbf{J}_{in}$,

$$d\sigma(\omega_q) = \frac{1}{2\,(2J_i+1)}\sum_{i,f,\lambda=\pm1}\frac{1}{\rho_t\,|\mathbf{J}_{in}|}\frac{|S_{fi}|^2}{VT}\prod_{i=0}^{2}\frac{V d\boldsymbol{\pi}_i'}{(2\pi)^3}\sqrt{\frac{m_i}{m}}\,, \tag{4.62}$$

[1] From Eq. (4.60) and recalling Eq. (4.42), one can recognize the long wave approximation used in the Siegert theorem approach.

The reaction examined here involves the absorption of a single photon ($|\mathbf{J}_{in}| = \frac{1}{V}$) on a single nucleus ($\rho_t = \frac{1}{V}$). Therefore using the relations,

$$\left[(2\pi)^3\delta^{(3)}(x)\right]^2 = (2\pi)^3 V\delta^{(3)}(x)\,, \tag{4.63}$$

$$[(2\pi)\delta(E)]^2 = 2\pi T\delta(E)\,, \tag{4.64}$$

and integrating on the $\boldsymbol{\pi}_i'$, one obtains that each delta function present in Eq. (4.61) eliminates an integral on the final momenta.
Finally, the expression of the cross-section results

$$\sigma(\omega_q) = \frac{2\pi}{2(2J_i+1)\omega_q}\delta(E_f - E_i - \omega_q)\sum_{i,f,\lambda=\pm1}|\langle\psi_f(\boldsymbol{\pi}_1,\boldsymbol{\pi}_2)|\hat{O}_\perp(\boldsymbol{\pi}_1)|\psi_i(\boldsymbol{\pi}_1,\boldsymbol{\pi}_2)\rangle|^2\,. \tag{4.65}$$

The Eq. (4.65) can be rewritten in the following form

$$\sigma(\omega_q) = \frac{2\pi}{2(2J_i+1)\omega_q}r(\omega_q) \tag{4.66}$$

defining the response function $r(\omega_q)$ as

$$r(\omega_q) = \sum_{i,f,\lambda=\pm1}|\langle\psi_f(\boldsymbol{\pi}_1,\boldsymbol{\pi}_2)|\hat{O}_\perp(\boldsymbol{\pi}_1)|\psi_i(\boldsymbol{\pi}_1,\boldsymbol{\pi}_2)\rangle|^2\delta(E_f - E_i - \omega_q)\,. \tag{4.67}$$

The next Chapter will focus on calculating the quantity shown above.

Chapter 5

The Lorentz Integral Transform

Once the current operator and ground state are calculated, a procedure for calculating all possible final states would, in principle, be required. This Chapter focuses on the description of the Lorentz Integral Transform (LIT) approach for the computation of the response function associated with inclusive processes. In Section 5.1 we present a general introduction to the LIT method, emphasizing its importance in the calculation of nuclear reactions and in particular in our case to calculate the cross-section of the ^{9}Be photodisintegration. In Section 5.2 we explain how the LIT allows us to calculate the response function based only on the knowledge of the ground state energy, wave function and of the current operator. In Section 5.2, we discuss the implementation methods for the computation of the LIT and in Section 5.4 the issues related to the inversion of the transform. Finally in Section 5.5 the application of the LIT method to ^{9}Be photodisintegration reaction is presented. The general approach to the LIT shown in this Chapter follow the lines of Ref. [34].

5.1 Introduction to the LIT

The ab initio calculation of the cross-section for a many-body nuclear process is a very challenging problem. By ab initio we mean a computation that requires an Hamiltonian $\hat{H}$ and the kinematics of the reaction as input only, and treats all the chosen degrees of freedom of the many-body system explicitly. Often the final states of a nuclear reaction belong to the continuum and the wave function for these states could be calculable only with approximations even for a few-body system. The approximations, are particularly unsatisfactory in cases where experiments cannot be performed, such as for some nuclear reactions of astrophysical significance. On the other hand, often the calculation of the cross-sections must be precise as it is the aim to test the model inputs like the potential and the degrees of freedom used. This situation is typical of nuclear physics as well as of any non-fundamental theory, where we would like to test the reliability of the effective degrees of freedom in the Hamiltonian and of the interaction. In this case, the comparison between theoretical results and experimental data is expected to provide this information, but the comparison risks be inconclusive if the quality of the applied approximation is not under control. In both cases described above, an accurate ab initio calculation may be required.

The difficulty in calculating a cross-section with many body involving continuous states can be understood if we consider that at a given energy the wave function of the system can have many different components (channels) corresponding to all its different fragmentations. Already in a rather small system of four constituents the two-, three- and four-body break-up channels contribute to the energies beyond the so-called four-body break-up threshold. The task consists in finding the solution of the four-body Schrödinger equation with the appropriate boundary conditions and the implementation of the latter constitutes the main obstacle to the practical solution of the problem. The great advantage of the LIT method is that it allows to avoid all the complications of a continuous calculation, reducing all the difficulties to those of a typical bound state problem.

In general, when we approach the calculation of a cross-section, two different cases are possible. The first one is when we are interested in a specific channel of that reaction, hence to a particular final state of the system under consideration, these are the exclusive reactions. The other possible case occurs when we want to study reactions containing all the possible final states. In this case we speak of an inclusive reaction and here the LIT approach gives the major simplification to the calculation [34]. In this work we will use the LIT approach for the inclusive reactions. Our purpose is to calculate the photodisintegration of the ^{9}Be nucleus, given by:

$$^9\mathrm{Be} + \gamma \rightarrow \alpha + \alpha + n. \tag{5.1}$$

Although in reaction (5.1) we consider a specific fragmentation channel for ^{9}Be, one can use the LIT method for inclusive processes, since it is the only open channel at low energy. In fact, since we are describing the internal structure of ^{9}Be as a $\alpha\alpha n$ configuration in a Cluster EFT framework, the photodisintegration cross-section will be analysed in the same energy range in which this theory holds, specifically, energies from the $\alpha\alpha n$ threshold (−1.572 MeV) to the α-particle separation energy ($\simeq$ 20 MeV).

5.2 LIT approach for inclusive processes

In general for perturbation induced reactions the following quantity must be calculated [34]

$$r(E) = \sum\!\!\!\!\!\!\int d\lambda \langle \Psi_0 | \hat{O} | \Psi_\lambda \rangle \langle \Psi_\lambda | \hat{O}' | \Psi_0 \rangle \delta (E_\lambda - E) \,, \tag{5.2}$$

where $\hat{O}, \hat{O}'$ are transition operators, Ψ_0 the ground state wave function and Ψ_λ are solutions to the equation

$$\left(\hat{H} - E_\lambda\right) |\Psi_\lambda\rangle = 0 \,, \tag{5.3}$$

with $\hat{H}$ the Hamiltonian of the system.
The set $|\Psi_\lambda\rangle$ is assumed to be complete and orthonormal,

$$\sum\!\!\!\!\!\!\int d\lambda \, |\Psi_\lambda\rangle \langle\Psi_\lambda| = 1 \, . \tag{5.4}$$

The integration and summation here and in (5.2) go over all discrete and continuum states of the Hamiltonian. If $\hat{O} = \hat{O}'$, the quantity (5.2) represents a response function of the type seen in Eq. (4.67).

When the energy E and the number of particles in a system increase the direct calculation of the quantity $r(E)$ becomes infeasible. The difficulty is related to the fact that in these cases a great number of continuum spectrum states $|\Psi_\lambda\rangle$ contribute to $r(E)$ and the structure of these states is very complicated. In order to overcome this difficulty we present here an approach that is based on the closure property of the Hamiltonian eigenstates. Let us define $|Q\rangle = \hat{O}\,|\Psi_0\rangle\,, |Q'\rangle = \hat{O}'\,|\Psi_0\rangle$.
We suppose that the norms $\langle Q \mid Q\rangle$ and $\langle Q' \mid Q'\rangle$ are finite. We consider an integral transform

$$\Phi(\sigma) = \sum\!\!\!\!\!\!\int K(\sigma, E) r(E) dE \, , \tag{5.5}$$

with a smooth kernel K. This yields

$$\Phi(\sigma) = \sum\!\!\!\!\!\!\int d\lambda \, \langle Q \mid \Psi_\lambda\rangle \, K\left(\sigma, E_\lambda\right) \left\langle \Psi_\lambda \mid Q'\right\rangle \tag{5.6}$$

$$= \sum\!\!\!\!\!\!\int d\lambda \left\langle Q|\hat{K}(\sigma, \hat{H})|\Psi_\lambda\right\rangle \left\langle \Psi_\lambda \mid Q'\right\rangle \, . \tag{5.7}$$

Using the closure property (5.4) one obtains

$$\Phi(\sigma) = \left\langle Q|\hat{K}(\sigma, \hat{H})|Q'\right\rangle \, . \tag{5.8}$$

With a proper choice of the kernel K the right-hand side of (5.8) may be calculated using bound-state type methods. Once $\Phi(\sigma)$ is available, the Eq. (5.5) can be solved to obtain $r(E)$ via an inversion of the transform.

The choice of the kernel $K(\sigma, E)$ is such that both the calculation of $\Phi(\sigma)$ and the inversion of (5.5) are possible. We choose [34]

$$K(\sigma, E) = \frac{1}{\left(E - \sigma^*\right)\left(E - \sigma\right)} \, . \tag{5.9}$$

For convenience we define

$$\sigma = E_0 + \sigma_R + i\sigma_I \, , \tag{5.10}$$

where E_0 is the ground state energy, and $\sigma_I \neq 0$.
Hence $K(\sigma, E)$ is a Lorentzian function centred at $E_0 + \sigma_R$, having σ_I as a half width

$$K\left(\sigma_R, \sigma_I, E\right) = \frac{1}{\left(E - E_0 - \sigma_R\right)^2 + \sigma_I^2} . \tag{5.11}$$

Then the integral transform (5.5) becomes

$$L(\sigma_R, \sigma_I) = \frac{\sigma_I}{\pi} \int\!\!\!\!\!\!\diagup dE \frac{r(E)}{(E - E_0 - \sigma_R)^2 + \sigma_I^2}. \tag{5.12}$$

Since the Lorentzian is a representation of the delta function for convenience we normalize to one. Notice that in the limit $\sigma_I \to 0$ $L(\sigma_R)$ coincides with $r(e)$. Here and in the following the integral transform $\Phi(\sigma)$ with a Lorentz kernel is denoted by $L(\sigma_R, \sigma_I)$. Using the definitions (5.8), (5.9) it is easy to show that the quantity (5.12) may be represented as

$$L(\sigma_R, \sigma_I) = \left\langle \tilde{\Psi} \mid \tilde{\Psi}' \right\rangle , \tag{5.13}$$

where the 'LIT functions' $\tilde{\Psi}$ and $\tilde{\Psi}'$ are given by

$$|\tilde{\Psi}\rangle = \left(\bar{H} - E_0 - \sigma_R - i\sigma_I\right)^{-1} \hat{O} |\Psi_0\rangle , \tag{5.14}$$

$$\left|\tilde{\Psi}'\right\rangle = \left(\hat{H} - E_0 - \sigma_R - i\sigma_I\right)^{-1} \hat{O}' |\Psi_0\rangle . \tag{5.15}$$

These functions are solutions to the inhomogeneous equations

$$\left(\hat{H} - E_0 - \sigma_R - i\sigma_I\right) |\tilde{\Psi}\rangle = \hat{O} |\Psi_0\rangle , \tag{5.16}$$

$$\left(\hat{H} - E_0 - \sigma_R - i\sigma_I\right) \left|\tilde{\Psi}'\right\rangle = \hat{O}' |\Psi_0\rangle . \tag{5.17}$$

The solutions are unique, since the homogeneous equations have only the trivial solution being the eigenvalues of the Hamiltonian real.

Let us suppose that $\hat{O}' = \hat{O}$. In this case $L(\sigma)$ equals to $\langle \tilde{\Psi} \mid \tilde{\Psi} \rangle$. Since for $\sigma_I \neq 0$ the integral in (5.12) does exist, the norm of $|\tilde{\Psi}\rangle$ is finite. This implies that $|\tilde{\Psi}\rangle$ is a localized function. Consequently, (5.16) and (5.17) can be solved with bound state type methods.

If the Hamiltonian is rotationally invariant it is useful to expand $\hat{O}|\Psi_0\rangle$ and $\hat{O}'|\Psi_0\rangle$ over states possessing given values of the angular momentum J and its projection M. Then the whole calculation may be done in separate subspaces of states belonging to given J and M, see later in the text Section 5.3.3. Furthermore the calculations will be M independent, as we will explicitly see in Section 5.5.

5.3 Implementation method

Before analyzing how to implement the LIT method it is useful to try to understand how to separate in $r(E)$, defined in (5.2), the discrete and continuum spectrum contributions, one may write

$$L(\sigma_R,\sigma_I) = \frac{\sigma_I}{\pi}\left(\sum_n \frac{r_n}{(\sigma_R-e_n)^2+\sigma_I^2} + \int_{e_{th}}^{\infty} de \frac{r(e)}{(\sigma_R-e)^2+\sigma_I^2}\right) \tag{5.18}$$

$$\equiv L_D(\sigma_R,\sigma_I) + L_C(\sigma_R,\sigma_I)\ , \tag{5.19}$$

where we have introduced the excitation energy $e = E - E_0$ and the discrete excitation energies $e_n = E_n - E_0$ with r_n representing the corresponding contributions to the function r

$$r_n = |\langle Q \mid \Psi_n\rangle|^2 . \tag{5.20}$$

The second term in (5.19) is related to the continuum part of the spectrum with e_{th} representing the continuum threshold energy ($e_n < e_{th}$) and

$$r(e) = \int_{\varepsilon_{th}}^{\infty} dE_\lambda |\langle Q \mid \Psi_\lambda\rangle|^2 \delta(E_\lambda - E)\ . \tag{5.21}$$

The aim of the LIT method is to obtain both r_n and $r(e)$ solving (5.19) using $L(\sigma_R,\sigma_I)$, calculated at a fixed σ_I in a range of σ_R values, as an input.

One way to get the contributions from the discrete levels in Eq. (5.19) is to calculate these levels explicitly to obtain $|\Psi_n\rangle$ and e_n, then evaluate directly the overlaps (5.20) and their contributions to the response function. Alternatively one can extract these contributions by calculating the transform $L = \langle \tilde{\Psi} \mid \tilde{\Psi}\rangle$ at a very small σ_I value for a range of σ_R values between zero and e_{th}. After calculating $L(\sigma_R,\sigma_I)$ from (5.13) and subtracting the discrete contributions from it, the following integral equation has to be solved to obtain $r(e)$

$$L_C(\sigma_R,\sigma_I) = \frac{\sigma_I}{\pi}\int_{e_{th}}^{\infty} de \frac{r(e)}{(\sigma_R-e)^2+\sigma_I^2}\ . \tag{5.22}$$

To simplify the notation in the following we will omit the σ_I dependence and use $L(\sigma)$ to indicate its continuum part only.

Let us comment on the choice of the σ_I and σ_R values. The resulting response function $r(e)$ should be independent of the σ_I value, however the rate of convergence of the LIT may be influenced by this choice. Smaller σ_I values are preferable, since they reproduce better the structure details of the response function. On the other hand, when σ_I decreases one approaches the scattering regime in Eq. (5.16), which makes it harder to obtain L with bound-state type methods. Therefore performing a calculation with too small a value of σ_I is not expedient. All these aspects discussed here from a theoretical point of view will then be better understood in practice in the final Chapter 6, where we will show the results of the LIT calculation for the ^{9}Be

photodisintegration. Regarding the σ_R values for which (5.22) is to be solved, if one assumes that the spectrum $r(e)$ to be obtained extends over the range $e_{th} \leq e \leq e_{\max}$ then it is reasonable to employ $L(\sigma_R)$ approximately in the range $e_{th} - \sigma_I \leq \sigma_R \leq e_{max} + \sigma_I$. At such conditions complete information on $r(e)$ contained in $L(\sigma_R)$ is used.

5.3.1 Calculation of the LIT via the eigenvalue method

As we have shown in Section 5.2 the LIT method can be used to reformulate a scattering problem as a Schrödinger-like equation. We can therefore use an expansion on proper a basis in the same way we proceeded in the bound state problem. We want to calculate the following overlap

$$\begin{aligned} L(\sigma) &= \left\langle \tilde{\Psi} \mid \tilde{\Psi} \right\rangle \\ &= \frac{\sigma_I}{\pi} \left\langle Q \left| \frac{1}{\left(\hat{H} - E_0 - \sigma_R + i\sigma_I\right)} \frac{1}{\left(\hat{H} - E_0 - \sigma_R - i\sigma_I\right)} \right| Q' \right\rangle , \end{aligned} \tag{5.23}$$

where $|Q\rangle$ contains the information about the type of reaction one is considering. We write now $|\tilde{\Psi}\rangle$ as expansion over N localized basis states. Denoting the eigenvectors $|\Psi_\lambda\rangle$ and the eigenvalues ϵ_λ, resulting from the diagonalization of the Hamiltonian represented on the chosen basis, the expansions of our localized LIT functions will be

$$|\tilde{\Psi}\rangle = \sum_{\lambda}^{N} \frac{\langle \Psi_\lambda \mid Q \rangle}{\epsilon_\lambda - E_0 - \sigma_R - i\sigma_I} |\Psi_\lambda\rangle \, . \tag{5.24}$$

Substitution of (5.24) into (5.23) yields the following expression for the LIT,

$$L(\sigma) = \sum_{\lambda} \frac{|\langle \Psi_\lambda \mid Q \rangle|^2}{(\epsilon_\lambda - E_0 - \sigma_R)^2 + \sigma_I^2} \, . \tag{5.25}$$

From (5.25) it is clear that $L(\sigma)$ is a sum of Lorentzian. If the continuum starts at $E = e_{th}$, the inversion of the LIT contributions from the states with $\epsilon_\lambda < e_{th}$ gives the discrete part of the spectrum, whereas the inversion of the rest gives its continuum part. The gap between the eigenvalues with $\epsilon_\lambda > e_{th}$ depends on the chosen basis. To obtain an accuracy in the inversion procedure one needs to reach the regime when one has a sufficient number of levels ϵ_λ.

5.3.2 Calculation of the LIT via the Lanczos algorithm

In this Section a second strategy to practically solve the LIT is described. This approach utilizes the Lanczos algorithm [58] to express the LIT as a continuous fraction. The great advantage of using this algorithm is that only a relatively small number of Lanczos steps are required to obtain an accurate LIT. When the number of particles in the system under consideration increases and, thus, the number of basis

states grows very rapidly, the Lanczos method seems to be the only mean to calculate the LIT. Assuming that the source state $|Q\rangle$ is real, the LIT can be expressed as,

$$L(\sigma) = -\frac{1}{\pi}\,\mathrm{Im}\left\{\left\langle Q\left|\frac{1}{\sigma_R + i\sigma_I + E_0 - \hat{H}}\right|Q\right\rangle\right\}. \tag{5.26}$$

One can reformulate the above expression as follows,

$$L(\sigma) = -\frac{1}{\pi}\,\mathrm{Im}\left\{\left\langle Q\left|\frac{1}{z - \hat{H}}\right|Q\right\rangle\right\}, \tag{5.27}$$

with $z = E_0 + \sigma_R + i\sigma_I$.

In the limit $\sigma_I \to 0$ Eq. (5.27) is the well known relation between response function and dynamic polarization [82].

It is interesting to note that even in the case of $Q \neq Q'$

$$\begin{aligned}
&\langle Q|\frac{1}{z - \hat{H}}|Q'\rangle = \\
&\frac{1}{4}\left(\left(\langle Q| + \langle Q'|\right)\frac{1}{z - \hat{H}}\left(|Q\rangle + ||Q'\rangle\right)\right) - \frac{1}{4}\left(\left(\langle Q| - \langle Q'|\right)\frac{1}{z - \hat{H}}\left(|Q\rangle - |Q'\rangle\right)\right) \\
- &\frac{i}{4}\left(\left(\langle Q| + i\langle Q'|\right)\frac{1}{z - \hat{H}}\left(|Q\rangle + i|Q'\rangle\right)\right) \\
+ &\frac{i}{4}\left(\left(\langle Q| - i\langle Q'|\right)\frac{1}{z - \hat{H}}\left(|Q\rangle - i|Q'\rangle\right)\right),
\end{aligned} \tag{5.28}$$

one can reduce to analyse only the symmetric case $|Q'\rangle = |Q\rangle$.
The application of the Lanczos algorithm to the LIT,

$$L(\sigma) = -\frac{1}{\pi}\,\mathrm{Im}\left\{\left\langle Q\left|\frac{1}{\sigma_R + i\sigma_I + E_0 - \hat{H}}\right|Q\right\rangle\right\}, \tag{5.29}$$

starts by choosing the normalized source vector

$$|\phi_0\rangle = \frac{|Q\rangle}{\sqrt{\langle Q \mid Q\rangle}} \tag{5.30}$$

as the pivot for the Lanczos basis, see Appendix B.
With the help of these definitions one can rewrite $L(\sigma)$ as

$$L(\sigma) = -\frac{1}{\pi}\,\mathrm{Im}\left\{\left\langle \phi_0\left|\frac{1}{z - \hat{H}}\right|\phi_0\right\rangle\right\}. \tag{5.31}$$

Therefore the LIT depends on the matrix element

$$x_{00} = \left\langle \phi_0\left|\frac{1}{z - \hat{H}}\right|\phi_0\right\rangle. \tag{5.32}$$

This matrix element can be calculated applying Cramer's rule to the solution of the linear system [83]

$$\sum_n (z - \hat{H})_{mn} x_{n0} = \delta_{m0} \tag{5.33}$$

(where $x_{n0} = \left\langle \phi_n \left| \frac{1}{z-\hat{H}} \right| \phi_0 \right\rangle$)which arises from the identity

$$(z - \hat{H})(z - \hat{H})^{-1} = I \tag{5.34}$$

on the Lanczos basis $\{|\phi_i\rangle\, ; i = 0, \ldots, n-1\}$.
Using Cramer's rule one gets

$$x_{00} = \frac{\det(M_{00})}{\det(z - \hat{H})}, \tag{5.35}$$

where

$$M_{00} = \begin{pmatrix} 1 & -b_1 & 0 & \cdots \\ 0 & z - a_i & -b_2 & \cdots \\ 0 & -b_2 & z - a_2 & \cdots \\ \vdots & \vdots & \vdots & \ddots \end{pmatrix} \tag{5.36}$$

and the a_n and b_n are the Lanczos coefficients. Defining D_i as the matrix obtained by removing the first i rows and i columns from $(z - \hat{H})$, one find that $D_0 = (z - \hat{H})$,

$$\det(M_{00}) = \det(D_1) \tag{5.37}$$

and

$$\det(D_0) = (z - a_0)\det(D_1) - b_1^2 \det(D_2)\ . \tag{5.38}$$

Thus one has

$$x_{00} = \frac{1}{z - a_0 - b_1^2 \frac{det(D_2)}{det(D_1)}}\ . \tag{5.39}$$

The recurrence relation (5.39), is valid for any sub matrix D_i. In this way x_{00} can be written as a continued fraction containing the Lanczos coefficients a_i and b_i, thus also the LIT becomes a function of the Lanczos coefficients like

$$L(\sigma) = -\frac{1}{\pi} \mathrm{Im} \left\{ \frac{\langle Q \mid Q \rangle}{z - a_0 - \cfrac{b_1^2}{z - a_1 - \cfrac{b_2^2}{z - a_2 - b_{3\cdots}^2}}} \right\}. \tag{5.40}$$

5.3.3 Transition to different channels

A special feature, that we will need later to analyze our cross-section, is the calculation of the LIT between states with defined J and M values. Let us now consider the LIT expressed in the following form

$$L(\sigma) = -\frac{1}{\pi} \mathrm{Im} \left(\left\langle Q \left| \frac{1}{z - \hat{H}} \right| Q \right\rangle \right). \tag{5.41}$$

We want to show that in order to calculate a transition to different channels with distinct value of J and M, the LIT can be calculated in each channel separately and

then summed up. The transition state $|Q\rangle$ can be written as

$$|Q\rangle = \hat{O}\,|\Psi_0\rangle = \begin{pmatrix} Q_a \\ 0 \\ 0 \\ \cdots \end{pmatrix} + \begin{pmatrix} 0 \\ Q_b \\ 0 \\ \cdots \end{pmatrix} + \begin{pmatrix} 0 \\ 0 \\ Q_c \\ \cdots \end{pmatrix} + \cdots$$
$$\equiv |Q_a\rangle + |Q_b\rangle + |Q_c\rangle + \cdots . \tag{5.42}$$

The different channels are defined by different good quantum numbers, which can be in this instance J and M. Hence they are not connected with each other through the Hamiltonian of the system

$$\left\langle Q_i|\hat{H}|Q_j\right\rangle = \delta_{ij}\left\langle Q_i|\hat{H}|Q_i\right\rangle , \tag{5.43}$$

and also

$$\left\langle Q_i|\frac{1}{z-\hat{H}}|Q_j\right\rangle = \delta_{ij}\left\langle Q_i|\frac{1}{z-\hat{H}}|Q_i\right\rangle . \tag{5.44}$$

Therefore

$$\begin{aligned} L(\sigma) &= -\frac{1}{\pi}\,\mathrm{Im}\left(\sum_{i,j}\left\langle Q_i\left|\frac{1}{z-\hat{H}}\right|Q_j\right\rangle\right) \\ &= \sum_i -\frac{1}{\pi}\,\mathrm{Im}\left(\left\langle Q_i\left|\frac{1}{z-\hat{H}}\right|Q_i\right\rangle\right) \\ &\equiv \sum_i L(\sigma)_i . \end{aligned} \tag{5.45}$$

A better strategy is to keep the LIT contributions of each channel separate and sum them up only after inversions of the integral transforms.

5.4 Inversion of the LIT

A crucial part of the LIT method is then the inversion of the integral transform. This inversion has to be made with care, since it is unstable with respect to high frequency oscillations, in this sense the LIT inversion problem belongs to the class of so-called ill posed problems. In [84] the mathematical aspects of such problems are studied. The 'standard' LIT inversion method consists in the following ansatz for the response function [34]

$$r\left(e'\right) = \sum_{n=1}^{N_{\max}} c_n \chi_n\left(e', \alpha_i\right) , \tag{5.46}$$

with $e' = e - e_{th}$, where e_{th} is the threshold energy for the break-up into the continuum. The χ_n are given functions with parameters α_i. A basis set often used for LIT

inversions is

$$\chi_n\left(e', \alpha_i\right) = e'^{\alpha_1} \exp\left(-\frac{\alpha_2 e'}{n}\right). \tag{5.47}$$

Regarding the parameters α_i, α_2 is a non-linear variational parameter while α_1 describes the proper threshold behaviour. The latter can be obtained from the case in which the short-range interaction between fragments is absent or, alternatively, one may include this one in the least-square fit. Substituting this expansion into the right side of (5.22) one obtains

$$L\left(\sigma_R\right) = \sum_{n=1}^{N_{\max}} c_n \bar{\chi}_n\left(\sigma_R, \alpha_i\right), \tag{5.48}$$

where

$$\bar{\chi}_n\left(\sigma_R, \alpha_i\right) = \frac{\sigma_I}{\pi} \int_0^\infty de' \frac{\chi_n\left(e', \alpha_i\right)}{\left(e' - \sigma_R\right)^2 + \sigma_I^2}. \tag{5.49}$$

For given α_i the linear parameters c_n are determined from a least-square best fit of Eq. (5.48) to the calculated $L\left(\sigma_R\right)$ of Eq. (5.13).
For each value of $N_{\max}$ the best fit is selected and then the procedure is repeated for $N'_{\max} = N_{\max} + 1$ until the stability of the inverted response is reached. A further increase, beyond a certain saturation value, of N_{max} would favour the appearance of random oscillations. This is due to the accuracy of Eq. (5.47) as a LIT estimate, which results not so elevated to prevent the case where a randomly oscillating $r(e)$ fits the LIT better than a smoother result. Varying the α_i parameters is equivalent to trying different basis sets and usually finding a proper basis is not so problematic.

Nevertheless in the presence of narrow resonances, an explicit resonance should be added to the basis [85]. In general, a Lorentzian with free parameters γ and ω_R, $\left[(\omega - \omega_R)^2 + (\gamma/2)^2\right]^{-1}$, is used. If the LIT is calculated with a sufficiently small σ_I, then the position, width, and strength of the resonance can still be found in the inversion.

5.5 ^{9}Be photodisintegration

Our aim is to calculate the ^{9}Be photodisintegration cross-section of Eq. (4.65) using the LIT method.

As we have seen in the Section 5.3, both via eigenvalues and Lanczos method one has to represent $|Q\rangle = \hat{O}_\perp|\Psi_i\rangle$, where $|\Psi_i\rangle$ indicates the initial ground state, as a vector on $\varphi_a^{N'}$

$$|Q_a\rangle = \sum_{N'} |\varphi_a^{N'}\rangle\langle\varphi_a^{N'}|\hat{O}_\perp|\Psi_i\rangle, \tag{5.50}$$

being $\varphi_a^{N'}$ a complete basis of the considered a channel.
In each of the two cases it is necessary to calculate the following quantity,

$$\langle\varphi_a^{N'}|\hat{O}_\perp|\Psi_i\rangle. \tag{5.51}$$

Therefore we can start to see how to implement the matrix element written in Eq. (5.51). The transverse current operator in function of single particle momenta is given in Eq. (4.60) and we already showed in Eq. (4.59) as, if the neutron is the third particle, setting $\pi_0 = 0$ the operator is proportional only to $\boldsymbol{\pi}_1$. It should be emphasized that the form of the Jacobi coordinate operator also depends on the order of the three particles. In our ordering the neutron is in the first position and the two alpha particles at the last positions, hence in Eq. (3.35) $\boldsymbol{p}_1$, m_1 correspond to the momentum and mass of the neutron, $\boldsymbol{p}_2$, $\boldsymbol{p}_3$ to the α momenta, m_2, m_3 to the α masses. In this case, it is easy to prove that:

$$\begin{aligned}\hat{O}_\perp &= -\sqrt{\tfrac{2\pi}{3}}\tfrac{ie}{m_\alpha}\Big(\sqrt{\tfrac{m_\alpha}{m_\alpha+m_n}}\boldsymbol{\pi}_{2\perp} \\ &\quad +\sqrt{\tfrac{m_\alpha m_n}{(m_\alpha+m_n)(2m_\alpha+m_n)}}\boldsymbol{\pi}_{1\perp}\Big)\,. \end{aligned} \tag{5.52}$$

However with the help of permutation matrices, seen in Section 3.5, it is always possible to move the neutron to the third position and use the expression (4.59).

A third and final option is based on the same mechanism already used for the two-body potential. Using the relations between the Jacobi and relative momenta one finds,

$$\boldsymbol{\pi}_2 = \sqrt{\frac{m_n(m_n+m_\alpha)}{m_n m_\alpha}}\boldsymbol{p}_{12}\,, \qquad \boldsymbol{\pi}_1 = \sqrt{\frac{m_n(m_\alpha+m_n)}{m_\alpha(2m_\alpha+m_n)}}\left(\boldsymbol{p}_{13}+\frac{2m_\alpha}{m_\alpha+m_n}\boldsymbol{p}_{23}\right). \tag{5.53}$$

From Eq. (5.52) the operator is written in terms the relative momenta as

$$\begin{aligned}\hat{O}_\perp &= -\sqrt{\frac{2\pi}{3}}\frac{ie}{m_\alpha}\left(\sqrt{\frac{m_\alpha}{m_\alpha+m_n}}\boldsymbol{\pi}_{2\perp}+\sqrt{\frac{m_\alpha m_n}{(m_\alpha+m_n)(2m_\alpha+m_n)}}\boldsymbol{\pi}_{1\perp}\right) \\ &= -\sqrt{\frac{2\pi}{3}}\frac{ie}{m_\alpha}\left(\boldsymbol{p}_{12_\perp}+\frac{m_n}{(2m_\alpha+m_n)}\left(\boldsymbol{p}_{13_\perp}+\frac{2m_\alpha}{2m_\alpha+m_n}\boldsymbol{p}_{23_\perp}\right)\right), \end{aligned} \tag{5.54}$$

hence it can be seen as the sum of two-body operators

$$\hat{O}_\perp = \sqrt{\frac{m_\alpha}{m_\alpha+m_n}}(\hat{O}_{12})_\perp + \sqrt{\frac{m_\alpha}{m_\alpha+m_n}}\frac{m}{(2m_\alpha+m_n)}\left((\hat{O}_{13})_\perp+\frac{2m_\alpha}{2m_\alpha+m_n}(\hat{O}_{23})_\perp\right). \tag{5.55}$$

With the same mechanism of permutations already seen in Section 3.5 we limit ourselves to considering $(\hat{O}_{12})_\perp$ and the other operators will be calculated starting from the latter by multiplying by the appropriate permutation of particles.
Here we follow this last formulation[1] considering therefore only the operator $(\hat{O}_{12})_\perp$ given by,

$$(\hat{O}_{12})_\perp = -\sqrt{\tfrac{2\pi}{3}}\tfrac{ie}{m_\alpha}\pi_2(Y_1^1(\theta_2,\phi_2)+Y_1^{-1}(\theta_2,\phi_2))\,, \tag{5.56}$$

[1] As further check we have implemented all three operator formulations obtaining clearly the same results.

in hyperspherical coordinates π_2 is given by,

$$\pi_2 = Q \sin\alpha_2 \,. \tag{5.57}$$

Let us focus on the calculation of the operator matrix element seen in Eq. (5.51),

$$\langle \varphi_a^{N'} | (\hat{O}_{12})_\perp | \varphi^N \rangle = -\sqrt{\frac{2\pi}{3}} \frac{ie}{m_\alpha} \sum_{\lambda=\pm 1} \langle g_{n'}(Q) | Q | g_n(Q) \rangle \, \langle [K'] | Y_1^\lambda(\theta_N, \phi_N) \sin\alpha_N | [K] \rangle \,, \tag{5.58}$$

here $\varphi_a^{N'}$ and φ^N correspond to the basis of final and initial state.

In order to calculate the hypermomentum part of the transition matrix element one has to solve numerically the following integral

$$\langle g_{n'}(Q) | Q | g_n(Q) \rangle = \sqrt{\frac{n! n'!}{\beta^{\nu+1} \beta'^{\nu+1} (n+\nu)! \, (n'+\nu)!}} \int_0^\infty L_{n'}^\nu \left(\frac{Q}{\beta'} \right) Q L_n^\nu \left(\frac{Q}{\beta} \right) Q^\nu e^{-\frac{Q}{2\beta}} e^{-\frac{Q}{2\beta'}} dQ \tag{5.59}$$

while the angular part is given by

$$\begin{aligned}
\langle [K'] | Y_1^\lambda(\theta_N, \phi_N) \sin\alpha_N | [K] \rangle = & \int_0^{\pi/2} d\alpha_N \, (\sin\alpha_N)^{2+l'_N+l_N} \, (\cos\alpha_N)^{3N-5+2K_{N-1}} \\
& \times \mathcal{N}_N \left(K'_N; l'_N, K_{N-1} \right) P_{\mu'_N}^{[l_N+1/2, K'_{N-1}+(3N-5)/2]} (\cos 2\alpha_N) \\
& \times \mathcal{N}_N \left(K_N; l_N, K_{N-1} \right) P_{\mu_N}^{[l_N+1/2, K_{N-1}+(3N-5)/2]} (\cos 2\alpha_N) \\
& \times \langle J', M' | Y_1^\lambda(\theta_N, \phi_N) | JM \rangle \\
& \mathcal{N}_N \left(K'_{Ni} l'_N, K_{N-1} \right) \mathcal{N}_N \left(K_N; l_N, K_{N-1} \right) \\
& \times \quad 2^{-\frac{1}{2}(3N+1+l'_N+l_N+2K_{N-1})} \\
& \times \quad \int_{-1}^{1} dx (1-x)^{\frac{1}{2}(l_N+l_N+2)} (1+x)^{\frac{1}{2}(2K_{N-1}+3N-5)} \\
& \times P_{\mu'_N}^{[l_N+1/2, K_{N-1}+(3N-5)/2]}(x) P_{\mu_N}^{[l_N+1/2, K_{N-1}+(3N-5)/2]}(x) \\
& \times \langle J', M' | Y_1^\lambda(\theta_N, \phi_N) | JM \rangle \,,
\end{aligned} \tag{5.60}$$

where in the last line $x = \cos 2\alpha_N$.

Regarding the Y_1^λ term in Eq. (5.60), we can firstly consider the case of a specific projection of the total angular momentum a the operator as

$$\left\langle \left[\left[\{ L'_{N-1} \} \otimes l'_N \right]_{L'_N} \otimes \{ S' \} \right]_{J'}, M' \left| Y_{1,\lambda} (\Omega_N) \right| \left[\left[\{ L_{N-1} \} \otimes l_N \right]_{L_N} \otimes \{ S \} \right]_J, M \right\rangle . \tag{5.61}$$

In Eq. (5.61) we can recouple the quantum numbers, using

$$\left|\left[\left[l_N \otimes L_{N-1}\right]_{L_N} \otimes S\right]_j\right\rangle = (-1)^{l_N+L_{N-1}+S+J} \sum_{J_{N-1}} \hat{L}_N \hat{J}_{N-1} \begin{Bmatrix} l_N & L_{N-1} & L_N \\ S & J & J_{N-1} \end{Bmatrix} \times \left|\left[l_N \otimes \left[L_{N-1} \otimes S\right]_{J_{N-1}}\right]_J\right\rangle , \tag{5.62}$$

in order to have the angular momentum of the Jacobi coordinate N in the first place. In Eq. (5.62) the hat on the symbols stands for $\hat{J} = \sqrt{2J+1}$. The additional parameter over which the expression in (5.62) is summed, is called J_{N-1} and J'_{N-1} respectively. Now we can use

$$\left\langle\left[l'_N \otimes J'_{N-1}\right]J', M' \left|Y_{1,\lambda}\left(\Omega_N\right)\right| \left[l_N \otimes J_{N-1}\right] J, M\right\rangle = \delta_{J_{N-1}J'_{N-1}} (-1)^{J+l'_N+J_{N-1}-1} C^{J'M'}_{JM1\lambda} \begin{Bmatrix} l_N & J_{N-1} & J \\ J' & 1 & l'_N \end{Bmatrix} \left\langle l'_N \| Y_1\left(\Omega_N\right) \| l_N\right\rangle , \tag{5.63}$$

being $Y_{1,\lambda}\left(\Omega_N\right)$ an operator depending only on the N subsystem. We simplify the sum over J_{N-1} and J'_{N-1} with the $\delta_{J_{N-1}J'_{N-1}}$ obtaining

$$\begin{aligned} \left\langle\left\{J'\right\}, M' \left|Y_{1,\lambda}\left(\Omega_N\right)\right| \left\{J\right\}, M\right\rangle = & \sum_{J_{N-1}} \delta_{\{S'\},\{S\}} \delta_{\{L'_{N-1}\},\{L_{N-1}\}} \delta_{\{l'_{N-1}\},\{l_{N-1}\}} \\ & \times (-1)^{2J+J'+J_{N-1}-L_N-L'_N+4L_{N-1}+2l_N+3l'_N+2S-1} \\ & \times \quad (2J_{N-1}+1)\, \hat{L}_N \hat{L}'_N \hat{J} C^{J'M'}_{JM1\lambda} \\ & \times \begin{Bmatrix} l_N & L_{N-1} & L_N \\ S & J & J_{N-1} \end{Bmatrix} \begin{Bmatrix} l'_N & L_{N-1} & L'_N \\ S & J' & J_{N-1} \end{Bmatrix} \\ & \times \quad \begin{Bmatrix} l_N & J_{N-1} & J \\ J' & 1 & l'_N \end{Bmatrix} \left\langle l'_N \| Y_1\left(\Omega_N\right) \| l_N\right\rangle . \end{aligned} \tag{5.64}$$

The reduced matrix element of the spherical harmonics is

$$\left\langle l'_N \| Y_1(\Omega_N) \| l_N\right\rangle = (-1)^{l'_N} \sqrt{\frac{3}{4\pi}}\, \hat{l}'_N \hat{l}_N \begin{pmatrix} l'_N & 1 & l_N \\ 0 & 0 & 0 \end{pmatrix} \tag{5.65}$$

and using the relation of the Clebsch-Gordan coefficients

$$C^{J'M'}_{JM1\lambda} = (-)^{M'+J-1} \hat{J}' \begin{pmatrix} J & 1 & J' \\ M & \lambda & M' \end{pmatrix} , \tag{5.66}$$

in addition to the following property of 3j-symbols

$$\begin{aligned} & \sum_x (-1)^{a+b+c+d+e+f+g+h+x+j} (2x+1) \begin{Bmatrix} a & b & x \\ c & d & g \end{Bmatrix} \begin{Bmatrix} c & d & x \\ e & f & h \end{Bmatrix} \begin{Bmatrix} e & f & x \\ b & a & j \end{Bmatrix} \\ & = \begin{Bmatrix} g & h & j \\ e & a & d \end{Bmatrix} \begin{Bmatrix} g & \hbar & j \\ f & b & c \end{Bmatrix} , \end{aligned} \tag{5.67}$$

we get

$$\begin{aligned}\left\langle \{J'\}, M' \left| Y_{1,\lambda}\left(\Omega_N\right) \right| \{J\}, M \right\rangle = \quad & \delta_{\{S'\},\{S\}} \delta_{\{L'_{N-1}\},\{L_{N-1}\}} \delta_{\{l_{N-1}\},\{l_{N-1}\}} \\ & \times (-1)^{S+L_{N-1}+l_N+l_N+J+J'-M'} \sqrt{\frac{3}{4\pi}} \hat{L}_N \hat{L}'_N \hat{J} \hat{J}' \hat{l}_N \hat{l}_N \\ & \times \begin{pmatrix} J & 1 & J' \\ M & \lambda & -M' \end{pmatrix} \begin{pmatrix} l'_N & 1 & l_N \\ 0 & 0 & 0 \end{pmatrix} \\ & \times \begin{Bmatrix} L'_N & J' & S \\ J & L_N & 1 \end{Bmatrix} \begin{Bmatrix} l'_N & L'_N & L_{N-1} \\ L_N & l_N & 1 \end{Bmatrix}. \end{aligned} \tag{5.68}$$

The matrix element (5.68) depends on M, however recalling the definition of the cross-section (4.67) and using the orthogonality proprieties of the $3j$ symbols,

$$\begin{aligned} & \sum_{\lambda=\pm1,M'} \begin{pmatrix} J' & 1 & J \\ -M' & \lambda & M \end{pmatrix} \begin{pmatrix} J' & 1 & J \\ -M' & \lambda & M \end{pmatrix} \\ = & \frac{2}{3} \sum_{\lambda=0,\pm1,M'} \begin{pmatrix} J' & 1 & J \\ -M' & \lambda & M \end{pmatrix} \begin{pmatrix} J' & 1 & J \\ -M' & \lambda & M \end{pmatrix} \\ = & \frac{1}{(2J+1)}, \end{aligned} \tag{5.69}$$

the dependence on the longitudinal component of the total angular momentum in the response function and in the cross-section (4.65) vanishes. Above, in Eq. (5.69) J is the total angular momentum of the ^{9}Be ground state $J = \frac{3}{2}$.

After calculating all the terms of Eq. (5.58), we use the permutation matrices P_{ij} given in Eq. (3.50) to calculate all the contributions of the two body operators and finally to sum them up as

$$\langle \varphi_a^{N'} | \hat{O}_\perp | \Psi_i \rangle = \langle \varphi_a^{N'} | (\hat{O}_{12})_\perp + P_{13}^{-1} (\hat{O}_{12})_\perp P_{13} + P_{23}^{-1} (\hat{O}_{12})_\perp P_{23} | \Psi_i \rangle , \tag{5.70}$$

where $\langle \Psi_i | = \sum_N C_N \varphi^N$ is the ground state wave function. In this way we obtain the LIT numerator. The last step for calculating the LIT will be to use the methods seen in Section 5.3.1 and Section 5.3.2 to rewrite it as in Eq. (5.25) or (5.40).
Explicitly in the case of calculation of LIT with the eigenvalue method we have

$$\begin{aligned} L(\sigma) &= \langle \Psi_i | \hat{O}_\perp^\dagger \hat{K}(\sigma, \hat{H} - E_0) \hat{O}_\perp | \Psi_i \rangle \\ &= \sum_\lambda \langle \Psi_i | \hat{O}_\perp^\dagger | \Psi_\lambda \rangle \langle \Psi_\lambda | \hat{O}_\perp | \Psi_i \rangle \frac{1}{(\epsilon_\lambda - E_0 - \sigma_R)^2 + \sigma_I^2}, \\ &= \sum_\lambda | \langle \Psi_\lambda | \hat{O}_\perp | \Psi_i \rangle |^2 \frac{1}{(\epsilon_\lambda - E_0 - \sigma_R)^2 + \sigma_I^2} \end{aligned} \tag{5.71}$$

with $|\Psi_\lambda\rangle$ the eigenstates of the Hamiltonian $\hat{H} |\lambda\rangle = \epsilon_\lambda |\lambda\rangle$ given by

$$\langle \Psi_\lambda | = \sum_{N'} C_{N'} \varphi_a^{N'} . \tag{5.72}$$

Hence following this approach we should calculate the coefficients C_N and the respective eigenvalue of each λ state, with the same method used in calculating the bound state, and inserting it in Eq. (5.71) to obtain the desired result. Clearly, the knowledge of a sufficient number of eigenfunctions of the Hamiltonian is crucial to obtain a convergent LIT and consequently a successful inversion.
According to the Lanczos method instead one has

$$L(\sigma)_a = -\frac{1}{\sigma_I}\,\mathrm{Im}\left\{\frac{\langle Q_a \mid Q_a\rangle}{z - a_0 - \cfrac{b_1^2}{z-a_1-\cfrac{b_2^2}{z-a_2-b_3^2\cdots}}}\right\}, \tag{5.73}$$

where $|Q_a\rangle$ is given in Eq. (5.50) with $\varphi_a^{N'}$ the basis system obtained from the Lanczos technique. Therefore in this case, calculated the numerator, the knowledge of the coefficients a_i and b_i is enough to calculate the integral transform.

Regarding the possible final states that we are going to analyze, since in the energy range of interest the major contribution is given by the electric dipole term, they must satisfy the following selection rules

$$\pi_f = -\pi_i \tag{5.74}$$

$$\Delta L = \pm 1, 0 \tag{5.75}$$

$$\Delta S = 0 \tag{5.76}$$

where L (S) is the total orbital angular momentum (spin) and π indicates the parity of the system. The ground state of ^{9}Be is characterised by $J^\pi = \frac{3}{2}^-$, hence there are three possible final channels corresponding to $\frac{1}{2}^+$, $\frac{3}{2}^+$ and $\frac{5}{2}^+$. We will analyze the contributions of each channel separately and then the total LIT will be given by the sum of the individual LITs, as seen in Section 5.3.3 (Eq. (5.45)).

Chapter 6

Halo EFT applications

This Chapter collects the final results obtained from the application of the Cluster EFT theory on the NSHH and LIT method. In this context we analyze the convergence and stability of the calculated quantities by varying the variational parameters. We also discuss the dependence of our results on EFT parameters, in particular on the cutoffs Λ. After some technical details on the integration of the Coulomb potential in momentum space, Section 6.1, in Section 6.2 we start showing the analysis of the ground state of ^{12}C described as three α particle system. We also analyse the α particle four-body system provided by the ^{16}O and the ^{20}Ne as a five-body system, Section 6.3. Then we move on to examine the ^{9}Be nucleus depicted with $\alpha\alpha$n structure, Section 6.4. In Section 6.5 the LITs for all three possible channels of the ^{9}Be photodisintegration process are discussed. Finally, in Section 6.6 the result obtained for the ^{9}Be photointegration cross-section is shown.

6.1 Coulomb potential in momentum space

In order to calculate the ground state energy and wave function of a system, one has to solve the integrals of the potential in Eq. (3.73) and in Eq. (3.74). The Coulomb potential in momentum space is given by the following form

$$V_C(\pi_N, \pi'_N, t) = \frac{1}{2\pi^2} \frac{4e^2}{\pi_N^2 + \pi_N'^2 - 2\pi_N \pi'_N t}, \tag{6.1}$$

therefore the S-wave component can be calculated as

$$V_{C,l=0}(\pi'_N, \pi_N) = \frac{1}{2} \int_{-1}^{1} dt V_C(\pi'_N, \pi_N) P_{l=0}(t). \tag{6.2}$$

The result of the above integral presents a logarithmic divergence

$$V_{C,l=0}(\pi'_N, \pi_N) = \tfrac{1}{2} \textstyle\int_{-1}^{1} V_C(\pi_N, \pi'_N, t) P^0_{l_N}(t) dt \tag{6.3}$$

$$= \tfrac{1}{2} \tfrac{1}{2\pi^2} \tfrac{4e^2}{2\pi_N \pi'_N} \ln \tfrac{(\pi_N^2 + \pi_N'^2 - 2\pi_N \pi'_N)}{(\pi_N^2 + \pi_N'^2 + 2\pi_N \pi'_N)} \tag{6.4}$$

and this makes the potential not only divergent but also highly oscillatory near the singularity, as shown in Figure 6.1. To avoid this divergence we computed the integral (6.2) numerically on a grid of ~ 500 angular points with a Gauss-Legendre integration [86]. Then the result is placed in the integral of Eq. (3.73). The radial part of the latter is performed with a Gauss-Legendre integration shifted in the range 0 infinity. This shift is accomplished with a change of variable

$$x' = \frac{S(\frac{x+1}{2})^n}{(1-\frac{x+1}{2})^m}, \tag{6.5}$$

where $x \in [0,\infty[$, $x' \in [-1,1]$ and m,n,S are real parameters. This quadrature with $m = n = 0.9$ and $S = 10$ and a number of radial point of ~ 550 gives a more accurate and stable result than the classical Gauss-Laguerre quadrature. The integral in the hyperangle is then performed with standard Gauss-Legendre integration and again a large number of integration points is used. We recall that in the presence of potentials in momentum space the radial and hyperangular integrations are tightly connected thanks to the relation that binds ϕ' hyperangle and Q' hypermomentum, that eliminates an integration on one of the two primate variables. For this reason the number of hyperangular points required is ~ 500.

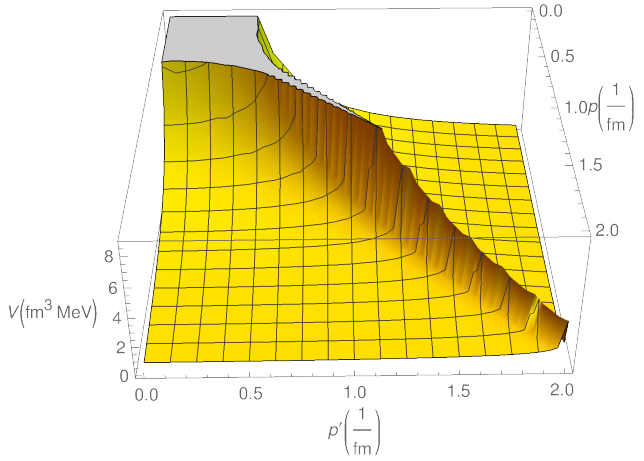

FIGURE 6.1: S-wave Coulomb potential in momentum space.

Another method we test to integrate the S-wave Coulomb potential consists on a change of variable. We need to integrate the Eq. (6.4) which diverges for $\pi = \pi'$ with

$$\pi = \sqrt{1-x}\,Q, \quad \pi' = \sqrt{2-(1+x)Q^2/Q'^2}\,Q, \quad x = \cos 2\phi_N. \tag{6.6}$$

Instead of using the variables dQ and dQ' we can do the integral in dQ_1 and dQ_2 defined as

$$Q_1 = \frac{Q+Q'}{2}, \tag{6.7}$$
$$Q_2 = \frac{Q-Q'}{2}. \tag{6.8}$$

The integral in dQ_1 is done in an interval $[0, 2Q_{max}]$ using the shifted Gauss-Jacobi quadrature and the integral in dQ_2 in a range $[-Q_{2lim}(Q1), Q_{2lim}(Q1)]$ where

$$Q_{2lim}(Q1) = Q_1 \quad Q_1 \leq Q_{max}, \tag{6.9}$$
$$Q_{2lim}(Q1) = 2Q_{max} - Q_1 \quad Q_1 \geq Q_{max}. \tag{6.10}$$

Also for this latter integration we use the shifted Gauss-Jacobi quadrature.
We verified that for values of $Q_{max} \geq 100$ the integration is stable. Then for both the integrations on Q_1 and on Q_2 we make the following substitution:

$$t = \cos^2[\pi(x-1)/2] \quad x \geq 0, \tag{6.11}$$
$$t = -\cos^2[\pi(x-1)/2] \quad x \leq 0, \tag{6.12}$$

where x corresponds to the Gauss-Jacobi integration variables Q_1 and Q_2, the Jacobian of this transformation will be:

$$\mathcal{J} = \pi * |\cos(\pi(t-1)/2) * \sin(\pi(t-1)/2)|. \tag{6.13}$$

The number of grid points must be even to avoid $Q_2 = Q - Q' = 0$.
In this way we would have many points around the divergence without ever reaching the singularity. For each point $(Q_1, Q2)$ we have to calculate the Laguerre functions $g_n(Q(Q_1, Q_2))$ and $g_m(Q'(Q_1, Q_2))$.

Therefore this results in several loops in the code as we integrate on the Q_1 variable, on Q_2 (which depends on Q_1) for each pairs of radial functions $g_n(Q(Q_1, Q_2))$ and $g_m(Q'(Q_1, Q_2))$.

To save computational time this integral is calculated separately in a module at the beginning of the program and is recorded for points. Then, it is added to the total potential and integrated in the hyperangle coordinates (this integration must be done when the program is running because it depends on quantum numbers and changes every time according the input variables).

The results obtained with the two integration methods are in agreement with an accuracy of one per thousand. In addition, we tested the stability of these integrations by considering a two-body system whose binding energy result with a chosen potential is known. Using the second method already with 200 grid points for Q_1 and Q_2 we reproduce the expected result up to the fourth decimal place.

6.2 ^{12}C

The first nucleus we analyze is ^{12}C described as a system of three alpha particles. The expected ground state energy in the three-body model is ~ −7.27 MeV to which the binding energy of the three alpha particles, of ~ −28.29 MeV, must be added in order to reach the experimental energy of −92.16 MeV.

The potential used in this case is the $\alpha\alpha$ S-wave interaction, described in Chapter 2, and the Coulomb repulsive potential still in S-wave. To begin the study of the convergence we need to set the potential parameters. We recall the form of the potential in S-wave,

$$V_{l=0}(p,p') = e^{\left(\frac{-p}{\Lambda}\right)^{2m}} e^{\left(\frac{-p}{\Lambda}\right)^{2m}} (\lambda_0 + \lambda_1 (p'+p)^2)\,, \tag{6.14}$$

where for the $\alpha\alpha$ interaction we set $m = 1$. As seen in the Section 2.4.1, the potential coefficients λ_0 and λ_1 were obtained as a solution pair of a quadratic equation, thus for each cutoff we would get two solutions, the first with negative λ_0 while the second with positive λ_0. We choose $\Lambda = 190$ MeV and λ_0, λ_1 the couple of the solutions of the quadratic equation with λ_0 attractive, in the following this coupling constant set will be called λ_{0-}.

The first step in the variational calculation of the ground state is looking for the right parameter β present in the radial basis argument which can accelerate the convergence. Using $N = 30$ radial basis functions and selecting $K = 20$ for the maximum value of the hyperangular momentum quantum number, we calculate the ground state binding energy varying the β parameter. As it can be seen in Figure 6.2, the point of minimum binding energy is obtained with a very small beta of 0.02 fm^{-1} since the behaviour of this potential near zero requires many points concentrated in that range to achieve good convergence.

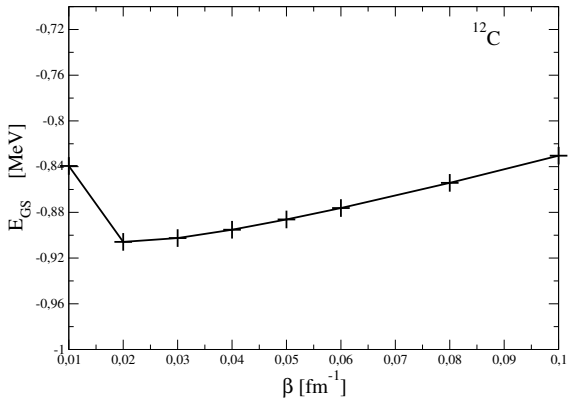

FIGURE 6.2: Ground state energy of ^{12}C varying the β parameter of the basis. Here $K = 20$, $N = 30$, n_i, $n_r = 500, 550$.

The convergence in the hyperangular momentum K is reached for a value $K > 10$. This is due to the simple form of the S-wave potential, being in this case $p^l \cdot p'^l = 1$

and $P_l(\boldsymbol{p}\cdot\boldsymbol{p}') = 1$ the resulting potential is a soft, fast converging potential. We emphasize that with $K = 20$ we get a stable result up to the fourth decimal place.

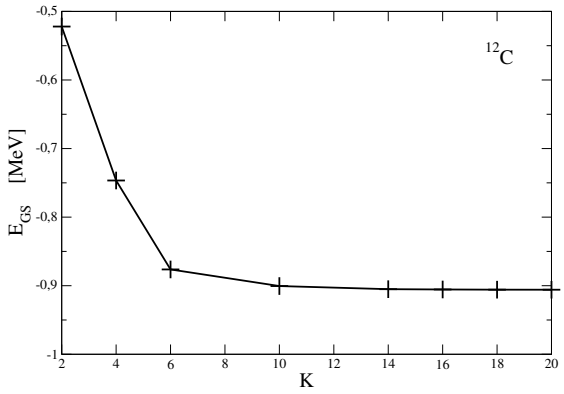

FIGURE 6.3: Ground state energy of ^{12}C increasing the hyperangular momentum K. We set $\beta = 0.02$ fm^{-1}, $N = 30$, n_i, $n_r = 500, 550$.

As shown in Table 6.1 the convergence in the number of radial functions is obtained for $N > 30$ with an accuracy up to the third decimal place. Same precision was obtained in the numbers of angular and radial integration points of 500, 550.

N	E_{GS} [MeV]
20	$-9.037 \cdot 10^{-1}$
30	$-9.060 \cdot 10^{-1}$
40	$-9.062 \cdot 10^{-1}$

$n_i - n_r$	E_{GS} [MeV]
500 – 550	$-9.060 \cdot 10^{-1}$
550 – 600	$-9.066 \cdot 10^{-1}$

TABLE 6.1: Ground state energy of ^{12}C increasing the number of basis function N and number of hyperangular radial integration points n_i, n_r.

Therefore we set $\beta = 0.02$ fm^{-1}, $K = 20$, $N = 30$, n_i, $n_R = 500, 550$ as optimal values for the convergence.

Once the variational parameters are selected, we can focus on the result obtained. The binding energy obtained for the ^{12}C nucleus, of −0.91 MeV, is less than the expected energy −7.27 MeV.

However, the result seems to be in agreement with other works which has attempted to describe the ^{12}C using the same micro-clustering model with halo EFT potentials, see for example [87]. This binding energy is obtained with a cutoff of 190 MeV and with the pair solution including an attractive λ_0 value. By varying the cutoff and examining all the two pairs of the solutions we can examine how the ground state energy of this system changes. In Figure 6.4 the variation of the binding energy with the cutoff for the λ_{0-} and λ_{0+} solutions is shown. As it can be seen, the first pair produces less cutoff-dependent and lower ground state energies. The second one, λ_{0+}, leads to binding energies which vary greatly over the examined range reaching a maximum value of −4.752 for 170 MeV. The Wigner bound limits the value of the cutoff up to 230 MeV and the results for $\Lambda = 210$ MeV indicate the approach of the maximum limit. This spectrum created by varying the cutoff of the two-body force

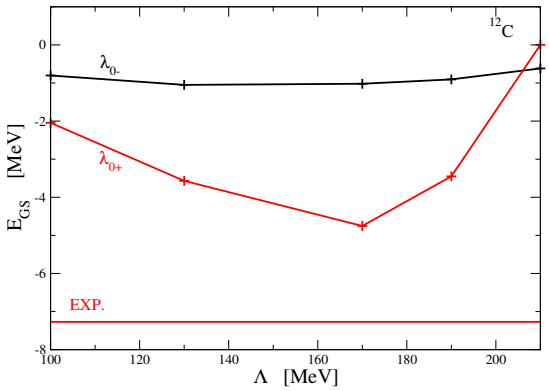

FIGURE 6.4: ^{12}C ground state energy varying the cutoff value of the EFT theory.

Λ [MeV]	λ_{-3} [fm^5]	λ_{+3} [fm^5]
100	−8.221	−3.930
130	−5.932	−2.070
170	−6.808	−1.771
190	−8.422	−3.402
210	−9.075	−4.407

TABLE 6.2: Three-body force strength for different cutoff values. With λ_{-3} (λ_{+3}) we indicate the three-body force coupling constant associated with the solution pair $\lambda_{0,-}$ ($\lambda_{0,+}$). The cutoff of this force is set to Λ_3 = 130 MeV.

could be interpreted as a remaining discrete scale invariance, despite the long-range Coulomb potential and despite the finite cutoff introducing another energy scale in the theory. These cutoff effects are curable by the inclusion of a three-body force.

We added a three-body force to our description by fixing the coupling constant for each two-body cutoff in order to reproduce the experimental energy. Some values of the coupling constant of the three-body force are shown in the Table 6.2. In Figure 6.5 we show the ground state energy obtained with the addition of the three-body potential.

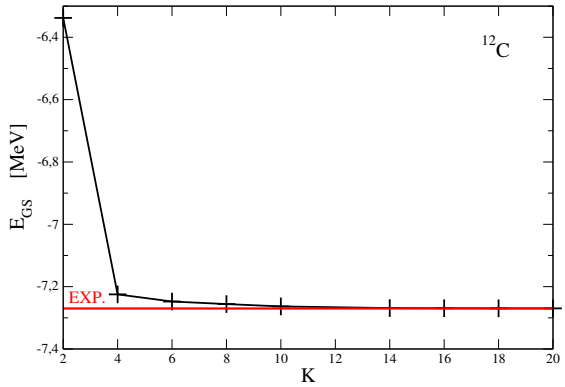

FIGURE 6.5: Ground state energy of ^{12}C increasing the hyperangular momentum K. Here the three-body force is included.

To verify the accuracy of the model we then calculated the spin 2^+ excited state

of ^{12}C, Figure 6.6. With the three-body force inserted in the model we manage to obtain a 2^+ bound state for all λ_3 values, the energy however varies depending on the constant of the three-body force from a minimum value of −0.875 MeV up to −7.028 MeV, Table 6.3. In order to have a more detailed description of this state probably a D-wave interaction should be also included so as to reduce the three-body force. Our three-body potential, in fact, includes several effects as well as additional partial waves not considered in the model. Moreover, one might consider calculating the NLO contribution of the three-body force.

λ_3 [fm^5]	E [MeV]
−3.402	−0.875
−3.930	−1.545
−6.808	−4.780
−8.422	−7.028

TABLE 6.3: Variation of the binding energy of 2^+ state changing the three-body force strength, with fixed cutoff Λ_3 = 130 MeV.

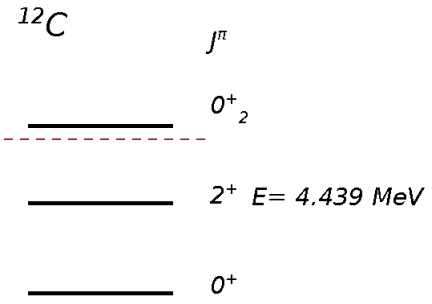

FIGURE 6.6: Energy levels of ^{12}C.

Further analysis of this point is required. Implementing other contributions to the potential, in principle of higher orders in our EFT and for this reason neglected here, one could have a more precise indication of the system in examination.

6.3 ^{16}O and ^{20}Ne systems

In this Section we review some results obtained for ^{16}O and ^{20}Ne nuclei.

The Oxygen nucleus described as a 4-alpha particle system has an experimental binding energy of −14.44 MeV, while the expected energy of ^{20}Ne 5-alpha particle system is of −19.17 MeV. As we already mentioned, our EFT with alpha particles as degrees of freedom is based on the assumption that the binding energy of the system is much larger than the separation energy of the degree of freedom used, thus ~ 20 MeV. Although for these two nuclei the binding energy of the system is comparable to 20 MeV, the description of their fundamental state within the theory is still possible since the binding energy of each single α particle within the nucleus results for the ^{16}O ~ −3.61 MeV and for the ^{20}Ne ~ −3.83 MeV. Therefore comparing the latter values with the excitation energy of the alpha particle, one can see that the assumptions for an effective theory approach could be considered still valid. This argument is based on the same principle used in the description of nuclear interaction in heavy nuclei when the Δ particle is neglected as a degree of freedom. The excitation $N \to \Delta$ is produced at energies of the order of the $\Delta - N$ mass difference, about 230 MeV. The binding energy of ^{208}Pb, for example, would be such that Δ particles could be produced, however these one are always neglected in the nuclear state description.

We first consider the 4-body system, the ^{16}O. We studied the variation of E_{GS} in function of the β parameter for both solution sets of the λ_i coefficients of the two-body potential. We set $K = 20$ and $N = 30$ and n_i, n_r=500, 550.

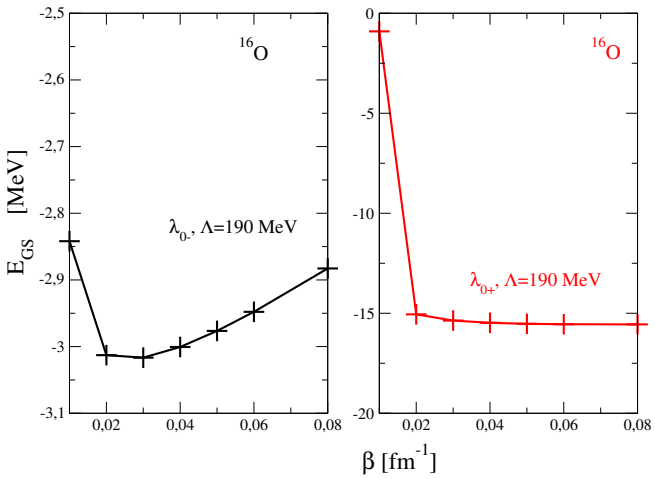

FIGURE 6.7: Ground state energy of ^{16}O varying the β parameter of the basis. Here $K = 20$, $N = 30$, $n_i, n_R = 500, 550$.

In Figure 6.7 one can see that while using the λ_{0-} solutions the optimal β is about ~ 0.03 fm^{-1}, for the λ_{0+} set the best β is bigger, in particular we reach the minimum of the binding energy for $\beta = 0.08$ fm^{-1} even if for β from 0.03 to 0.08 the result is stable up to the second decimal place.

Also in this case the potential with λ_{0-} gives a less bound nucleus with respect with the solution with λ_{0+}, see Figure 6.8. With a cutoff of $\Lambda = 150$ MeV we obtain $E_{GS} = -14.86$ MeV, therefore a value very close to the expected one.

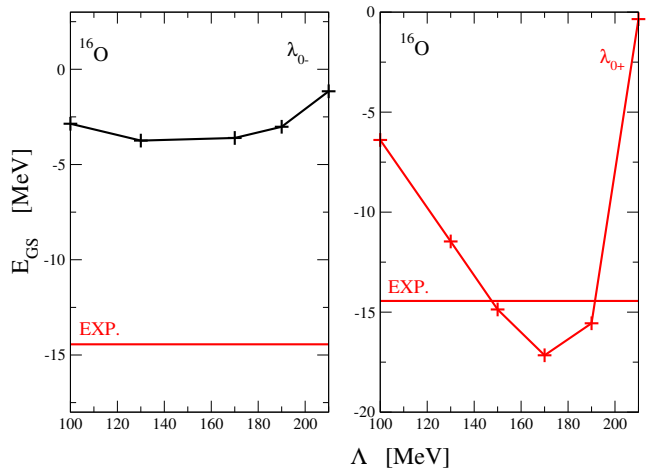

FIGURE 6.8: Ground state energy of ^{16}O varying the cutoff Λ. We set $K = 20$, $N = 30$, n_i, $n_R = 500, 550$ and $\beta = 0.03$ fm^{-1} for the λ_{0-} solution (left figure) while $\beta = 0.08$ fm^{-1} for the λ_{0+} solution (right figure).

As it can be seen in Figure 6.9, in case of a potential with λ_{0-} couplings the convergence in K is obtained to the second decimal place for $K > 10$, while already with

$K > 6$ with the other solution pair. With $K \sim 20$ we reach a precision up to the 4th-decimal place.

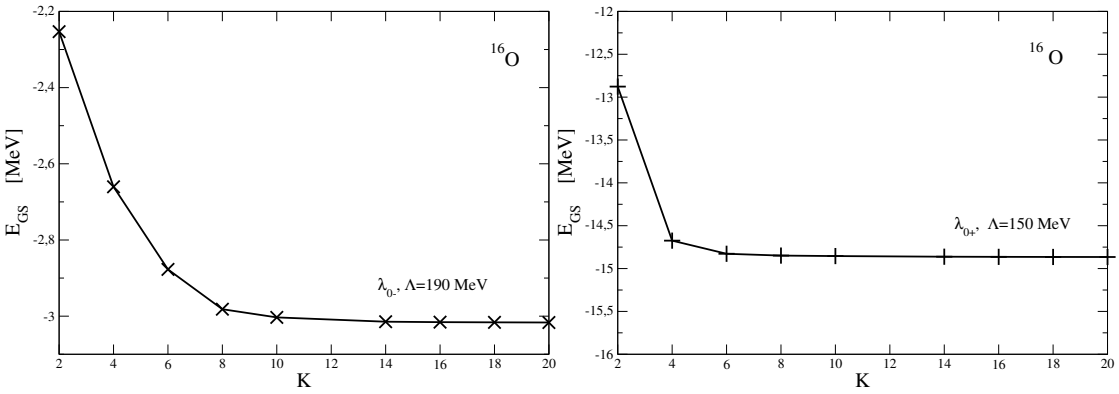

FIGURE 6.9: Ground state energy of ^{16}O increasing the hyperangular momentum K for λ_{0-} and λ_{0+} solution sets. Here $N = 30$, n_i, $n_R = 500, 550$ and $\beta = 0.03$ fm^{-1} in the left figure while $\beta = 0.08$ fm^{-1} in the right figure.

Regarding the ^{20}Ne the trends in β, in the cutoff and in K, shown in Figs. 6.10-6.12, are similar to those obtained for ^{16}O. However the calculation of a 5-body system is more demanding from the point of view of computational resources, for this reason here the maximum K value studied is 12. A more precise convergence would require a numerical optimization of the code. Nevertheless, thanks to the simplicity of the potentials used $K = 12$ leads to a result already stable up to the second decimal place, allowing us to make realistic considerations about the results obtained.

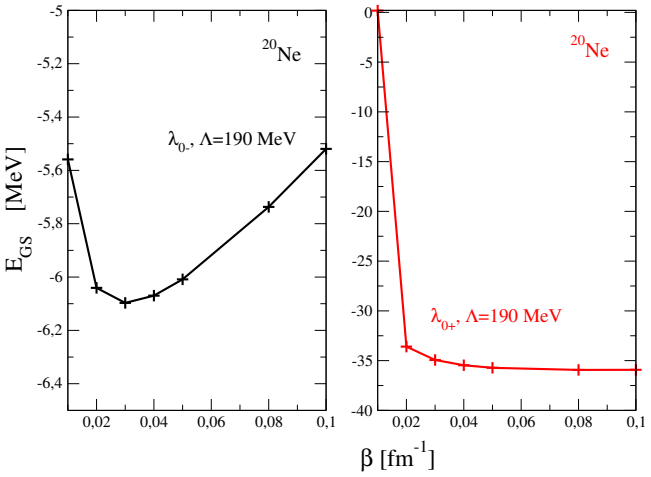

FIGURE 6.10: Ground state energy of ^{20}Ne varying the β parameter of the basis. We set $K = 12$, $N = 30$, n_i, $n_R = 500, 550$.

It is interesting to note that for both the ^{16}O and ^{20}Ne systems considering the λ_{0+} set the experimental binding energies are reproduced for $\Lambda_{\alpha\alpha} \sim$ 130-150 MeV, almost indicating a preferred energy scale for these systems. The dependence of the two-body cutoff is, however, preferably to be eliminated in order to make sure that the

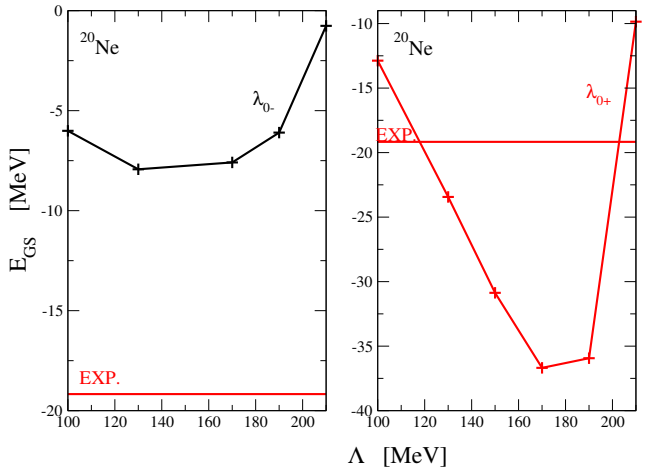

FIGURE 6.11: Ground state energy of ^{20}Ne varying the cutoff Λ. Here $K = 12$, $N = 30$, $n_i\, n_R = 500$, 550 and $\beta = 0.03$ fm^{-1} for the λ_{0-} solution while $\beta = 0.08$ fm^{-1} for the λ_{0+} solution

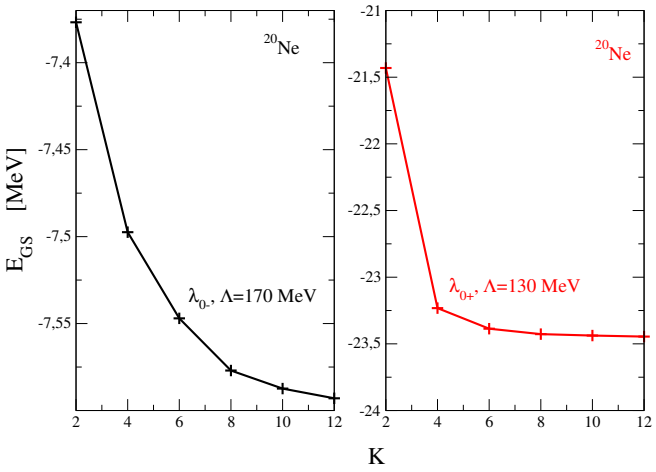

FIGURE 6.12: The ground state energy of ^{20}Ne increasing K. In this calculation we use the same convergence parameters of Figure 6.11.

states of the systems are not determined by it. In this direction, a future perspective will be to include a three-body force for these four- and five-body systems as well. To do this the implementation of three-body permutations in the code will be necessary.

After studying both sets of coupling constants for the alpha-alpha interaction on different systems, we conclude this section with a remark. Although the solutions with λ_{0+} provide deeper bound states and often a binding energy closer to the experimental values from here on we will not consider anymore these solution pairs. The strong dependence on the cutoff value of the theory makes these solutions less appropriate and furthermore their larger values are in contradiction with the principle of naturalness of the EFT coupling constants.

6.4 ^{9}Be

Let us now consider the ^{9}Be nucleus as a three-body system consisting of two alpha particles and one neutron. In this case the expected ground state energy is of −1.573 MeV to which one has to add the binding energy of two alpha particles to reach the experimental value of −58.158 MeV.

The interaction between the two alpha particles is the same as examined in the previous cases, shown in Eq. (6.14) and again the S-wave Coulomb potential. For the EFT potential we only consider the λ_{0-} set since, as we have seen in previous studies, it provides a binding energy that is less dependent on the cutoff and has natural size.

Regarding the α-n interaction we consider at first only the $P_{3/2}$ wave which, as already described in Section 2.4, has the form

$$V_{l=1}(p,p') = e^{\left(\frac{-p}{\Lambda}\right)^{2m}} e^{\left(\frac{-p}{\Lambda}\right)^{2m}} pp'(\lambda_0 + \lambda_1(p'+p)^2)\,. \tag{6.15}$$

In this case we set $m = 2$ and we still consider only the coupling constants which are of more natural size and provide a weakly attractive potential at large distance.

In order to study the convergence of the ground state energy on the variational parameters we set the cutoff $\Lambda_{\alpha\alpha} = 190$ MeV and $\Lambda_{\alpha n} = 300$ MeV. In Figure 6.13a the variation of the ground state energy as a function of the β parameter is shown.

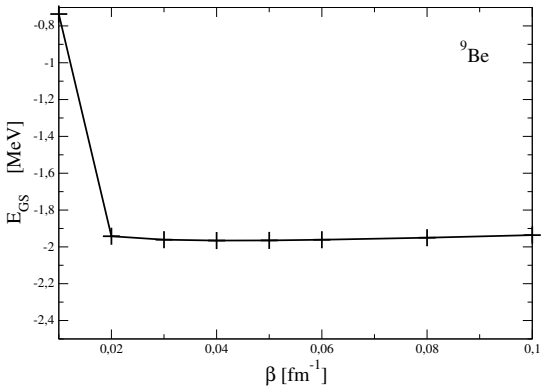

(A) Ground state energy of ^{9}Be varying the β parameter of the basis with $K = 23$, $N = 30$ and n_i, $n_R = 500, 550$.

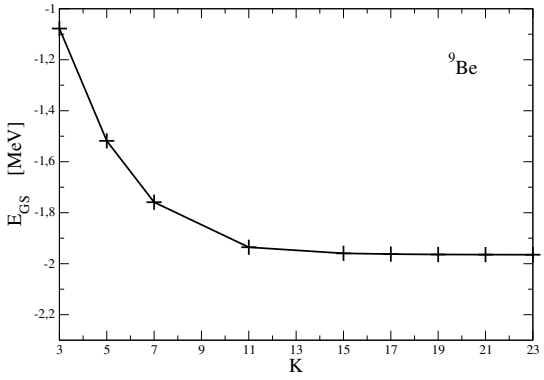

(B) Ground state energy of ^{9}Be increasing the hyperangular momentum K. Here $\beta = 0.05$ fm^{-1}, $N = 30$ and n_i, $n_R = 500, 550$

FIGURE 6.13: Convergence on K and β parameters of the ^{9}Be ground state energy.

The result is stable up to the third decimal place from $\beta = 0.03$ fm^{-1} up to 0.06 fm^{-1} and then decreasing again. The convergence in the hypermomentum K, Figure 6.13b and Table 6.4, is obtained with $K \sim 15$, a rather low value even if greater than the previous cases due to the presence of the P-wave α-n potential. With $K = 23$ we reach a precision up to the 4th decimal place. We achieve the same accuracy in the number of radial wave functions N, as shown in the Table 6.4. The integral

precision is one per thousand, Table 6.5, mainly due to the Coulomb potential in momentum space.

N	E_{GS} [MeV]
20	−1.9646
30	−1.9647
40	−1.9647

K	E_{GS} [MeV]
11	−1.9354
15	−1.9593
17	−1.9623
19	−1.9639
21	−1.9645
23	−1.9647

TABLE 6.4: Convergence of ground state energy of ^{9}Be increasing the number of basis function N and K with β = 0.05 fm^{-1} and n_i, n_R = 500, 550. In the Table on the left K = 23 while in the Table on the right N = 30.

n_i, n_r	E_{GS} [MeV]
450, 500	−1.960
500, 550	−1.965
550 – 600	−1.968

TABLE 6.5: Ground state energy variation with the number of integration points with β = 0.05 fm^{-1}, N = 30, K = 23.

We set β = 0.05 fm^{-1}, N = 30, K = 23 and n_i, n_R = 500, 550 as best parameters for convergence.

Now we can examine the cutoff dependence of the two-body potentials on our result. As one can see in Figure 6.14 the variation of the ground state energy with

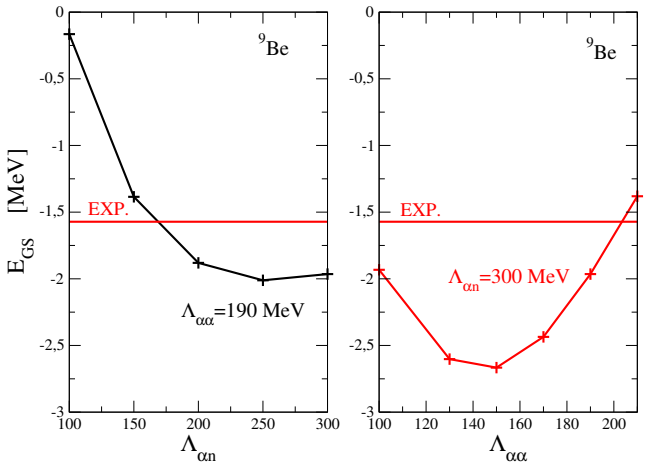

FIGURE 6.14: ^{9}Be ground state energy in function of the cutoffs of the theory.

the $\alpha\alpha$ cutoff is smaller than the one with the αn cutoff. By varying $\Lambda_{\alpha n}$ from 100 to 300 MeV the energy varies from −0.17 to −1.96 MeV. Even if the energy range is very wide we remember that in this case the maximum limit imposed by the Wigner bound for this cutoff is 340 MeV, therefore all the values examined are theoretically allowed. The situation is different by changing $\Lambda_{\alpha\alpha}$, increasing this parameter from

100 to 200 MeV the energy reaches a minimum at 150 MeV of −2.66 MeV and a maximum at 210 of −1.38 MeV. Probably this last value of 210 MeV is already affected by the incoming Wigner bound which gives a less reliable value of the binding energy. Therefore the ground state energy variation as a function of $\Lambda_{\alpha\alpha}$ can be considered of ~ 0.6 MeV. The difference between the behaviours of the two interactions as a function of the cutoffs could be interpreted as a stronger residue of the Efimov physics [57] in the α-n case. While for the α-α interaction the scale invariance is broken not only by the presence of the cutoff but also by the long range Coulomb potential, in the α-n case only 'contact' interactions are present. This could be reflected in a wider spectrum of different three-body bound state energies. The discrete scaling factor characteristic of the Efimov effect can occur, in fact, not only for three identical particles but also trying to describe two identical particles having a P-wave resonance with a third particle [88]. However, according to [89, 90], a real Efimov state in the P-wave case cannot be realized in nature.

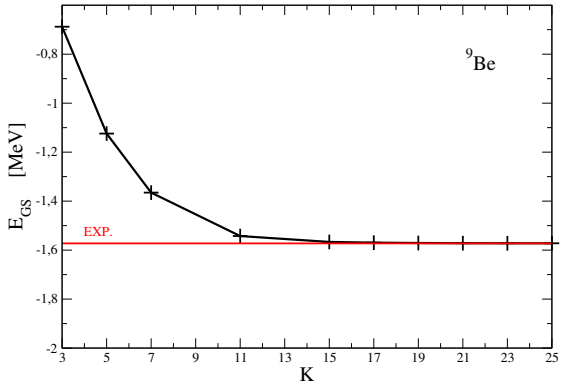

FIGURE 6.15: Ground state energy of ^{9}Be increasing the hyperangular momentum K with the three-body force.

As in ^{12}C case, in order to eliminate the cutoff dependence in the results we used a three-body force by fixing the coupling constant λ_3 to reproduce the experimental energy for each value of the two-body cutoff. The result of the binding energy convergence as a function of the hyperangular momentum K is shown in Figure 6.15, while the values of the three-body force coupling constant can be seen in the Table 6.6.

$\Lambda_{\alpha\alpha}$=190 MeV

$\Lambda_{\alpha n}$ [MeV]	λ_3 [fm^5]
100	−1.611
150	−0.015
200	+0.169
250	+0.2368
300	+0.2139

$\Lambda_{\alpha n}$=300 MeV

$\Lambda_{\alpha\alpha}$ [MeV]	λ_3 [fm^5]
100	+0.191
170	+0.454
210	−0.113

TABLE 6.6: Three-body force strength for different two body interaction cutoff values. Here the cutoff of the three-body force is set to Λ_3 = 130 MeV.

Clearly the variation of the three-body force constant increasing the two-body cutoff reflects the one of E_{GS}. Therefore changing $\Lambda_{\alpha\alpha}$ the λ_3 variation is smaller than that as a function of $\Lambda_{\alpha n}$.

6.4.1 NLO: The S-wave

To improve the description of the ^{9}Be, in view of the calculation of the photodisintegration cross-section, we added the S-wave α-n interaction to our potential. As explained in Section 2.4, this potential reads

$$V_{l=0}(p,p') = e^{(\frac{-p}{\Lambda})^{2m}} e^{(\frac{-p}{\Lambda})^{2m}} (\lambda_0 + \lambda_1 (p'+p)^2)\,, \tag{6.16}$$

and selecting $m = 2$ the coefficients λ_0, λ_1 are calculated by resumming the T matrix. This resumming operation results in poles of the T-matrix creating non-physical αn bound states. However, this does not happen for all values of the cutoff.

No bound states are observed for cutoffs less than 150 MeV. At 200 and 250 MeV a bound state of ~ -30 MeV appears, while for higher cutoffs a bound state of about -13 MeV is present. In the Table 6.7 we report the values of the binding energy of the forbidden state as the cutoff varies and in Figure 6.16 one can see the potential and the forbidden state wave functions for different values of Λ.

$\Lambda_{\alpha n}$ [MeV]	E [MeV]
200	27.89
250	31.38
300	12.25
525	13.97
400	13.39
500	13.90

TABLE 6.7: Forbidden S-wave state.

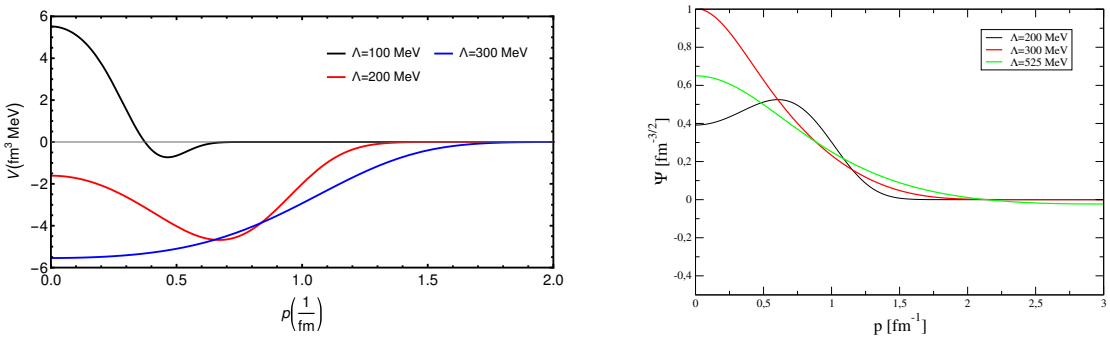

(A) Diagonal S-wave α-n potential for different cutoff values.

(B) Wave function of the forbidden state for three cutoff values.

FIGURE 6.16: S-wave α-n potential and wave function.

As we mentioned at the end of the Section 2.4, in order to remove this pole we follow the method of Ref. [50], adding to the S-wave α-n potential the term

$$V(p,p') = \Gamma|\Phi(p)\rangle\langle\Phi(p')|, \tag{6.17}$$

where $\Phi(p)$ is the wave function of the forbidden state and Γ the projection parameter.

Theoretically Γ should tend to infinity, but in practice it is sufficient to find a value for which the three-body bound state and scattering results are independent of it. For a cutoff greater than 300 MeV, we find a rather shallow bound state and a Γ value of ~ 40 MeV is sufficient to project out this state. In Figure 6.17 the diagonal part of the S-wave potential varying the projection parameter can be seen. A higher Γ value pushes the bound states, or nodes of the wave function, to higher energies until they are close to zero, thus unbound states. Furthermore, a Γ value of about 40 MeV does not affect the low-energy behaviour of the phase shift and reproduces accurately the experimental data, Figure 6.18.

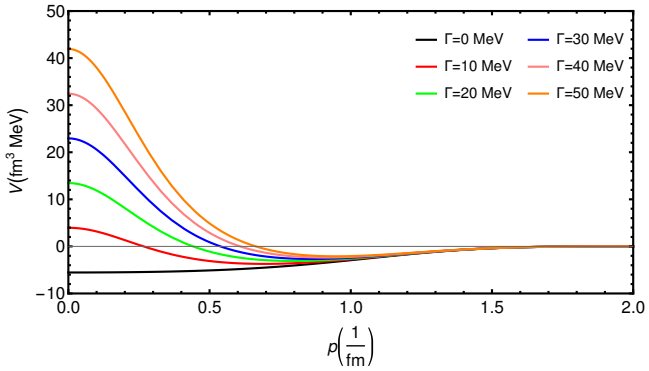

FIGURE 6.17: Total diagonal S-wave α-n potential with $\Lambda_{\alpha n}$ = 300 MeV.

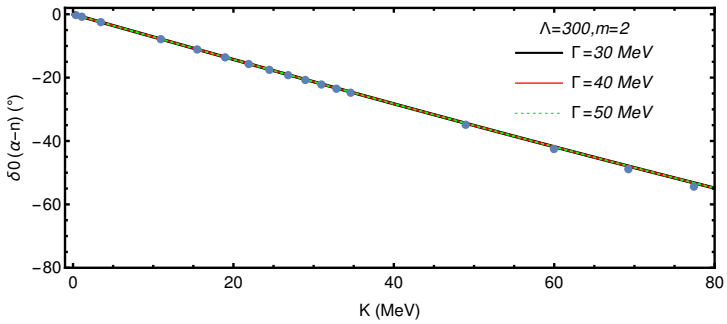

FIGURE 6.18: S-wave α-n phase shift with the projection of forbidden state. Here $\Lambda_{\alpha n}$ = 300 MeV and data from Ref.[46].

After implementing the NLO potential, we may compute the energy and wave function of the ^{9}Be ground state once more. Using only two-body potentials, the addition of the repulsive S-wave interaction results in a binding energy variation from

0.02 up to 0.07 MeV depending on the cutoff used. For example, using $\Lambda_{\alpha\alpha}$ = 190 MeV, $\Lambda_{\alpha n}$ = 130 MeV, without the S-wave contribution we obtained E_{GS} = −1.97 MeV and including the NLO contribution E_{GS} results of −1.99 MeV. The binding energy variation will be compensated by fitting again the three-body force coupling constant in such a way as to reproduce the experimental energy of the system. This will then produce, for fixed Λ_3, a corresponding change in the three-body force constant λ_3 still at percent level.

In Figure 6.19 we show the trend of λ_3 in function of Λ_3, until now kept fixed at 130 MeV. In principle, the λ_3 behaviour should reflect and cure the dependence of the two body cutoffs and on Λ_3 such that the potential and the obtained binding energy will remain always the same. The three different color curves shown correspond to different values $\Lambda_{\alpha n}$ while the $\Lambda_{\alpha\alpha}$ parameter is 190 MeV for all the three studied cases. In the bottom panel of the Figure 6.19 the trend of $c_3 = \lambda_3\Lambda^5$ is shown. As

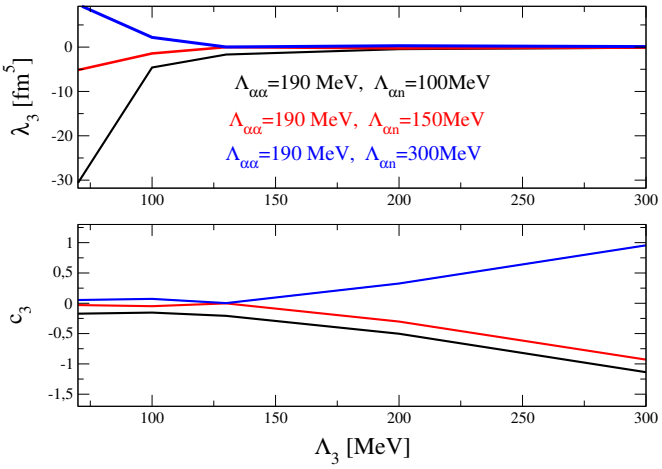

FIGURE 6.19: λ_3 and $c_3 = \lambda_3\Lambda^5$ variation in function of the cutoff Λ_3, described in the text.

it can be seen approaching high cutoffs values ~ 300 MeV the constant c_3 assume natural size ~ ±1. A visible influence of the addition of the NLO potential and of the three-body force variation will be better shown in the next Section by the LIT calculation results.

6.5 LIT for ^{9}Be photodisintegration

Once the binding energy and the wave function of the ^{9}Be $3/2^-$ ground state are calculated, we can consider the LIT of the response function for the photodisintegration reaction. The relevant channels for this process are $1/2^+$,$5/2^+$ and $3/2^+$.
Regarding the ^{9}Be wave function we use the result obtained in the previous Section with $\beta = 0.05$ fm^{-1}, $N = 30$, $K = 25$, n_i, $n_R = 500, 550$ and a NLO potential with $\Lambda_{\alpha\alpha} = 190$ MeV, $\Lambda_{\alpha n} = 100$ MeV, $\Lambda_3 = 300$ MeV. The same Hamiltonian is used for the calculation of the integral transform.

The operator we implemented in the code in order to calculate the response function is,

$$\hat{O}_\perp = \frac{1}{m_\alpha}\left(\sqrt{\frac{m_\alpha}{m_\alpha + m_n}}\boldsymbol{\pi}_{1\perp} + \sqrt{\frac{m_\alpha m_n}{(m_\alpha + m_n)(2m_\alpha + m_n)}}\boldsymbol{\pi}_{2\perp}\right). \tag{6.18}$$

Thus leaving out, with respect with the Eq. (5.52), only the constant factors. In this way, the implemented operator is dimensionless and the only units of the LIT come from the denominator of the integral transform of Eq. (5.71). The quantity in Eq. (6.18) is calculated solving the radial and hyperangular integrals numerically, separating the contributions as seen in Eq. (5.58). Since the expression of $\hat{O}_\perp$ is quite simple, the radial integral is convergent already with ~ 100 integration points and the hyperangular one with ~ 80. However we integrate this operator with the same integration grid used for the Hamiltonian matrix.

The first checks on the calculation we propose are about the validity of the sum rules which can be a good feedback on the correctness and credibility of the outcomes of the LIT. We firstly test the completeness of the basis chosen to expand the H eigenstates. We consider the moment of zero order $m_0 = \int d\omega r(\omega)$ in the following form,

$$m_0 = \int \sum_{\lambda=0}^{N_\lambda} \langle\lambda|\hat{O}_\perp^\dagger|0\rangle\langle\lambda|\hat{O}_\perp|0\rangle\delta(\omega - \epsilon_\lambda + E_0)d\omega \tag{6.19}$$

$$= \sum_{\lambda=0}^{N_\lambda} \langle\lambda|\hat{O}_\perp^\dagger|0\rangle\langle\lambda|\hat{O}_\perp|0\rangle \tag{6.20}$$

$$= \langle 0|\hat{O}_\perp^\dagger\hat{O}_\perp|0\rangle\,. \tag{6.21}$$

If we separately compute the expressions in the second and third lines we have quantitatively verified the completeness relation of the chosen basis for the states λ. We obtain for $m_0 = 7.602\cdot10^{-4}$ and the sum of $\langle\lambda|\hat{O}_\perp|0\rangle$ on all possible channels gives ~ $7.593\cdot10^{-4}$. The relation is therefore verified with precision of one per thousand.

Another useful test concerns the behaviour of $L(\sigma_R)$

$$L(\sigma) = \int d\omega \frac{r(\omega)}{(\omega - E_0 - \sigma_R)^2 + \sigma_I^2} \tag{6.22}$$

for σ_R tending to infinity, one has

$$L(\sigma) = \int d\omega \frac{r(\omega)}{\sigma_R^2} = \frac{m_0}{\sigma_R^2}. \tag{6.23}$$

Considering only one channel, for example the $1/2^+$ channel, for $\sigma_R = 10^6$ MeV we get $L(\sigma) = 2.48803 \cdot 10^{-16}$ MeV $^{-2}$ in good agreement with $2.48800 \cdot 10^{-16}$ MeV $^{-2}$ obtained from $(m_0)_{1/2^+}/\sigma_R^2$. The same relation is also satisfied for the other two channels and for the total LIT.

The computation of the LIT requires setting the parameter σ_I which corresponds to the Lorentzian width. Smaller values of σ_I ensure a better resolution of the transformation, but imply a slower convergence depending on the size of the basis. We start by selecting $\sigma_I = 1$ MeV which can be considered a good compromise for the resolution of the final result.

The evaluation of the convergence of the transform involves several steps, one of these is the study of the stability of the method used to calculate it. As we have seen in Section 5.3, there are two practical methods for the calculation of the LIT: the method through the Lanczos algorithm (5.73) and the calculation of eigenvalues method (5.71). In Figure 6.20 we present the study of these two approaches. With the first method the number of steps of the Lanczos algorithm needed to reach convergence is around 100. In the right panel we can see that the number of eigenvectors and eigenvalues needed to reconstruct the LIT must be greater, also in this case, than ~ 100. Clearly the two approaches are totally equivalent once convergence is achieved. The method we use principally to calculate the LIT is the Lanczos method, using ~ 500 of the a_i, b_i coefficients of the Hamiltonian matrix, i.e. ~ 500 number of steps.

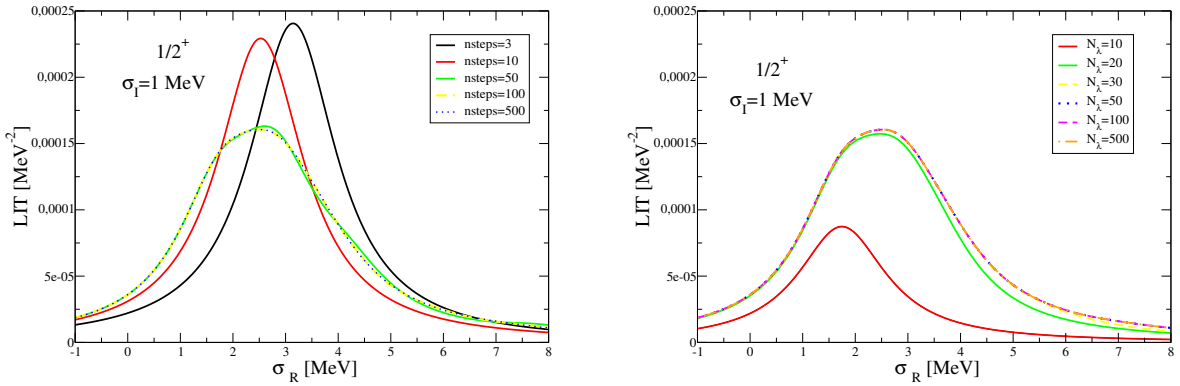

(A) LIT with Lanczos method.

(B) LIT with eigenvalues method.

FIGURE 6.20: LIT convergence in the number of eigenstates and Lanczos steps.

Let us now study the results as the β parameter of the radial basis changes. This parameter as shown in Ref. [91] turned out to be critical for incrementing the eigenvalues in the range of interest. There the authors used the pseudostates method to compute the continuum states via bound state method and analytical transformed

harmonic oscillator (THO) as radial basis. However, even in our case the choice of β is important to have a denser spectrum of eigenvalues, as shown in Figure 6.22 with a too small β value the eigenvalues at energies higher are missing and this causes a peak of the LIT visibly lower, Figure 6.21a. A β range from 0.04 to 0.06 fm^{-1} ensures a good convergence of the integral transform providing a good distribution of Hamiltonian eigenvalues, see Figures 6.21. With a Lorentzian width of 1 MeV, the

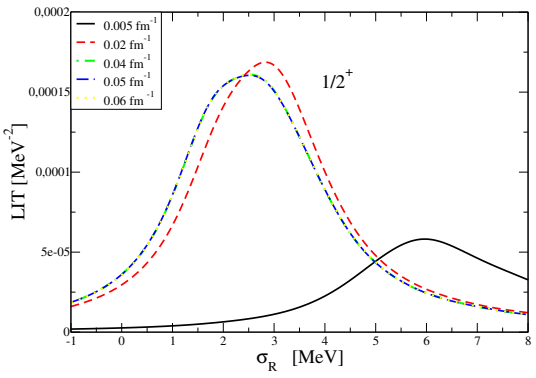

(A) LIT for $1/2^+$ channel varying the β parameter of the radial basis. We set K = 24, N = 30 and n_i, n_R = 500, 550 and σ_I = 1 MeV.

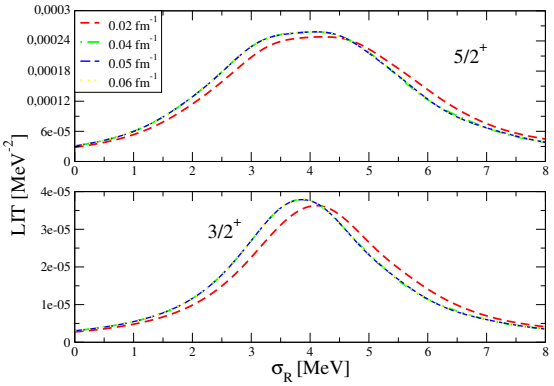

(B) LITs for $5/2^+$, $3/2^+$ channels in function of the β parameter of the radial basis. We set K = 24, N = 30 and n_i, n_R = 500, 550 and σ_I = 1 MeV.

FIGURE 6.21: LIT results in function of the β parameter.

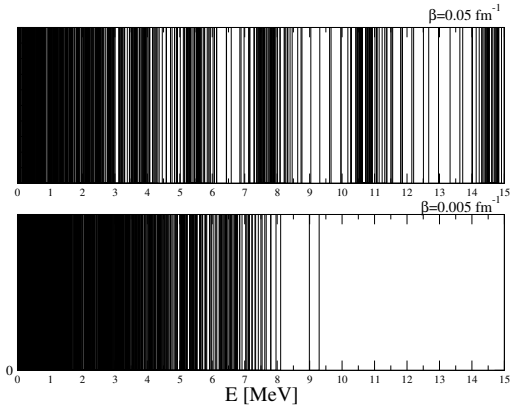

FIGURE 6.22: Comparison of the eigenvalues for $1/2^+$ channel for two different β values. Each bar represents an eigenvalue relative to the energy reported in the x-axis.

convergence in the hyperangular momentum K and in the number of radial functions N is easily achieved. In Figure 6.23 it can be seen that the result is already stable for $K > 6$ in each of the three channels. This is mainly due to the σ_I used which is large enough to ensure convergence at low values of K and in part to the potential used which includes few partial waves. Regarding the N convergence it can be seen that in $1/2^+$ channel there is no visible difference in the position or height of the peak from N = 20 up to 40. Looking closely it is possible to notice only a very small difference in the $3/2^+$ and $5/2^+$ channels, at energies greater than 4 MeV, between the

curve calculated with N = 20 and the N = 30/40 curves. However with N = 30 the convergence is achieved even in these cases.

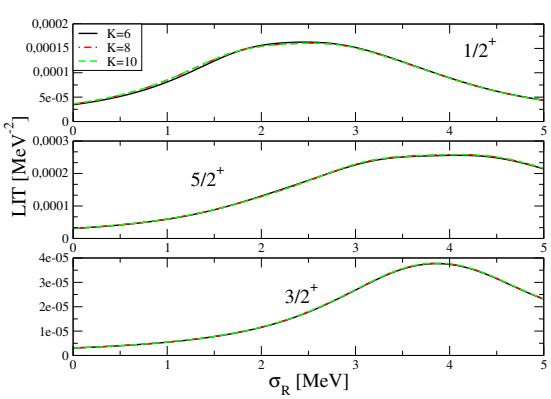

(A) LIT result increasing K with β = 0.05 fm^{-1}, N = 30 and n_i, n_R = 500, 550 and σ_I = 1 MeV.

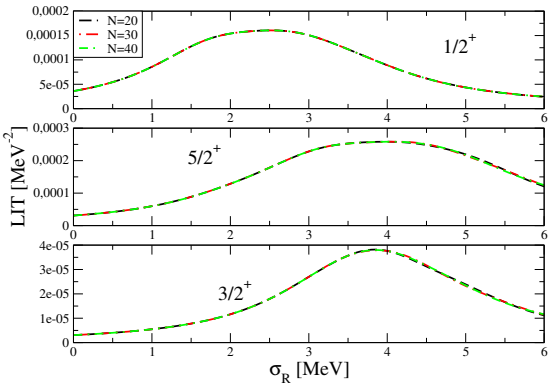

(B) LIT result in function of N with β = 0.05 fm^{-1}, K = 26 and n_i, n_R = 500, 550 and σ_I = 1 MeV.

FIGURE 6.23: LIT results varying the variational parameters N and K.

Now we can focus on the results obtained and in particular on how they vary according to the EFT parameters, i.e. according to the interaction used. Clearly as the potential varies in the LIT calculation, we calculated the ground state of ^{9}Be with the same potentials therefore keeping the same Hamiltonian for the ground state and resonances. The experimental photodisintegration cross-section exhibits plainly the $1/2^+$ channel peak at around 1.7 MeV and the $5/2^+$ channel peak at ~ 3 MeV. The obtained results, for $\Lambda_{\alpha\alpha}$ = 190 MeV, $\Lambda_{\alpha n}$ = 100 MeV, Λ_3 = 300 MeV and σ_I = 1 MeV, show the $1/2^+$ channel peak at ~ 2.2 MeV and the $5/2^+$ peak at ~ 3.7 MeV. Therefore the values are not too far from the expected ones.

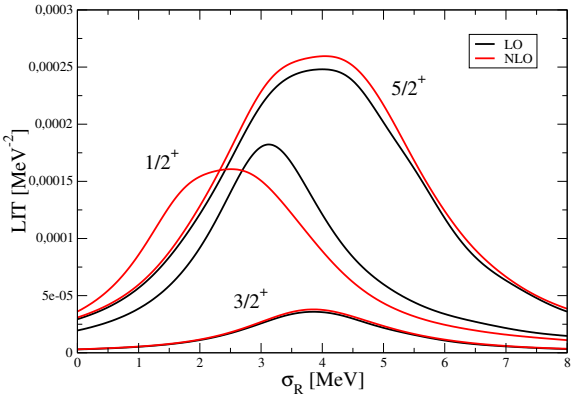

FIGURE 6.24: LIT results calculated at leading order and next to leading order. Here $\Lambda_{\alpha\alpha}$ = 190 MeV, $\Lambda_{\alpha n}$ = 100 MeV, Λ_3 = 300 MeV.

Comparing the calculation of the LIT carried out at the leading order and at the next to leading order, Figure 6.24, one can see that the greatest influence of the NLO contribution is in the $1/2^+$ channel. At the LO in our EFT for the α-n interaction only the $P_{3/2}$ wave is included while at the NLO also the $S_{1/2}$ wave is present. So

the greater influence on the $1/2^+$ channel is easily explainable since this channel has $L = 0$ and depends more on the S-wave potential. The NLO contribution of the theory causes amplitude variation of the $1/2^+$ peak of $\sim 2.4 \cdot 10^{-5}$ MeV^{-2} and a leftward shift of ~ 0.8 MeV. For the $5/2^+$ channel a visibly small increase and leftward shift of the peak is present while for the $3/2^+$ channel there is almost no influence of the NLO contribution.

Regarding the influence of the two-body cutoffs and thus of the three-body force coupling constant, while no noticeable differences arise by varying the $\alpha\alpha$ cutoff, Figure 6.25, the LIT result for all three channels considered are susceptible to the choice of αn cutoff.

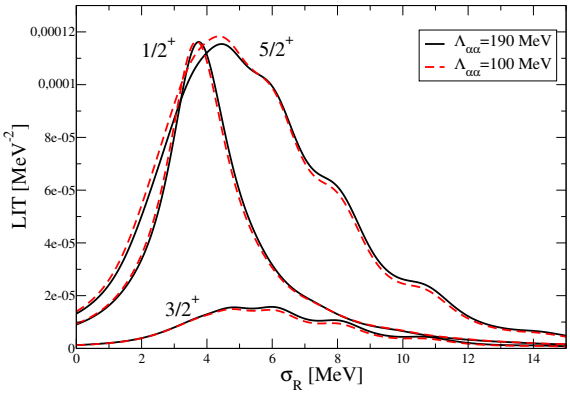

FIGURE 6.25: Comparison between LIT results calculated with $\Lambda_{\alpha\alpha}$ = 100 MeV and $\Lambda_{\alpha\alpha}$ = 190 MeV. Here $\Lambda_{\alpha n}$ = 100 MeV and Λ_3 = 130 MeV.

By varying $\Lambda_{\alpha n}$ the ground state energy of ^{9}Be has the largest variation and consequently λ_3 can also take on a rather wide range of values. This constant vary from positive to negative values making the three-body force can be either attractive or repulsive. In Figure 6.26 we show the calculation of the LITs for all three channels for

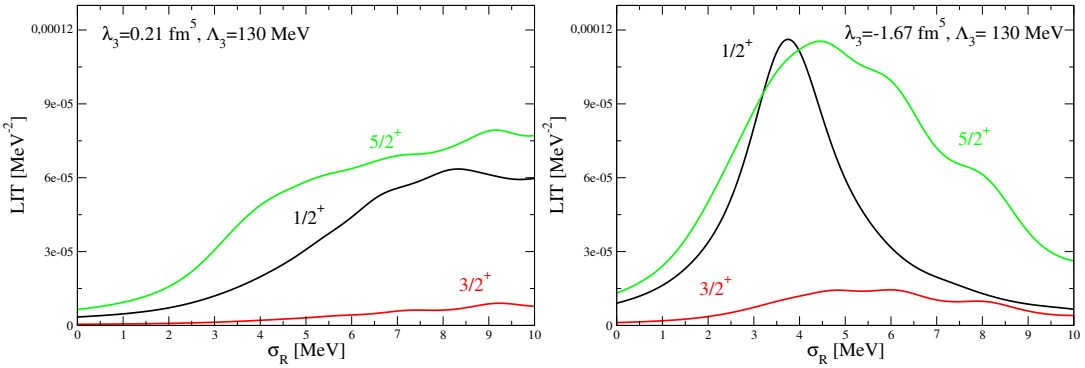

FIGURE 6.26: Comparison between two LIT results obtained with two different αn potential.

two different values of the αn cutoff and thus two respective values of the three-body force coupling constant. The results show an interesting aspect. Although the three-body force has been promoted to leading order in the EFT, to remove in the ground state of ^{9}Be the cutoff dependence, the latter still affects the computed observables

through the coupling constant λ_3. This is analogous to what happened in the prediction of the 2^+ state of Carbon, which showed a strong dependence on the three-body force. In particular for a Λ_3 cutoff of 130 MeV a three-body force with $\lambda_3 = -1.67$ fm^5 seems to produce lower energy resonances. The shift to higher energies of the LIT strength for higher $\Lambda_{\alpha n}$ values could be also interpreted as a possible indication that the low-energy peaks are obtained with a system configuration where the alpha particles are much closer to each other than to the neutron. The Fourier transform of a Gaussian cutoff $e^{-(p/\Lambda)^2}$ with $\Lambda = 300$ MeV corresponds, in fact, in coordinate space to $e^{-(r/r_0)^2}$ with $r_0 = \frac{2}{\Lambda} \sim 1.3$ fm, while for $\Lambda_{\alpha n} = 100$ MeV one has $r_0 \sim 3.9$ fm. Therefore the αn interaction in the first case vanishes for distances greater than 1.3 fm while in the second one is a longer range interaction. Moreover the mean value of the hypermomentum on the ground state wave function, defined as $\sqrt{\langle 0|\hat{Q}^2|0\rangle}$, at $\Lambda_{\alpha n} \sim 300$ MeV is about two times bigger that the value calculated with $\Lambda_{\alpha n} \sim 100$ MeV, suggesting the inverse proportion for the values of the RMS radius.

The need of an attractive three-body force is also in agreement with the works of Refs.[22, 21]. There phenomenological potentials were used and the resonance of channel $1/2^+$ was obtained by placing a three-body force more attractive than the one included in the ^{9}Be wave function calculation, thus a channel-dependent three-body force. In this work, instead, fixing the three-body force in the $3/2^-$ channel by the binding energy of ^{9}Be, we tried to reproduce all resonances with the same Hamiltonian.

Another interesting aspect is the study of the variation of the results as the three-body force cutoff changes. As it can be seen in Figure 6.27 by increasing the value

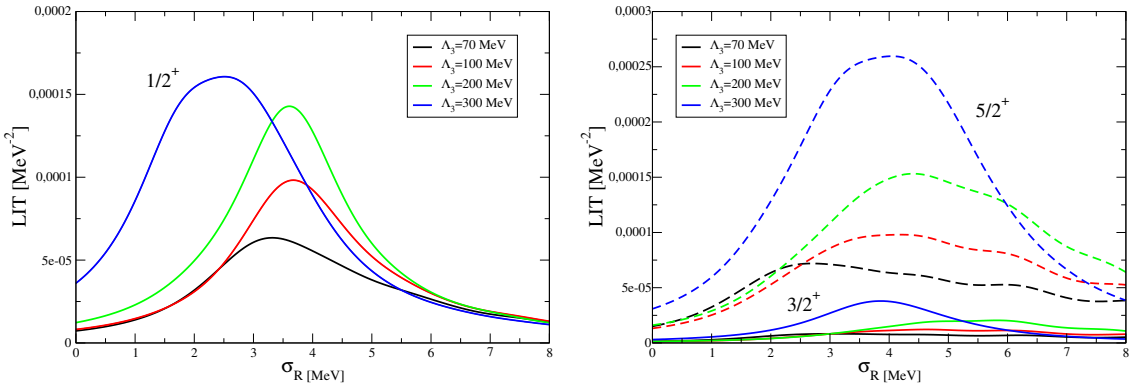

(A) LIT result for $1/2^+$ channel. (B) LIT results for $3/2^+$ and $5/2^+$ channels.

FIGURE 6.27: LIT results varying the three-body cutoff Λ_3 value. Here $\sigma_I = 1$ MeV.

of Λ_3 the peaks have a rather significant shift to the left until they reach about the expected position for 300 MeV. Using the same parallelism presented above, one could say that increasing the cutoff Λ_3 one gradually incorporates the short hyperradius components of the interaction and this could affect the description of the near-threshold resonances. We also recall that with a cutoff of about 300 MeV the

value of the coupling constants of the three-body force c_3 is of natural size ~ 1, Figure 6.19. Furthermore in Ref. [92], where a similar cluster EFT was used, it is shown that it is necessary to fine tuning the three-body force parameters in order to adequately reproduce the considered resonances. There the $3/2^+$ resonance of ^{11}Be was examined.

On the other hand, the previous results would point in the direction of a demand of a more accurate three-body force capable of unambiguously describing the system described here. This might be a hint that the theory requires higher order contributions of the three-body force. From the results obtained here, we can conclude that the three-body force that best reproduces the low-energy resonances of the three channels has a coupling constant $\lambda_3 = -0.14$ fm^5 and a cutoff $\Lambda_3 = 300$ MeV.

In order to perform the inversion of this LIT, more resolution in the calculation needs to be achieved and thus we decrease the width of the Lorentzian up to σ_I = 0.2 MeV, Figure 6.28. With this value of σ_I the number of steps required for the convergence with Lanczos algorithm is greater than 1500.

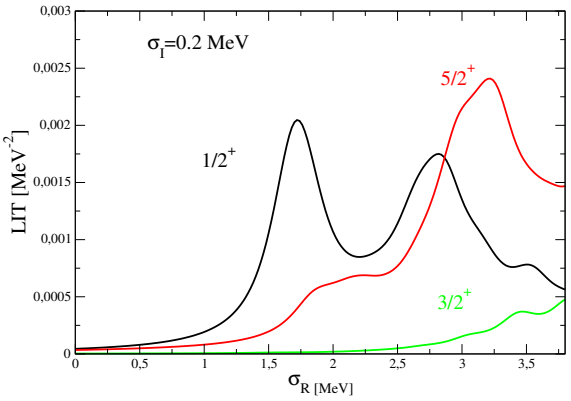

FIGURE 6.28: LIT for the three channels studied with σ_I = 0.2 MeV. As it can be seen for the $1/2^+$ channel the dominant peak is at ~ 1.7 MeV and for the $5/2^+$ channel at ~ 3 MeV. However for both channels minor peaks are also present.

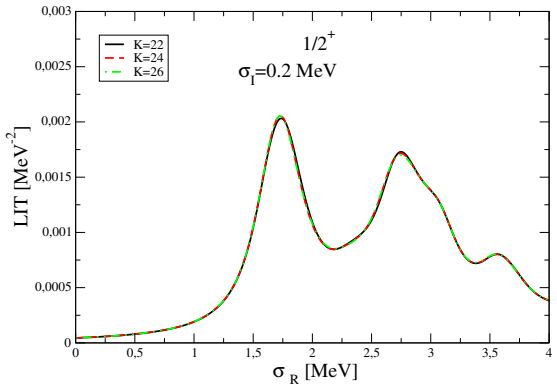

(A) $1/2^+$ channel LIT increasing K. Here N = 30, n_i, n_R = 500, 550 and β = 0.05 fm $^{-1}$.

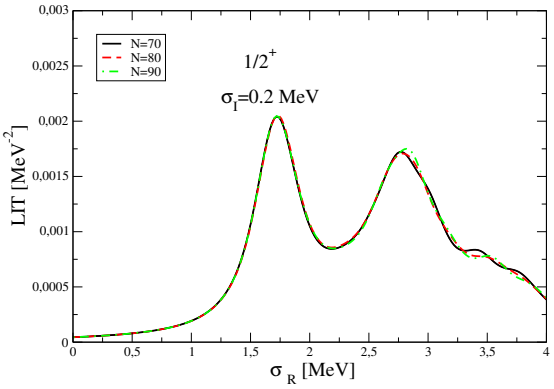

(B) $1/2^+$ channel LIT increasing the number of radial function N, we use K = 26, n_i, n_R = 500, 550 and β = 0.05 fm $^{-1}$.

FIGURE 6.29: $1/2^+$ LIT with σ_I = 0.2 MeV.

As it can be seen in Figure 6.29, for the $1/2^+$ channel the convergence on K is reached for K greater than 24 and the number of radial functions needed for convergence increases up to 70. Regarding the other two channels, as shown in Figure 6.30, with such σ_I a good convergence in N and K for the $5/2^+$ channel is obtained, while for the $3/2^+$ channel with $N = 90$ the full convergence is not still achieved. However in this case we used $\sigma_I = 1$ MeV for the LIT inversion due to the fact that the experimental resonance is wide.

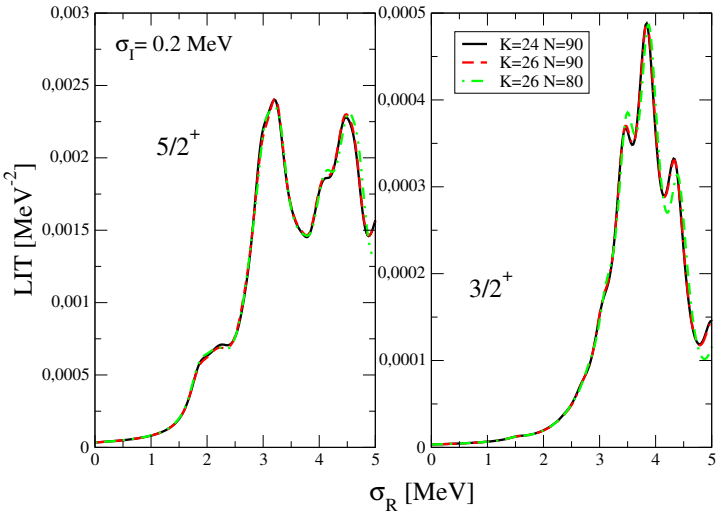

FIGURE 6.30: $3/2^+$ and $5/2^+$ LITs with $\sigma_I = 0.2$ MeV.

This confirms that the higher is the resolution, required for the integral transform, the slower is the convergence in the size of the basis. Moreover at such a small resolution we can see the presence of more than one distinct peak for the $1/2^+$ and $5/2^+$ channels.

6.6 ^{9}Be photointegration cross-section

Using the results shown in Figures 6.29 and 6.30, the integral transforms are inverted. During this procedure each channel is examined individually, in this way no information is lost about the characteristics of the identified resonances. In our case considering narrow resonances, as mentioned in Section 5.4, it is necessary to add to the inversion basis Lorentzian functions with two non-linear parameters: the position and the width. In Figure 6.31 we show the result of the LIT inversion for the $1/2^+$ channel.

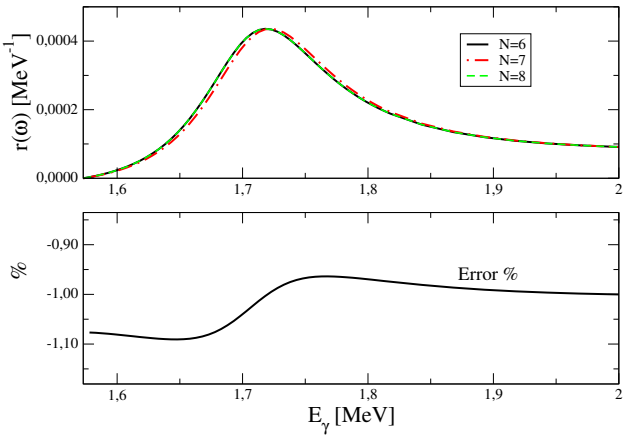

FIGURE 6.31: Inversions of LIT $1/2^+$ by increasing the number of basis functions. In the Figure above N denotes the number of basis functions comprising one Lorentzian. In the Figure below the percent error associated with the inversion is shown.

As it can be seen, using six basis functions a good stability of the result can be achieved. The error associated with the inversion, shown in the panel below, is calculated using the percentage difference between the curves with $N = 6$ and $N = 8$.

In the $5/2^+$ case, shown in Figure 6.32, it is necessary to include two Lorenzians in the set.

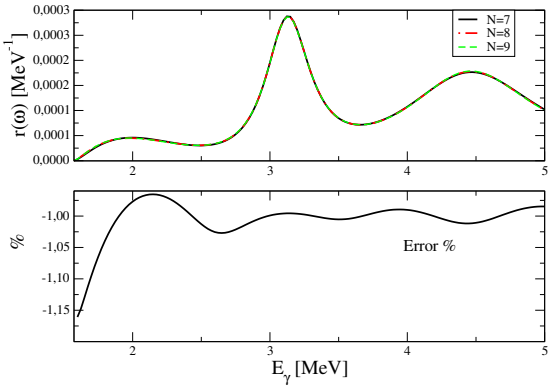

(A) Convergence of the results by increasing the number of basis functions (top figure) and error associated with inversion (bottom figure).

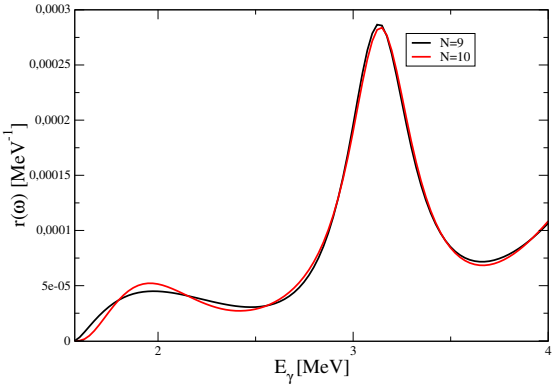

(B) LIT inversions with $N = 9$ and $N = 10$ basis function. With $N = 10$, random oscillation start to appear

FIGURE 6.32: Inversion results for $5/2^+$ channel.

The convergence is achieved for $7 \leq N \leq 9$ with a relative error of around 1%, calculated from the difference between the $N = 7$ and $N = 9$ curves. For $N > 9$ artificial oscillations start to appear. This is an example of when the number of basis functions becomes too high and instabilities arise.

The results of these inversions are then multiplied by the square of the constants present in the operator $\hat{O}_\perp$ of Eq. (5.52) and by the factors relating the cross-section to the response function of Eq. (4.66).

The response function has the same units as LIT multiplied by MeV, hence MeV^{-1}. The factor $\frac{1}{\omega_q}$ multiplied by $(\hbar c)^2$ in MeV^2 mb gives the right units to the cross-section.

In Figure 6.33 we show the comparison between the experimental data, already presented in Figure 1.2, and our theoretical result. There we can see the individual contributions of the channels $1/2^+, 3/2^+, 5/2^+$ and the total cross-section σ_{tot} obtained from the sum of the single cross-sections.

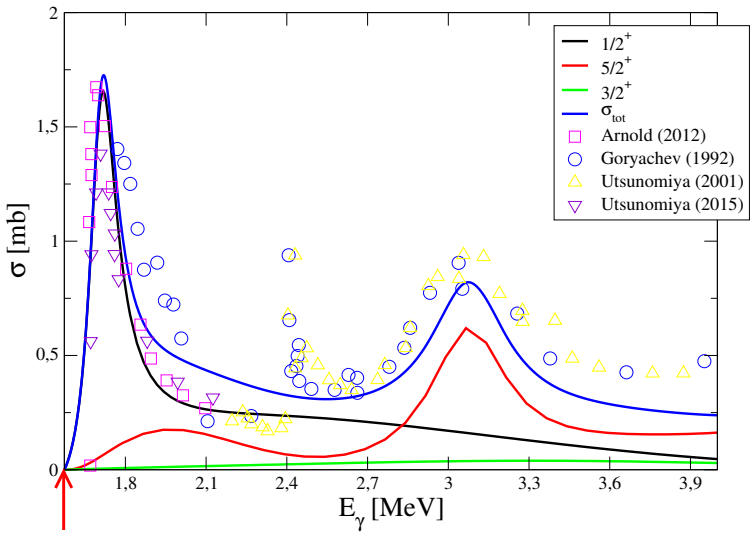

FIGURE 6.33: Comparison of our result obtained for the ^{9}Be photodisintegration cross-section and the experimental data shown in Figure 1.2. The red arrow indicates the threshold.

Our results reproduce the positions of the experimental resonances quite well. In the spectrum it is possible to identify the $1/2^+$ channel resonance at 1.7 MeV and the $5/2^+$ resonance at 3 MeV. The amplitude and width of the $1/2^+$ peak appears to be in better agreement with the data obtained by Arnold et al. [29]. Regarding the $5/2^+$ resonance, the peak turns out to be 0.1 mb lower than the experimental data, while position and width are in agreement with the expected values. Compared to the experimental data, the cross-section slightly overestimates the 1.9 – 2.4 MeV range and underestimates around 3.2 – 4 MeV. This could be improved with the NLO of the three-body force or by implementing higher order of the electromagnetic currents, described in Section 4.2. Moreover going beyond the minimal coupling with the electromagnetic field, in order to study additional negative parity channels, could help in this direction. The experimental peak at 2.5 MeV is related to the $5/2^-$ channel

resonance produced by an M1 transition. To study this part of the spectrum, the transition operator coupling the neutron spin to the electromagnetic field will also have to be taken into account,

$$\hat{O}_n = i\mu_N \sigma_n \times \boldsymbol{q} \tag{6.24}$$

being $\mu_N = -1.913\frac{e}{2m_n}$ the neutron magnetic moment. This term derived from the so-called Pauli coupling.

It is worth noting that in this work we have focused on analyzing low-energy range. With the used potential we manage to describe resonances up to ~ 4 MeV while for higher energies the cross-section decreases rather fast. We have shown in the previous section how the variation of the two body αn cutoff results in an energy shift of the calculated resonances. With $\Lambda_{\alpha n} = 300$ MeV, Figure 6.26, the dipole strength of calculated LIT would seem closer to the experimental data with energy below the GDR. From the inversion of the LIT shown in Figure 6.26 we obtain the total cross-section presented in Figure 6.34.

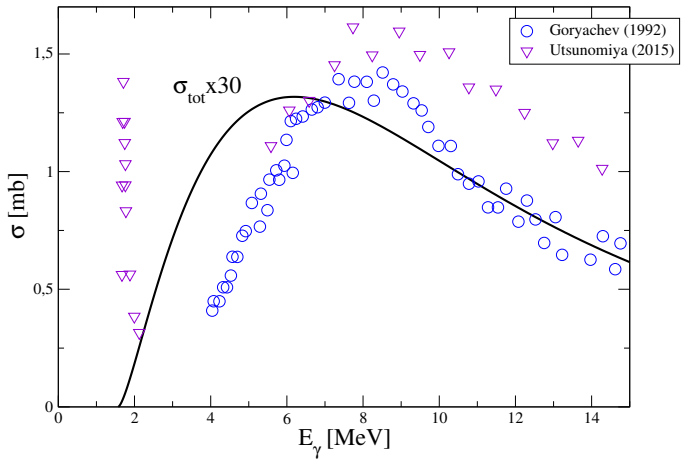

FIGURE 6.34: Cross-section result with a three-body force with strength $\lambda_3 = 0.21\text{fm}^5$, $\Lambda_3 = 130$ MeV and αn two-body potential with $\Lambda_{\alpha n} = 300$ MeV.

In the experimental spectrum the region > 6 MeV presents a wide peak whose dominant contribution seem to come from the channels $3/2^+$ and $5/2^+$ [22]. The obtained cross-section results to be thirty times smaller than the experimental one. This could be due to the lack of the $\alpha\alpha$ D-wave potential in our EFT.

As stated in Ref. [22] the cross-section in the energy range $6\,\text{MeV} < E_\gamma < 16\,\text{MeV}$ seems to acquire the main contribution by the single neutron excitation from the $^8\text{Be}(2^+) + n$ configuration of the ground state. To describe this range of the spectrum one would need of a significant percentage of $^8\text{Be}(2^+)$ state in the wave function. In our case this one is around 2%. The addition of the D-wave to the $\alpha\alpha$ potential could increase this contribution allowing a better description of the resonance. Using as a check a phenomenological α-α interaction, the Ali-Bodmer potential [93], which includes S and D partial waves, we verified how this percentage changes due to the effect of the D-wave. Using only the S-wave potential the contribution of $^8\text{Be}(2^+)$

state to the wave function is around 2% while inserting also D-wave raise up to 50%. Therefore it would be interesting to introduce such an interaction in our EFT ansatz.

Nevertheless, one should consider that for E_γ around 16 MeV we are approaching the break-down scale of our EFT given by the excitation energy of the alpha particle ~ 20 MeV. Furthermore for such energy range also the hypothesis of low-energy photon could not be fully satisfied.

Chapter 7

Conclusions and future perspectives

In this Thesis we present a description of α cluster nuclei, in particular focusing on the case of ^{9}Be, with αn and $\alpha\alpha$ contact interactions derived from Cluster Effective Field Theory (EFT).

The peculiarity of the treated systems is the separation of energy scales shown by them. The energy required to break the system is much lower compared to the excitation energy of the alpha particle. This motivation makes them candidates to be described through an EFT with clusters, namely alpha particles and nucleons as degree of freedom.

Cluster EFT is a variation of the much better known pionless EFT used to treat nuclear phenomena at an energy scale lower than the pion mass.

The potentials extracted from the theory are regularized by a Gaussian cutoff which regulates the short-distance dependence of the interaction. We choose the cutoff regularization because of its ability to reproduce known features, such as the correct sign of the effective range parameter in the T-matrix expansion or the right scaling of the renormalized scattering amplitude [23, 24]. Then, the potential low-energy constants are fitted to reproduce these scattering parameters in the calculated scattering T-matrix. The Cluster EFT loses its perturbative character trying to describe bound states and resonances. In these cases the non-natural size of the scattering length and effective range suggest a low-energy scale in the theory which distorts the perturbative power counting and makes the resummation of all the possible T-matrix diagrams necessary. To calculate the scattering matrix and find the potential coupling constants we then solved the Lippmann-Schwinger equation summing all the diagrams of the T-matrix. The non-perturbative approach is also more consistent with our approach to computing ground states ab initio, i.e., by solving the Schrödinger equation. Due to the infinite number of counterterms and to the limits imposed by the Wigner bound it is no longer possible to make the cutoff tend to infinity. The correct renormalization procedure in this case is given by the so-called implicit renormalization that keeps the cutoff at finite values and calculates at each order and for each cutoff values the low-energy constants. With the adopted power

counting the $\alpha\alpha$ system has a S-wave interaction contribution at LO and no contribution at NLO. In the αn case the $P_{3/2}$ resonance gives the LO contribution and the $S_{1/2}$ partial wave the NLO. Once the two-body potentials are obtained, the calculation of the ground-state energies is carried out by diagonalizing the Hamiltonian on a Non-symmetryzed Hyperspherical Harmonics basis in momentum space. The choice to work in the momentum space is due to the use of EFT potentials which are born naturally in this space.

From the results obtained for the ground states of the considered nuclei, it is clear that the use of only two-body forces results in general in a rather strong cutoff dependence. This is a well known feature within pionless EFT, this theory with two-body contact interactions and thus zero range force by describing three-body systems exhibits features of Efimovian physics. When only two-body contact forces are present this EFT exhibits a discrete scale invariance that gives rise to a tower of the three-body system bound states. For this reason the inclusion of the three-body force at the leading order is required in order to break this invariance. In our case although the long-range Coulomb potential, for the alpha alpha interaction, and the finite cutoff introduce a scale in the theory there still remains a residual of the discrete scale invariance shown by the rather strong dependence of the two-body cutoff.

For the Oxygen and Neon systems the binding energies are approximately reproduced using an alpha alpha cutoff value of $\Lambda_{\alpha\alpha}$ = 150 MeV and 130 MeV, respectively. Regarding the ^{12}C nucleus no value of the two-body force cutoff can reproduce the ground state energy. The obtained binding energy is much lower than the experimental one.

In any case without the three-body force the scale of the 3-body ground state is only a cutoff effect, which often leads to instability and uncertainty in the bound states obtained.

For these reasons, we introduced in our EFT at LO the three-body force by fixing its coupling constant λ_3 to describe the ground state binding energies for each value of the two body cutoff, in order to predict other physical quantities. In this way as the cutoff of the two-body force varies, the coupling constant of the three-body force varies as well, eliminating, in principle, the dependence on the cutoff.

As a first check, we tried to see if the ^{12}C excited state 2^+ was reproduced by our potential model. We found this excited state for all the values of the three-body force coupling constant λ_3 analyzed, nevertheless, its energy turns out to be dependent on the λ_3 value. This effect could in principle indicate the lack of the D-wave interaction for the $\alpha\alpha$ potential, which turns out to be of higher order in our EFT and for this reason not considered in this work. Another possibility is that this effect shows the need to include the NLO contribution of the three-body force by fixing the coupling constants to other physical quantities of the three-body system.

Finally, we studied the photodisintegration cross-section of ^{9}Be, the inverse process of the reaction $\alpha + \alpha + n \rightarrow ^9\text{Be}+\gamma$. The latter could be an important contribution to carbon nucleosynthesis during particular events, as neutron star mergers or supernova explosions, where due to the strong conditions of pressure and temperature a high number of free neutrons are present. The strong Coulomb barrier in the low-energy range makes the measurement of this reaction quite challenging and although the experimental data identify quite well the resonance peaks of interest, among them there is still some uncertainty. In this work we have considered the inverse reaction which thanks to the time reversal symmetry gives the same transition amplitude.

The electromagnetic current, or transition operator, is derived from the alpha particle free Lagrangian via minimal coupling with the electromagnetic field. Further diagrams and other electromagnetic field couplings result to be of higher order.

In order to calculate the response function of the cross-section the Lorentz integral transform approach is used. This method avoids the calculation of a final state, which may in principle belong to the continuous spectrum, by means of an integral transform of the response function; the LIT. In this way the problem is reduced to calculating this transform which can be solved by bound state methods with only the knowledge of the ground state wave function. Considering the dominant electric dipole transitions three channels are available for this reaction: $1/2^+$, $5/2^+$ and $3/2^+$.

The results obtained, for all the three channel considered, exhibit a dependence on the three-body force coupling constant and cutoffs used. In particular we found that the three-body force which best reproduces the low-energy resonances of the three channels has a coupling constant of $\lambda_3 = -0.14$ fm^5 and a cutoff of $\Lambda_3 = 300$ MeV.

From the inversion of the LIT, the response function and thus the cross-section is calculated. Our results reproduce the experimental resonances rather accurately. In the spectrum it is possible to identify the $1/2^+$ channel resonance at 1.7 MeV and the $5/2^+$ resonance at 3 MeV.

The amplitude and width of the $1/2^+$ peak appears to be in better agreement with the experimental data obtained by Arnold et al. [29]. Regarding the $5/2^+$ resonance, the peak turns out to be 0.1 mb lower than the data, while position and width are in agreement with the expected values.

The main difference with other works in the literature concerns the use of EFT potentials and a single Hamiltonian able to describe the ground state and the resonances of the system. In Refs. [22, 21] phenomenological potentials were used and the $1/2^+$ peak is obtained by placing a three-body force more attractive than the one included in the ^{9}Be wave function calculation, suggesting a channel-dependent three-body force. In this work, instead, we tried, once the three-body force in the $3/2^-$ channel is fixed by the binding energy of ^{9}Be, to reproduce all resonances with the same three-body force.

This Thesis arises from an idea whose theoretical basis was first presented in Ref. [47]. Later in Ref. [60] a code able of using potentials in momentum space was realized. There the first calculations for the αn P-wave potential and for a preliminary version, with a theta cutoff, of the $\alpha\alpha$ S-wave potential have been performed. In Ref. [59] the LIT of the ^{9}Be photodisintegration for the $1/2^+$ channel was calculated, with the dipole operator in coordinate space and using the potentials of Ref. [60].

The original contributions of this work result mainly in the further development of EFT potentials, the calculation of electromagnetic currents and their subsequent use in the LIT approach. Here, an S-wave $\alpha\alpha$ potential with Gaussian cutoff was added in the code. In addition, with regard to the potential αn we have calculated the NLO by implementing the S-wave interaction. A three-body force was also introduced in the description.

All these steps have led to the analysis of the systems ^{12}C, ^{16}O, ^{20}Ne and ^{9}Be.

The calculation of electromagnetic currents within our EFT paves the way for further studies of reaction processes. Finally, the implementation of the LIT method for the calculation of the response function with EFT currents has allowed the study of the photodisintegration cross-section. At this point several new lines of research are open.

A future perspective could be calculate a more accurate three-body interaction up to NLO in order to remove the dependence shown in our theory on the three-body force cutoff Λ_3. While the two-body interactions are, in fact, computed at NLO for the three-body force we stopped at LO and this might explain dependence on the cutoff Λ_3 shown by the results.

Furthermore implementing the three-particle permutations one could, fixed the three-body interaction parameters for example on the ^{12}C experimental data, try to predict the binding energy of the ^{16}O. In this way it could be seen whether with two- and three-body forces the four-body system will be predicted.

In this direction one could also improve the $\alpha\alpha$ interaction by inserting the D-wave of the two-body potential.

Another possible application concerns the calculation of electromagnetic currents. Going to higher orders in the calculation and beyond the minimal coupling with the electromagnetic field it would be possible to see how it affects the results. In addition negative parity reaction channels could be also investigated.

Appendix A

T-matrix

A.1 T-matrix formalism

In this Appendix we specify some details about the Lippmann-Schwinger equation.

Starting from a free particle Hamiltonian H_0 and from its solution to Schrödinger equation $|\psi_0\rangle$, we can add a potential V obtaining,

$$(E - H_0)|\psi\rangle = V|\psi\rangle\,. \tag{A.1}$$

This equation can be solved to get a solution with the required asymptotic form, introducing the Green's function G_0 for the operator on the left-hand side

$$|\psi\rangle = |\psi_0\rangle + G_0 V|\psi\rangle\,, \tag{A.2}$$

with

$$G_0 = \lim_{\epsilon\to 0} \frac{1}{E - H_0 + i\epsilon}\,. \tag{A.3}$$

The Eq. (A.2) is the Lippman-Schwinger equation, the basic integral equation of time-independent scattering theory. For more details on the derivation of this equation see for example Ref. [94]. The solution of Eq. (A.2) can be obtained by starting with $|\psi\rangle = |\psi_0\rangle$ and iterate infinite times as

$$|\psi\rangle = (1 + G_0 V + G_0 V G_0 V + \ldots)\,|\psi_0\rangle\ . \tag{A.4}$$

Defining the scattered state as

$$|\psi_s\rangle = |\psi\rangle - |\psi_0\rangle\ , \tag{A.5}$$

one has

$$|\psi_s\rangle = G_0\,(V + V G_0 V + V G_0 V G_0 V + \ldots)\,|\psi_0\rangle\,. \tag{A.6}$$

In the above expression we can recognize the operator definition of the T-matrix

$$|\psi_s\rangle = G_0 T\,|\psi_0\rangle\ , \tag{A.7}$$

or equivalently

$$T = \frac{V}{1 - G_0 V} = V + V G_0 V + V G_0 V G_0 V + \dots . \tag{A.8}$$

The expression (A.8) can be represented as an infinite sum of diagrams as in Figure A.1.

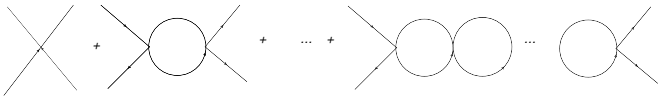

FIGURE A.1: T-matrix as infinite sum of loop corrections to the tree diagram.

It is important to note that in order to obtain a bound or virtual state all the loop corrections to the first diagram are needed. The virtual or real bound states represent in fact the poles of the T-matrix and the tree diagram does not have any pole.

A.2 Effective range theory

Let us now briefly review the effective range expansion or the T-matrix expansion as a function of the scattering length and the effective range , following Ref [95]. We consider the radial non-relativistic time-independent Schroedinger equation

$$\left(\frac{d^2}{dr^2} - \frac{l(l+1)}{r^2} - U(r) + k^2 \right) u_l(r) = 0 , \tag{A.9}$$

where $u_l(r)$ is the radial part of the following wave function expansion

$$\psi(r) = \sum_{l=0}^{\infty} B_l(k) \frac{u_l(r)}{r} P_l(\cos\theta) , \tag{A.10}$$

being $B_l(k)$ expansion coefficients, $P_l(\cos\theta)$ the Legendre polynomial and $U(r) = 2\mu V(r)$, where μ is the reduced mass.
We want to find solutions in the case of a short range potential which satisfies

$$U(r) = 0 \quad \text{for} \quad r \le R . \tag{A.11}$$

In this case the $u_l(r)$ boundary condition for $r \to 0$ is given by

$$u_l(r) = N r^{l+1} , \tag{A.12}$$

where N is a normalization factor.
The asymptotic behaviour is defined by the Bessel functions as

$$k u_l(r) = a_l s_l(kr) + b_l c_l(kr) , \tag{A.13}$$

with

$$s_l(kr) = krj_l(kr)(r \to \infty)sin(kr - \frac{l\pi}{2}), \tag{A.14}$$

$$c_l(kr) = -kr\eta_l(kr)(r \to \infty)cos(kr - \frac{l\pi}{2}). \tag{A.15}$$

Hence for $r \to \infty$

$$ku_l(kr) = a_l \sin\left(kr - \frac{l}{2}\pi\right) + b_l \cos\left(kr - \frac{l}{2}\pi\right) = \sqrt{a_l^2 + b_l^2} \sin\left(kr - \frac{l}{2}\pi + \delta_l\right), \tag{A.16}$$

with

$$\frac{b_l}{a_l} = \tan(\delta_l). \tag{A.17}$$

Therefore we can write

$$u_l(r) = a_l \left[s_l(kr) + \tan\delta_l c_l(kr)\right]. \tag{A.18}$$

Choosing $a_l = -2i\cos\delta_l e^{i\delta_l}$ we can rewrite Eq. (A.18) as

$$u_l(r \to \infty) = e^{-i\left(kr - \frac{1}{2}\pi\right)} - e^{i\left(kr - \frac{1}{2}\pi\right)} S_l(k). \tag{A.19}$$

The quantity $S_l(k)$ is then a diagonal element of the S-matrix are given by

$$S_l(k) = e^{2i\delta_l(k)} = \frac{1 + i\tan\delta_l(k)}{1 - i\tan\delta_l(k)}. \tag{A.20}$$

In general it is useful define $R_l(E)$ as

$$u_l(R) = R_l(E)\left(R\frac{du_l}{dr} - eu_l\right)_{r=R}, \tag{A.21}$$

with e an arbitrary constant, then it is possible to prove that

$$\frac{1}{\tan\delta_l(k)} = \frac{c_l(kR) - R_l(E)\left[kRc_l'(kR) - ec_l(kR)\right]}{-s_l(kR) + R_l(E)\left[kRs_l'(kR) - es_l(kR)\right]}, \tag{A.22}$$

where the derivatives are with respect to kr.

Looking at the expansion near 0 of the Bessel functions

$$j(z) = \frac{1}{(2l+1)!!}z^l + \mathcal{O}\left(z^{l+2}\right), \tag{A.23}$$

$$n_l(z) = -(2l-1)!!z^{-l-1} + 0\left(z^{-l+1}\right), \tag{A.24}$$

one can see that $\frac{k^{2l+1}}{\tan\delta_l(k)}$ is a function of k^2 which we call $F(k^2)$.

Finally recalling the relation between the on-shell T-matrix and the S-matrix,

$$T_l^{on}(E) = -\frac{2\pi}{\mu}\frac{S_l(k) - 1}{2ik}, \tag{A.25}$$

by Taylor expanding $F\left(k^2\right)$ one finds that

$$\frac{k^{2l}}{T_l^{on}(E)} = -\frac{\mu}{2\pi}\left(-\frac{1}{\alpha_l} + \frac{1}{2}r_l k^2 - ik^{2l+1}\right), \tag{A.26}$$

being the coefficients of the expansion the scattering length α_l and the effective range r_l.

It is interesting to note that in general, having used the boundary condition in R to determine T_l^{on} in powers of k^2, $r_l \sim R$, with R the range of the potential. Regarding α_l in general its size can be anything. If $\alpha_l \sim R$, it is called "natural", if $|\alpha_l| \gg R$ "unnatural".

Appendix B

The Lanczos algorithm

As already mentioned in Section 3.5 and 5.3.2, we adopt the stabilized Lanczos algorithm [58] both to calculate the ground state of the pseudo-Hamiltonian matrix and the LIT transform. The basic idea of the Lanczos method is that a special basis can be constructed when the Hamiltonian has a tridiagonal form [83]. This is carried out iteratively. First, it is necessary to select an arbitrary vector $|\phi_0\rangle$ in the Hilbert space of the studied model. If the Lanczos method is used to obtain the ground-state $|\psi_0\rangle$, then it is crucial that the overlap between $|\psi_0\rangle$ and $|\phi_0\rangle$ be non-zero. If no information about the ground state is known, this condition is usually satisfied by selecting an initial state with random chosen coefficients in the used working basis. After selecting the so-called Lanczos pivot $|\phi_0\rangle$, we can define a new vector by applying the Hamiltonian $\hat{H}$ to $|\phi_0\rangle$. Subtracting the projection over $|\phi_0\rangle$, we get

$$|\phi_1\rangle = \hat{H}\,|\phi_0\rangle - \frac{\langle\phi_0|\hat{H}|\phi_0\rangle}{\langle\phi_0 \mid \phi_0\rangle}\,|\phi_0\rangle\,, \tag{B.1}$$

which satisfies $\langle\phi_0 \mid \phi_1\rangle = 0$.
Now we can construct a new state orthogonal to the previous two as

$$|\phi_2\rangle = \hat{H}\,|\phi_1\rangle - \frac{\langle\phi_1|\hat{H}|\phi_1\rangle}{\langle\phi_1 \mid \phi_1\rangle}\,|\phi_1\rangle - \frac{\langle\phi_1 \mid \phi_1\rangle}{\langle\phi_0 \mid \phi_0\rangle}\,|\phi_0\rangle\,. \tag{B.2}$$

It can be easily verified that $\langle\phi_0 \mid \phi_2\rangle = \langle\phi_1 \mid \phi_2\rangle = 0$.
The procedure can be generalized by defining an orthogonal basis recursively as

$$|\phi_{n+1}\rangle = \hat{H}\,|\phi_n\rangle - a_n\,|\phi_n\rangle - b_n^2\,|\phi_{n-1}\rangle\,, \tag{B.3}$$

where $n = 0, 1, 2$ and the coefficients are given by

$$a_n = \frac{\langle\phi_n|\hat{H}|\phi_n\rangle}{\langle\phi_n \mid \phi_n\rangle}, \quad b_n^2 = \frac{\langle\phi_n \mid \phi_n\rangle}{\langle\phi_{n-1} \mid \phi_{n-1}\rangle} \tag{B.4}$$

supplemented by $b_0 = 0, |\phi_{-1}\rangle = 0$.
In this basis, it can be shown that the Hamiltonian matrix becomes

$$H = \begin{pmatrix} a_0 & b_1 & 0 & 0 & \cdots \\ b_1 & a_1 & b_2 & 0 & \cdots \\ 0 & b_2 & a_2 & b_3 & \cdots \\ 0 & 0 & b_3 & a_3 & \cdots \\ \vdots & \vdots & \vdots & \vdots & \end{pmatrix} \tag{B.5}$$

which is tridiagonal. Once in this form the matrix can be diagonalized easily using standard library subroutines. To diagonalize completely the Hamiltonian, a number of iterations equal to the dimension of the model are needed. However, one of the advantages of this technique is that accurate enough information about the lowest eigenstates of the problem can be obtained after a small number of iterations (typically of the order of ~ 100 or less).

In our code for each 2-body term involving an (i, j) couple, the Lanczos vector is multiplied for the potential matrix in the reference Jacobi set, whose matrix elements are stored on file. So for each (i, j) term the two particles involved in the interaction are temporarily moved in the first two positions of the Jacobi set. This means that at each step the total potential matrix is built on flight starting from the 2-body potential matrix elements.

Appendix C

Notations

C.1 Notations

In this Thesis

- We adopt the natural units $\hbar = c = 1$ and $\alpha = \frac{e^2}{4\pi}$.
- Three dimension vectors are indicated with the bold font, i.e. $\boldsymbol{q}$.
- The modulus of a vector is denoted by $|\boldsymbol{q}| \equiv q$.
- We define four vectors as $p_\mu = (E_p, \boldsymbol{p})$ with $E_p = \sqrt{m^2 + p^2}$ and $q_\mu = (\omega_{\boldsymbol{q}}, \boldsymbol{q})$ with $\omega_{\boldsymbol{q}} = q$.
- We define $\eta_{\mu\nu} = \begin{pmatrix} 1 & 0 & 0 & 0 \\ 0 & -1 & 0 & 0 \\ 0 & 0 & -1 & 0 \\ 0 & 0 & 0 & -1 \end{pmatrix}$.
- The neutron, alpha and photon fields in interaction picture are written as

$$\Psi(x) = V \int \frac{d\boldsymbol{k}}{(2\pi)^3} \frac{1}{\sqrt{V}} \left(a_{\boldsymbol{k}} e^{-ik_\mu x^\mu} + a^\dagger_{\boldsymbol{k}} e^{ik_\mu x^\mu} \right), \tag{C.1}$$

$$n(x) = V \int \frac{d\boldsymbol{k}}{(2\pi)^3} b_{\boldsymbol{k}}\, u(\boldsymbol{k}) \frac{e^{-ik_\mu x^\mu}}{\sqrt{V}}, \tag{C.2}$$

$$A^\mu(x) = \sum_{\lambda=4,\pm1,0} V \int \frac{d\boldsymbol{q}}{(2\pi)^3} \frac{1}{\sqrt{2\omega_{\boldsymbol{q}}}} (a_{\boldsymbol{q},\lambda} \epsilon^\mu_{\boldsymbol{q},\lambda} \frac{e^{iq_\mu x^\mu}}{\sqrt{V}} + a^\dagger_{\boldsymbol{q},\lambda} \epsilon^{\mu\,*}_{\boldsymbol{q},\lambda} \frac{e^{-iq_\mu x^\mu}}{\sqrt{V}}), \tag{C.3}$$

  being the dependency of the fields on the variable $x \equiv x^\mu = (t, \boldsymbol{x})$.

- The transition amplitude from an initial state $|i\rangle$ to a final state $|f\rangle$ is given by the matrix element $\langle f|S|i\rangle$, where S in the interaction picture reads [96]

$$S = 1 + \sum_{n=1}^{\infty} \frac{(-i)^n}{n!} \int d^4x_1 ... d^4x_n\, \mathcal{T}\left(\mathcal{H}_{INT}(x_1) ... \mathcal{H}_{INT}(x_n)\right), \tag{C.4}$$

  where again $x \equiv x^\mu = (t, \boldsymbol{x})$, $\mathcal{T}$ indicates the time-ordered product and $\mathcal{H}_{INT}(x)$ is the part of the Hamiltonian density containing the interaction between the

particles in interaction picture. Usually $\mathcal{H}_{INT}$ is written as a sum of terms given by products of fields and their derivatives

$$\mathcal{H}_{INT}(x) = \int d^3x \bar{n}(x)...\Psi(x)...\partial_\mu\Psi(x)...n(x)...A^\mu(x) \tag{C.5}$$

which is defined from the interaction Lagrangian density. Working in Heisenberg picture, the Hamiltonian density $\mathcal{H}$ is related to the chiral Lagrangian $\mathcal{L}$ via the Legendre transformation

$$\mathcal{H} = \Pi_\gamma \partial_0 A_\mu + \Pi_n \partial_0 n + \Pi_\Psi \partial_0 \Psi - \mathcal{L}, \tag{C.6}$$

where

$$\Pi_\gamma = \frac{\partial\mathcal{L}}{\partial(\partial_0 A^\mu(x))}, \qquad \Pi_n = \frac{\partial\mathcal{L}}{\partial(\partial_0 n)}, \qquad \Pi_\Psi = \frac{\partial\mathcal{L}}{\partial(\partial_0\Psi)} \tag{C.7}$$

are the conjugate momenta of photon, nucleon and alpha fields, respectively. Starting from the Lagrangian, performing the calculation and returning in interaction picture it is possible to prove that (see Ref. [75])

$$\mathcal{H}_{INT}(x) = -\mathcal{L}_{INT}(x) + \cdots, \tag{C.8}$$

where the correction terms can be neglected since of high order [75]. The Hamiltonian in interaction picture is defined as

$$H_{INT}(t) = \int d\boldsymbol{x}\, \mathcal{H}_{INT}(x), \tag{C.9}$$

and is related to H^{SR}_{INT} in Schrödinger picture by

$$H_{INT}(t) = e^{iH_0 t} H^{\text{SR}}_{INT} e^{-iH_0 t}, \tag{C.10}$$

where H_0 is the free Hamiltonian. Using Eq. (C.10) and integrating analytically over all the time variables, Eq. (C.4) can be written as [38]

$$\langle f|S|i\rangle = \delta_{f,i} - 2\pi\delta(E_f - E_i)\langle f|T|i\rangle, \tag{C.11}$$

where the operator T (the so-called T-matrix) is explicitly given by

$$\begin{aligned} T \;=\; & H^{SR}_{INT} + H^{SR}_{INT}\frac{1}{E_0 - H_0 + i\epsilon}H^{SR}_{INT} + \\ & + H^{SR}_{INT}\frac{1}{E_0 - H_0 + i\epsilon}H^{SR}_{INT}\frac{1}{E_0 - H_0 + i\epsilon}H^{SR}_{INT} + \cdots \end{aligned} \tag{C.12}$$

being ϵ an infinitesimal positive quantity.

In order to obtain the Hamiltonian terms expressed in Schrödinger picture, we must write the fields in this representation using

$$\psi^{\rm SR}(\boldsymbol{x}) = e^{-iH_0 t}\psi(\boldsymbol{x})e^{iH_0 t} \tag{C.13}$$

$$\psi^{\rm SR}(\boldsymbol{x}) = \psi(\boldsymbol{x}, t=0)\,. \tag{C.14}$$

In this way the fields of the photon, nucleon and alpha and their derivatives become as in Eqs. (2.3), (2.6), (4.5), (4.11).
Therefore,

$$H^{SR} = \int d\boldsymbol{x}\mathcal{H}(\boldsymbol{x}, t=0)\,, \tag{C.15}$$

where it is important to first act, if they appear, in $\mathcal{H}$ the derivatives on the fields and then put $t = 0$. In the main text although all quantities are in Schrödinger picture we omitted the superscript SR.

- When we write the matrix elements of a generic operator O

$$\langle\alpha_1|O|\alpha_1'\rangle \equiv \langle t_{\alpha_1}|\langle s_{\alpha_1}|\langle p_{\alpha_1}|O|p_{\alpha_1'}\rangle|s_{\alpha_1'}\rangle|t_{\alpha'}\rangle \tag{C.16}$$

although in general we do not write explicitly isospin and spin states and their delta functions.

Bibliography

[1] Martin Freer et al. "Microscopic clustering in light nuclei". In: *Reviews of Modern Physics* 90.3 (2018). ISSN: 1539-0756. DOI: 10.1103/revmodphys.90.035004. URL: http://dx.doi.org/10.1103/RevModPhys.90.035004.

[2] G. Gamow. "The Quantum Theory of Nuclear Disintegration". In: *Nature* 122 (3082 1928). DOI: 10.1038/122805b0. URL: https://doi.org/10.1038/122805b0.

[3] L. R. Hafstad and E. Teller. "The Alpha-Particle Model of the Nucleus". In: *Phys. Rev.* 54 (9 1938), pp. 681–692. DOI: 10.1103/PhysRev.54.681. URL: https://link.aps.org/doi/10.1103/PhysRev.54.681.

[4] David M. Dennison. "Excited States of the O-16 Nucleus". In: *Phys. Rev.* 57 (1940), pp. 454–456. DOI: 10.1103/PhysRev.57.454.

[5] David M. Dennison. "Energy Levels of the O-16 Nucleus". In: *Phys. Rev.* 96 (1954), pp. 378–380. DOI: 10.1103/PhysRev.96.378.

[6] H. Morinaga. "Interpretation of Some of the Excited States of $4n$ Self-Conjugate Nuclei". In: *Phys. Rev.* 101 (1 1956), pp. 254–258. DOI: 10.1103/PhysRev.101.254. URL: https://link.aps.org/doi/10.1103/PhysRev.101.254.

[7] F. Hoyle. "On Nuclear Reactions Occuring in Very Hot STARS.I. the Synthesis of Elements from Carbon to Nickel." In: *apjs* 1 (1954), p. 121. DOI: 10.1086/190005.

[8] C. W. Cook et al. "^{12}B, ^{12}C, and the Red Giants". In: *Phys. Rev.* 107 (2 1957), pp. 508–515. DOI: 10.1103/PhysRev.107.508. URL: https://link.aps.org/doi/10.1103/PhysRev.107.508.

[9] S. A. Afzal, A. A. Z. Ahmad, and S. Ali. "Systematic Survey of the $\alpha - \alpha$ Interaction". In: *Rev. Mod. Phys.* 41 (1 1969), pp. 247–273. DOI: 10.1103/RevModPhys.41.247. URL: https://link.aps.org/doi/10.1103/RevModPhys.41.247.

[10] N. P. Heydenburg and G. M. Temmer. "Coulomb Excitation and Cascade Decay of Rotational States in Odd-Mass Nuclei". In: *Phys. Rev.* 104 (4 1956), pp. 981–989. DOI: 10.1103/PhysRev.104.981. URL: https://link.aps.org/doi/10.1103/PhysRev.104.981.

[11] W G Nilson. "The effect of quenching and neutron irradiation on internal friction of a super purity Al-5 Mg alloy". In: (Sept. 1958). URL: https://www.osti.gov/biblio/4325592.

[12] S. Ali and A.R. Bodmer. "Phenomenological α-α potentials". In: *Nuclear Physics* 80.1 (1966), pp. 99–112. ISSN: 0029-5582. DOI: https://doi.org/10.1016/0029-5582(66)90829-7. URL: https://www.sciencedirect.com/science/article/pii/0029558266908297.

[13] Kiyomi Ikeda, Noboru Takigawa, and Hisashi Horiuchi. "The Systematic Structure Change into the Molecule-like Structures in the Self-Conjugate 4n Nuclei". In: *Progress of Theoretical Physics Supplement* E68 (July 1968), pp. 464–475. ISSN: 0375-9687. DOI: 10.1143/PTPS.E68.464. eprint: https://academic.oup.com/ptps/article-pdf/doi/10.1143/PTPS.E68.464/5216547/E68-464.pdf. URL: https://doi.org/10.1143/PTPS.E68.464.

[14] Tzany Kokalova Wheldon. "Over half a century of studying carbon-12". In: *Journal of Physics: Conference Series* 639 (Sept. 2015). DOI: 10.1088/1742-6596/639/1/012003.

[15] H Akimune et al. "Alpha cluster structure in 56Ni". In: *Journal of Physics: Conference Series* 436 (2013), p. 012010. DOI: 10.1088/1742-6596/436/1/012010. URL: https://doi.org/10.1088/1742-6596/436/1/012010.

[16] A A Cowley. "Alpha-cluster structure in the ground state of 40Ca displayed in a (p,pα) knockout reaction". In: *Journal of Physics: Conference Series* 436 (2013), p. 012011. DOI: 10.1088/1742-6596/436/1/012011. URL: https://doi.org/10.1088/1742-6596/436/1/012011.

[17] R. Higa, H.-W. Hammer, and U. van Kolck. "$\alpha\alpha$ scattering in halo effective field theory". In: *Nuclear Physics A* 809.3 (2008), pp. 171–188. ISSN: 0375-9474. DOI: https://doi.org/10.1016/j.nuclphysa.2008.06.003. URL: https://www.sciencedirect.com/science/article/pii/S0375947408005757.

[18] Paulo F. Bedaque and Ubirajara van Kolck. "Effective Field Theory for few-nucleons systems". In: *Annual Review of Nuclear and Particle Science* 52.1 (2002), 339–396. ISSN: 1545-4134. DOI: 10.1146/annurev.nucl.52.050102.090637. URL: http://dx.doi.org/10.1146/annurev.nucl.52.050102.090637.

[19] Silas R. Beane et al. "From hadrons to nuclei: crossing the border". In: *At The Frontier of Particle Physics* (2001), 133–269. DOI: 10.1142/9789812810458_0011. URL: http://dx.doi.org/10.1142/9789812810458_0011.

[20] V.D. Efros et al. "Low-energy photodisintegration of ^{9}Be and $\alpha+\alpha+n \to {}^9\mathrm{Be}+\gamma$ reactions at astrophysical conditions". In: *The European Physical Journal A* 1.4 (1998), 447–453. ISSN: 1434-601X. DOI: 10.1007/s100500050079. URL: http://dx.doi.org/10.1007/s100500050079.

[21] J. Casal et al. "Astrophysical reaction rate for Be9 formation within a three-body approach". In: *prc* 90.4, 044304 (2014), p. 044304. DOI: 10.1103/PhysRevC.90.044304. arXiv: 1407.6522 [nucl-th].

[22] Yuma Kikuchi et al. "Photodisintegration cross section of ^{9}Be up to 16 MeV in the $\alpha + \alpha + n$ three-body model". In: *Phys. Rev. C* 93 (5 2016), p. 054605. DOI: 10.1103/PhysRevC.93.054605. URL: https://link.aps.org/doi/10.1103/PhysRevC.93.054605.

[23] Daniel R. Phillips, Silas R. Beane, and Thomas D. Cohen. "Nonperturbative Regularization and Renormalization: Simple Examples from Nonrelativistic Quantum Mechanics". In: *Annals of Physics* 263.2 (1998), pp. 255–275. ISSN: 0003-4916. DOI: https://doi.org/10.1006/aphy.1997.5771. URL: https://www.sciencedirect.com/science/article/pii/S0003491697957717.

[24] Daniel R. Phillips and Thomas D. Cohen. "How short is too short? Constraining zero-range interactions in nucleon-nucleon scattering". In: *Physics Letters B* 390.1-4 (1997), 7–12. ISSN: 0370-2693. DOI: 10.1016/s0370-2693(96)01411-6. URL: http://dx.doi.org/10.1016/S0370-2693(96)01411-6.

[25] M. Fujishiro et al. "Cross section of the reaction 9Be(γ, n) near threshold". In: *Canadian Journal of Physics* 60.11 (1982), pp. 1672–1677. DOI: 10.1139/p82-224. eprint: https://doi.org/10.1139/p82-224. URL: https://doi.org/10.1139/p82-224.

[26] G. N. Zalesny A. M. Goryachev and I. V. Pozdnev. "Cross Section of (γn) Reaction on ^{9}Be in the Energy Range from Threshold to 20 MeV." In: *Bull. Russ. Acad. Sci. Phys.* 56 (1992), p. 762.

[27] H. Utsunomiya et al. "Photodisintegration of ^{9}Be through the $1/2^{+}$ state and cluster dipole resonance". In: *Phys. Rev. C* 92 (6 2015), p. 064323. DOI: 10.1103/PhysRevC.92.064323. URL: https://link.aps.org/doi/10.1103/PhysRevC.92.064323.

[28] H. Utsunomiya et al. "Photodisintegration of ^{9}Be with laser-induced Compton backscattered γ rays". In: *Phys. Rev. C* 63 (1 2000), p. 018801. DOI: 10.1103/PhysRevC.63.018801. URL: https://link.aps.org/doi/10.1103/PhysRevC.63.018801.

[29] C. W. Arnold et al. "Cross-section measurement of ^{9}Be(γ,n)^{8}Be and implications for α+α+n→^{9}Be in the *r* process". In: *Phys. Rev. C* 85 (4 2012), p. 044605. DOI: 10.1103/PhysRevC.85.044605. URL: https://link.aps.org/doi/10.1103/PhysRevC.85.044605.

[30] Takahiro Sasaqui et al. "Sensitivity of r-Process Nucleosynthesis to Light Element Nuclear Reactions". In: *The Astrophysical Journal* 634.2 (2005), 1173–1189. ISSN: 1538-4357. DOI: 10.1086/497061. URL: http://dx.doi.org/10.1086/497061.

[31] U. Kneissl et al. "Photoneutron cross sections for 9Be obtained with quasi-monoenergetic photons". In: *Nuclear Physics A* 247.1 (1975), pp. 91–102. ISSN: 0375-9474. DOI: https://doi.org/10.1016/0375-9474(75)90279-1. URL: https://www.sciencedirect.com/science/article/pii/0375947475902791.

[32] M. Gattobigio, A. Kievsky, and M. Viviani. "Nonsymmetrized hyperspherical harmonic basis for an A-body system". In: *Phys. Rev. C* 83 (2 2011), p. 024001. DOI: 10.1103/PhysRevC.83.024001. URL: https://link.aps.org/doi/10.1103/PhysRevC.83.024001.

[33] Sergio Deflorian et al. "Nonsymmetrized Hyperspherical Harmonics with Realistic Potentials". In: *Few Body Syst.* 55.8-10 (2014). Ed. by Roman Skibiński, Jacek Golak, and Stanislaw Kistryn, pp. 831–834. DOI: 10.1007/s00601-013-0781-3.

[34] V D Efros et al. "The Lorentz integral transform (LIT) method and its applications to perturbation-induced reactions". In: *Journal of Physics G: Nuclear and Particle Physics* 34.12 (2007), R459–R528. ISSN: 1361-6471. DOI: 10.1088/0954-3899/34/12/r02. URL: http://dx.doi.org/10.1088/0954-3899/34/12/R02.

[35] U. van Kolck. "Effective field theory of short-range forces". In: *Nuclear Physics A* 645.2 (1999), 273–302. ISSN: 0375-9474. DOI: 10.1016/s0375-9474(98)00612-5. URL: http://dx.doi.org/10.1016/S0375-9474(98)00612-5.

[36] H. A. Bethe. "Theory of the Effective Range in Nuclear Scattering". In: *Phys. Rev.* 76 (1 1949), pp. 38–50. DOI: 10.1103/PhysRev.76.38. URL: https://link.aps.org/doi/10.1103/PhysRev.76.38.

[37] Kenneth G. Wilson. "Renormalization Group and Strong Interactions". In: *Phys. Rev. D* 3 (8 1971), pp. 1818–1846. DOI: 10.1103/PhysRevD.3.1818. URL: https://link.aps.org/doi/10.1103/PhysRevD.3.1818.

[38] Steven Weinberg. *The Quantum Theory of Fields*. Vol. 2. Cambridge University Press, 1996. DOI: 10.1017/CBO9781139644174.

[39] H.-W. Hammer, Sebastian König, and U. van Kolck. "Nuclear effective field theory: Status and perspectives". In: *Reviews of Modern Physics* 92.2 (2020). ISSN: 1539-0756. DOI: 10.1103/revmodphys.92.025004. URL: http://dx.doi.org/10.1103/RevModPhys.92.025004.

[40] P.F. Bedaque and U. van Kolck. "Nucleon-deuteron scattering from an effective field theory". In: *Physics Letters B* 428.3-4 (1998), 221–226. ISSN: 0370-2693. DOI: 10.1016/s0370-2693(98)00430-4. URL: http://dx.doi.org/10.1016/S0370-2693(98)00430-4.

[41] Eric Braaten and H.-W. Hammer. "Universality in few-body systems with large scattering length". In: *Physics Reports* 428.5 (2006), pp. 259–390. ISSN: 0370-1573. DOI: https://doi.org/10.1016/j.physrep.2006.03.001. URL: https://www.sciencedirect.com/science/article/pii/S0370157306000822.

[42] C.A. Bertulani, H.-W. Hammer, and U. van Kolck. "Effective field theory for halo nuclei: shallow -wave states". In: *Nuclear Physics A* 712.1-2 (2002), 37–58. ISSN: 0375-9474. DOI: 10.1016/s0375-9474(02)01270-8. URL: http://dx.doi.org/10.1016/S0375-9474(02)01270-8.

[43] Elena Filandri et al. "Beryllium-9 in Cluster Effective Field Theory". In: *SciPost Phys. Proc. 3, 034* (2020).

[44] Lepage GP. In: *Proceedings of the VIII Jorge Andr e Swieca Summer School, 1995, Edited by C. A. Bertulani, et Al. World Scientific, Singapore* (1997).

[45] Richard A. Arndt, Dale D. Long, and L.David Roper. "Nucleon-alpha elastic scattering analyses: (I). Low-energy n-α and p-α analyses". In: *Nuclear Physics A* 209.3 (1973), pp. 429–446. ISSN: 0375-9474. DOI: https://doi.org/10.1016/0375-9474(73)90837-3. URL: https://www.sciencedirect.com/science/article/pii/0375947473908373.

[46] G. M. Hale. In: *private communication* (2021).

[47] Carlo Alberto Manzata. "Ground State and Photodisintegration of Beryllium-9 in Cluster Effective Field Theory". In: *Master thesis, University of Trento* (2016).

[48] D.R. Tilley et al. "Energy levels of light nuclei A=5, 6, 7". In: *Nuclear Physics A* 708.1 (2002), pp. 3–163. ISSN: 0375-9474. DOI: https://doi.org/10.1016/S0375-9474(02)00597-3. URL: https://www.sciencedirect.com/science/article/pii/S0375947402005973.

[49] G. L. Morgan and R. L. Walter. "Neutron-Helium Interaction. II. Angular Distributions and Phase Shifts from 0.2 to 7.0 MeV". In: *Phys. Rev.* 168 (4 1968), pp. 1114–1130. DOI: 10.1103/PhysRev.168.1114. URL: https://link.aps.org/doi/10.1103/PhysRev.168.1114.

[50] A. Deltuva. "Neutron– 19 C scattering: Towards including realistic interactions". In: *Physics Letters B* 772 (2017), 657–662. ISSN: 0370-2693. DOI: 10.1016/j.physletb.2017.07.036. URL: http://dx.doi.org/10.1016/j.physletb.2017.07.036.

[51] V. Eremenko et al. "Coulomb wave functions in momentum space". In: *Comput. Phys. Commun.* 187 (2015), pp. 195–203. DOI: 10.1016/j.cpc.2014.10.002.

[52] P.F. Bedaque, H.-W. Hammer, and U. van Kolck. "Narrow resonances in effective field theory". In: *Physics Letters B* 569.3-4 (2003), 159–167. ISSN: 0370-2693. DOI: 10.1016/j.physletb.2003.07.049. URL: http://dx.doi.org/10.1016/j.physletb.2003.07.049.

[53] E. P. Wigner. "Lower Limit for the Energy Derivative of the Scattering Phase Shift". In: *Phys. Rev.* 98 (1955), pp. 145–147.

[54] S.R. Beane, T.D. Cohen, and D.R. Phillips. "The potential of effective field theory in NN scattering". In: *Nuclear Physics A* 632.3 (1998), 445–469. ISSN: 0375-9474. DOI: 10.1016/s0375-9474(98)00007-4. URL: http://dx.doi.org/10.1016/S0375-9474(98)00007-4.

[55] K. A. Scaldeferri et al. "Short-range interactions in an effective field theory approach for nucleon-nucleon scattering". In: *Physical Review C* 56.2 (1997), 679–688. ISSN: 1089-490X. DOI: 10.1103/physrevc.56.679. URL: http://dx.doi.org/10.1103/PhysRevC.56.679.

[56] A. Kievsky et al. "Efimov Physics and Connections to Nuclear Physics". In: *Annual Review of Nuclear and Particle Science* 71 (2021).

[57] V. Efimov. "Energy levels arising from resonant two-body forces in a three-body system". In: *Physics Letters B* 33.8 (1970), pp. 563–564. ISSN: 0370-2693. DOI: https://doi.org/10.1016/0370-2693(70)90349-7. URL: https://www.sciencedirect.com/science/article/pii/0370269370903497.

[58] C. Lanczos. "An iteration method for the solution of the eigenvalue problem of linear differential and integral operators". In: *Journal of Research of the National Bureau of Standards* 45 (4 1950), 255–282.

[59] Francesca Bonaiti. "Application of the Lorentz Integral Transform method to 9 Be photodisintegration in a cluster effective model". In: *Master thesis, University of Trento* (2019).

[60] P. Andreatta. "Beryllium-9 in Cluster Effective Field Theory". In: *PhD thesis, University of Trento* (2019).

[61] F. F. Ruffino. "Non-Symmetrized Hyperspherical Harmonics Method Applied to Light Hypernuclei". In: *PhD thesis, University of Trento* (2017).

[62] M. Gattobigio et al. "Harmonic hyperspherical basis for identical particles without permutational symmetry". In: *Phys. Rev. A* 79 (3 2009), p. 032513. DOI: 10.1103/PhysRevA.79.032513. URL: https://link.aps.org/doi/10.1103/PhysRevA.79.032513.

[63] G. I. Kuznetsov N. Y. Vilenkin and Y. A. Smorodinskii. "Eigenfunctions of the Laplace Operator Providing Representations of U(2),SO(3),U(3) and SU(3) Groups and the Symbolic Method". In: *Sov. J. Nucl. Phys.* (1965), 906–917.

[64] J. Calais. "Hyperspherical harmonics. Applications in Quantum Theory. By. J. Avery, Kluwer Academic Publishers, Dordrecht, Boston, London, 1989". In: *International Journal of Quantum Chemistry* 38 (1990), pp. 867–867.

[65] M. Viviani et al. "Variational Calculation on A = 3 and 4 Nuclei with Non-Local Potentials". In: *Few-Body Systems* 39.3-4 (2006), 159–176. ISSN: 1432-5411. DOI: 10.1007/s00601-006-0158-y. URL: http://dx.doi.org/10.1007/s00601-006-0158-y.

[66] N. Barnea. "Exact solution of the Schrödinger and Faddeev equations for few body systems". In: *PhD thesis, Hebrew University* (1997).

[67] Sonia Bacca et al. "Ab initio calculation of Li-7 photodisintegration". In: *Phys. Lett. B* 603 (2004), pp. 159–164. DOI: 10.1016/j.physletb.2004.10.025. arXiv: nucl-th/0406080.

[68] J. Raynal and J. Revai. "Transformation coefficients in the hyperspherical approach to the three-body problem". In: *Il Nuovo Cimento A (1965-1970)* 68 (1970), 612–622.

[69] S. Pastore et al. "Two-nucleon electromagnetic charge operator in chiral effective field theory (χEFT) up to one loop". In: *Physical Review C* 84.2 (2011). ISSN: 1089-490X. DOI: 10.1103/physrevc.84.024001. URL: http://dx.doi.org/10.1103/PhysRevC.84.024001.

[70] H.-W Hammer and Daniel Phillips. "Electric properties of the Beryllium11 system in Halo EFT". In: *Fuel and Energy Abstracts* 865 (Aug. 2011), pp. 17–42. DOI: 10.1016/j.nuclphysa.2011.06.028.

[71] Steven Weinberg. *The Quantum Theory of Fields*. Vol. 2. Cambridge University Press, 1996. DOI: 10.1017/CBO9781139644174.

[72] M. Miorelli. "Electromagnetic properties of medium-mass nuclei from coupled-cluster theory". In: *PhD thesis (University of British Columbia)* (2017).

[73] M. Goldhaber and E. Teller. "On Nuclear Dipole Vibrations". In: *Phys. Rev.* 74 (9 1948), pp. 1046–1049. DOI: 10.1103/PhysRev.74.1046. URL: https://link.aps.org/doi/10.1103/PhysRev.74.1046.

[74] D. R. Phillips and H. W. Hammer. "Electromagnetic properties of the Beryllium-11 nucleus in Halo EFT". In: *EPJ Web Conf.* 3 (2010). Ed. by Evgeny Epelbaum, H. W. Hammer, and Ulf-G. Meissner, p. 06002. DOI: 10.1051/epjconf/20100306002. arXiv: 1001.1511 [nucl-th].

[75] A. Baroni et al. "Nuclear axial currents in chiral effective field theory". In: *Phys. Rev. C* 93 (1 2016), p. 015501. DOI: 10.1103/PhysRevC.93.015501. URL: https://link.aps.org/doi/10.1103/PhysRevC.93.015501.

[76] Steven Weinberg. "Effective chiral lagrangians for nucleon-pion interactions and nuclear forces". In: *Nuclear Physics B* 363.1 (1991), pp. 3–18. ISSN: 0550-3213. DOI: https://doi.org/10.1016/0550-3213(91)90231-L. URL: https://www.sciencedirect.com/science/article/pii/055032139190231L.

[77] J. Carlson and R. Schiavilla. "Structure and dynamics of few-nucleon systems". In: *Rev. Mod. Phys.* 70 (3 1998), pp. 743–841. DOI: 10.1103/RevModPhys.70.743. URL: https://link.aps.org/doi/10.1103/RevModPhys.70.743.

[78] J. D. Walecka. *Electron scattering for nuclear and nucleon structure*. Cambridge University Press, Jan. 2005. ISBN: 978-0-511-03483-1, 978-0-521-78043-8, 978-0-521-01839-5.

[79] A. J. F. Siegert. "Note on the Interaction Between Nuclei and Electromagnetic Radiation". In: *Phys. Rev.* 52 (8 1937), pp. 787–789. DOI: 10.1103/PhysRev.52.787. URL: https://link.aps.org/doi/10.1103/PhysRev.52.787.

[80] J. L. Friar and S. Fallieros. "Extended Siegert theorem". In: *Phys. Rev. C* 29 (5 1984), pp. 1645–1655. DOI: 10.1103/PhysRevC.29.1645. URL: https://link.aps.org/doi/10.1103/PhysRevC.29.1645.

[81] Sonia Bacca and Saori Pastore. "Electromagnetic reactions on light nuclei". In: *Journal of Physics G: Nuclear and Particle Physics* 41.12 (2014), p. 123002. DOI: 10.1088/0954-3899/41/12/123002. URL: https://doi.org/10.1088/0954-3899/41/12/123002.

[82] Enrico Lipparini. *Modern Many-Particle Physics: Atomic Gasses, Nanostructures and Quantum Liquids. 2nd Edition*. Feb. 2008, pp. 1–582. DOI: 10.1142/6551.

[83] Elbio Dagotto. "Correlated electrons in high-temperature superconductors". In: *Reviews of Modern Physics* 66.3 (1994), 763–840. ISSN: 1539-0756. DOI: 10.1103/revmodphys.66.763. URL: http://dx.doi.org/10.1103/RevModPhys.66.763.

[84] Andrey Nikolaevich Tikhonov and Vasiliy Yakolevich Arsenin. In: *Solutions of ill-posed problems. Washington D.C.: V.H. Winston.* (1977).

[85] Sonia Bacca et al. "Isoscalar Monopole Resonance of the Alpha Particle: A Prism to Nuclear Hamiltonians". In: *Physical Review Letters* 110.4 (2013). ISSN: 1079-7114. DOI: 10.1103/physrevlett.110.042503. URL: http://dx.doi.org/10.1103/PhysRevLett.110.042503.

[86] Stegun I. A. Abramowitz M. *Handbook of Mathematical Functions*. Dover Publ., Inc., New York., 1972.

[87] Francesco Alemanno. In: *Thesis, University of Salento* (2016).

[88] Eric Braaten et al. "Efimov Effect for P-wave Interactions". In: *Verhandlungen der Deutschen Physikalischen Gesellschaft* (Mar. 2012).

[89] H-W Hammer, C Ji, and D R Phillips. "Effective field theory description of halo nuclei". In: *Journal of Physics G: Nuclear and Particle Physics* 44.10 (2017), p. 103002. ISSN: 1361-6471. DOI: 10.1088/1361-6471/aa83db. URL: http://dx.doi.org/10.1088/1361-6471/aa83db.

[90] Yusuke Nishida. "Impossibility of the Efimov effect for p-wave interactions". In: *Physical Review A* 86.1 (2012). ISSN: 1094-1622. DOI: 10.1103/physreva.86.012710. URL: http://dx.doi.org/10.1103/PhysRevA.86.012710.

[91] J. Casal et al. "Description of continuum structures in a discrete basis: Three-body resonances and two-nucleon decays". In: *SciPost Phys. Proc.* (3 2020), p. 36. DOI: 10.21468/SciPostPhysProc.3.036. URL: https://scipost.org/10.21468/SciPostPhysProc.3.036.

[92] P. Capel, D.R. Phillips, and H.-W. Hammer. "Simulating core excitation in breakup reactions of halo nuclei using an effective three-body force". In: *Physics Letters B* 825 (2022), p. 136847. ISSN: 0370-2693. DOI: https://doi.org/10.1016/j.physletb.2021.136847. URL: https://www.sciencedirect.com/science/article/pii/S0370269321007875.

[93] S. Ali and A.R. Bodmer. "Phenomenological α-α potentials". In: *Nuclear Physics* 80.1 (1966), pp. 99–112. ISSN: 0029-5582. DOI: https://doi.org/10.1016/0029-5582(66)90829-7. URL: https://www.sciencedirect.com/science/article/pii/0029558266908297.

[94] J. J. Sakurai and Jim Napolitano. *Modern Quantum Mechanics*. 2nd ed. Cambridge University Press, 2017. DOI: 10.1017/9781108499996.

[95] P. G. Burke. *R-Matrix Theory of Atomic Collisions*. Springer Berlin Heidelberg, 2011.

[96] Franz Mandl and Graham Shaw. *Quantum Field Theory*. 1985.